Sustainable Microbial Production of 2-Oxoglutaric Acid as a Building Block for Bioplastics

Nachhaltige mikrobielle Produktion von 2-Oxoglutarsäure als Baustein für Biokunststoffe

Von der Fakultät für Maschinenwesen der Rheinisch-Westfälischen Technischen Hochschule Aachen zur Erlangung des akademischen Grades eines Doktors der Ingenieurwissenschaften genehmigte Dissertation

vorgelegt von

Lars Niklas Halle

Berichter: Univ.-Prof. Dr. rer. nat. Wolfgang Wiechert

Univ.-Prof. Dr.-Ing. Andreas Jupke

Tag der mündlichen Prüfung: 18. März 2026

Nanos gigantum humeris insidentes

(Bernhard von Chartres, anno 1120)

Nothing in biology makes sense, except in the light of evolution

(Theodosius Dobzhansky, anno 1964)

Declaration on oath

I hereby affirm in lieu of oath that I have prepared this thesis independently and without undue outside assistance. I have not used any sources or resources other than those listed. In the event that the work is additionally submitted on a data carrier, I declare that the written and the electronic form are completely identical.

Lars Niklas Halle

Mönchengladbach, October 2025

Published work

This work has been conducted at the Institute of Bio- and Geosciences – Biotechnology (IBG-1) at Forschungszentrum Jülich GmbH from February 2022 until August 2025 as part of the BioSC project "BioPlastiCycle – Transitioning bioplastics to the circular economy". The scientific activities of the Bioeconomy Science Center were financially supported by the Ministry of Culture and Science within the framework of the NRW Strategieprojekt BioSC (No. 313/323-400-002 13). Parts of this work have already been published in peer-reviewed journals, presented at conferences, or included in supervised student theses. Any ideas, methodologies, results, or conclusions that have previously appeared in my own publications are not referenced individually within this thesis, but are considered to be appropriately cited by the following listings:

Publications

1. Tenhaef, J., Halle, L., Müller, M. F., Tenhaef, N., Noack, S.: Automatisierte Wege der mikrobiellen Stammentwicklung. ***BIOspektrum***, 2022, *28*(4), 436-439.
2. Halle, L., Hollmann, N., Tenhaef, N., Mbengi, L., Glitz, C., Wiechert, W., Polen T., Baumgart, M., Bott, M., Noack, S.: Robotic workflows for automated long-term adaptive laboratory evolution: Improving ethanol utilization by *Corynebacterium glutamicum*. ***Microbial Cell Factories***, 2023, *22*(1), 175.
3. Halle, L., Höppner, D., Doser, M., Brüsseler, C., Gätgens, J., Conen, N., Jupke A., Marienhagen J., Noack, S.: From molasses to purified α-ketoglutarate with engineered *Corynebacterium glutamicum*. ***Bioresource Technology***, 2025, *416*, 131803.

Conference talks

***Himmelfahrtstagung on Bioprocess Engineering* 2024**, Regensburg/DE**,** 06. – 08.05.2024: Halle L., Gätgens J., Wiechert W., Marienhagen J., Noack S.: Microbially produced monomers for biopolymers: Bioprocess development for 2-oxoglutarate production with *Corynebacterium glutamicum*.

***8th BioProScale Symposium* 2024**, Berlin/DE, 09. – 11.04.2024. **Poster Award Talk:**
Halle L., Gätgens J., Wiechert W., Marienhagen J., Noack S.: Microbially produced monomers for biopolymers: Bioprocess development for 2-oxoglutarate production with *Corynebacterium glutamicum.*

Poster presentations

8th BioProScale Symposium, Berlin/DE, 09. – 11.04.2024:
Halle L., Brücker D., Doser M., Marienhagen J., Wiechert W., Noack S.: From molasses to α-ketoglutarate: Bioprocess development with *Corynebacterium glutamicum.*

8th International BioSC Symposium, Bonn/DE, 27. – 28.01.2025:
Halle L., Gätgens J., Wiechert W., Marienhagen J., Noack S.: Microbially produced monomers for biopolymers: Bioprocess development for 2-oxoglutarate production with *Corynebacterium glutamicum.*

***Himmelfahrtstagung on Bioprocess Engineering* 2025**, Bremen/DE**,** 26. – 28.05.2025:
Halle L.; Höppner D., Marienhagen J., Noack S.: Microbially produced monomers for biopolymers: Bioprocess development for 2-oxoglutarate: Improving C-source utilization by *Corynebacterium glutamicum.*

Supervised students´ projects

Hollmann N.: **Process modelling and analysis of microbial growth dynamics in selective environments**, Master Thesis 2022, RWTH Aachen/DE

Doser M.: **From molasses to α-ketoglutarate: Development of a *Corynebacterium glutamicum* based production process**, Master Thesis 2024, RWTH Aachen/DE

Awards

Best Poster Award: *8th BioProScale Symposium,* Berlin/DE, 09.–11.04.2024

Poster Award: *8th International BioSC Symposium,* Bonn/DE, 27.–28.01.2025

Acknowldegments

Diese Dissertation entstand im Rahmen meiner Tätigkeit als Doktorand am Forschungszentrum Jülich in der Arbeitsgruppe „Quantitative Microbial Phenotyping“ am IBG-1.

Mein besonderer Dank gilt Herrn Professor Dr. Wolfgang Wiechert, für seine wertvolle fachliche Begleitung als Gutachter und seine Unterstützung in der wissenschaftlichen Weiterentwicklung dieser Arbeit. Ebenso danke ich Herrn Professor Dr.-Ing. Andreas Jupke, der als zweiter Gutachter mit seiner Expertise wichtige Impulse gegeben und die Arbeit bereichert hat. Ein besonderer und herzlicher Dank gilt Herrn Dr.-Ing. Stephan Noack, Leiter der Arbeitsgruppe „Quantitative Microbial Phenotyping“ und mein direkter Betreuer und Mentor. Seine fachliche Expertise, sein unermüdliches Engagement und seine stetige Unterstützung haben mir während der gesamten Promotionszeit enorm geholfen. Ohne seine kompetente Betreuung und Ermutigung wäre dieses Projekt in dieser Form nicht möglich gewesen. Ich bedanke mich bei allen Mitarbeitenden der Arbeitsgruppen Noack und Oldiges, Doktorandinnen und Doktoranden, Technikerinnen und Technikern sowie Studierenden für die ausgezeichnete Zusammenarbeit, den freundschaftlichen Umgang und die inspirierende Atmosphäre in unseren Gruppen. Der kollegiale Austausch, die Hilfsbereitschaft und der Teamgeist haben diese Forschungszeit für mich besonders wertvoll gemacht. Besonderer Dank gilt Daniela Höppner für ihre wichtige Arbeit bei der Stammkonstruktion, die eine entscheidende Grundlage für die Prozessentwicklung im Projekt darstellt. Ebenso danke ich Herrn Professor Dr. Jan Marienhagen, der durch regelmäßige fachliche Diskussionen bei unseren AKG-Kaffeepausen die wissenschaftliche Qualität dieser Arbeit bereichert hat. Zuletzt danke ich von ganzem Herzen meiner Familie insbesondere meiner Frau, die mich in jeder Phase der Promotion begleitet, unterstützt und motiviert hat. Unsere gemeinsame Hochzeit und die Geburt unseres Sohnes waren für uns weitere Highlights der Promotionszeit, die wir mit viel gegenseitigem Verständnis und Zusammenhalt gemeistert haben. Die unerschütterliche Liebe und Geduld meiner Familie waren für mich eine wichtige Kraftquelle und Rückhalt während dieser intensiven Zeit. Mittlerweile ist unser Sohn zweieinhalb Jahre alt und bereichert unser Leben jeden Tag aufs Neue. Danke!

Zusammenfassung

Der globale Übergang zu einer nachhaltigen Bioökonomie erfordert effiziente mikrobiologische Plattformorganismen zur Umwandlung erneuerbarer Kohlenstoffquellen in wertvolle Chemikalien. Diese Dissertation widmet sich der Entwicklung eines nachhaltigen Bioprozesses zur mikrobiellen Produktion von α-Ketoglutarat (AKG), einer wichtigen Plattformchemikalie mit Anwendungen unter anderem in funktionellen Polymeren. Der erste Teil fokussiert auf die gesamte Bioprozessentwicklung mit *Corynebacterium glutamicum* auf Basis von Molasse, einem zuckerreichen industriellen Nebenstrom erster Generation. Im Upstream wurde durch die Kombination von rationalem Stamm-Engineering mit automatisierter Hochdurchsatz-Phänotypisierung und Skalierung ein effizienter Bioprozess entwickelt ($Y_{P/S}$ = 0.59 C_{mol} C_{mol}^{-1}). Die Erarbeitung eines Downstream-Konzeptes mit Flüssig-Flüssig-Extraktionsprozess und anschließender Kristallisation ermöglichte die Rückgewinnung von AKG in hoher Reinheit.

Der zweite Teil konzentriert sich auf die Nutzung lignocellulosehaltiger Reststoffströme zur Produktion von AKG. Dabei wurden sowohl die technischen Herausforderungen der Prozessentwicklung, insbesondere inhibitorische Nebenkomponenten im Hydrolysat und die effiziente Co-Verwertung von Glucose und Xylose adressiert. Nachhaltigkeits- und Wirtschaftlichkeitsaspekte werden diskutiert, wobei die Potenziale und Herausforderungen der Wertschöpfung aus agro-industriellen Reststoffen im Vordergrund stehen.

Im dritten Teil wird Ethanol als alternative Kohlenstoff- und Energiequelle zur mikrobiellen Produktion mit *C. glutamicum* untersucht. Um zunächst die metabolischen Limitierungen des Wildtypstammes bei der Verstoffwechselung von Ethanol zu überwinden, wurden adaptive Laborevolutionsexperimente (ALE) durchgeführt. Die Basistechnologie für miniaturisierte und automatisierte ALEs wurde dabei grundlegend erweitert und ermöglicht nun die Durchführung von Langzeit-ALEs. Der im Langzeit-ALE auf Ethanol evolvierte Stamm WT_EtOH-evo zeigte deutlich verbessertes Wachstum und Ethanolverwertung. Proteomische und genomische Analysen identifizierten eine Mutation eines einzelnen Nucleotid, die einen Einfluss auf die Regulation der Expression der Acetaldehyd-Dehydrogenase hat. Erste Versuche bestätigen die Machbarkeit der AKG-Produktion aus Ethanol ($Y_{P/S}$ = 0.11 C_{mol} C_{mol}^{-1}).

Insgesamt zeigt diese Arbeit die Entwicklung effizienter Prozesse für die Produktion von AKG und deren Erweiterung auf verschiedene erneuerbare Kohlenstoffquellen mit *C. glutamicum.*

Abstract

The global transition towards a sustainable bioeconomy requires efficient microbial platform organisms capable of converting renewable carbon sources into valuable chemicals. This dissertation is dedicated to the development of a sustainable bioprocess for the microbial production of α-ketoglutarate (AKG), an important platform chemical with applications including functional polymers. The first part focuses on comprehensive bioprocess development with *Corynebacterium glutamicum* using molasses, a sugar-rich industrial side stream of 1st generation. Through the combination of rational strain engineering with automated high-throughput phenotyping and scale-up in the upstream process, an efficient bioprocess was established ($Y_{P/S}$ = 0.59 C_{mol} C_{mol}^{-1}). The development of a downstream concept based on liquid-liquid extraction followed by crystallization enabled the recovery of highly pure AKG.

The second part focuses on the utilization of lignocellulosic side streams for AKG production. The technical challenges of process development, in particular inhibitory by-products in the hydrolysate and the efficient co-utilization of glucose and xylose were addressed. In addition, sustainability and economic aspects are discussed, with particular emphasis on the potentials and challenges of valorizing agro-industrial residues.

In the third part ethanol as an alternative carbon and energy source for microbial production with *C. glutamicum* is investigated. To overcome the metabolic limitations of the wild-type strain in ethanol utilization, adaptive laboratory evolution (ALE) experiments were conducted. The core technology for miniaturized and automated ALE was fundamentally expanded, enabling the implementation of long-term ALE. The ethanol-evolved strain WT_EtOH-evo exhibited significantly improved growth and ethanol utilization. Proteomic and genomic analyses identified a single nucleotide mutation affecting the regulation of acetaldehyde dehydrogenase expression. Initial experiments confirmed the feasibility of AKG production from ethanol ($Y_{P/S}$ = 0.11 C_{mol} C_{mol}^{-1}).

Taken together, this thesis demonstrates the establishment of an efficient bioprocess for AKG production and its extension to diverse renewable carbon sources, underlining the potential of *C. glutamicum* as a versatile platform organism for sustainable bioproduction.

Abbreviations and symbols

Abbreviation or Symbol	Full name or Description
1,4-BDO	1,4-Butanediol
ADHa	Alcohol dehydrogenase
ALDH	Aldehyde dehydrogenase
AKG	α-Ketoglutarate
ALE	Adaptive Laboratory Evolution
BS	Backscatter
CC	Carbon Capture
CCU	Carbon Capture and Utilization
CGXII	Defined medium for *C. glutamicum*
DO	Dissolved oxygen
DSP	Downstream processing
EG	Ethylene glycol
FC	Fold changes
FDA	Food and Drug Administration
GDH	Glutamate dehydrogenase
GRAS	Generally Recognized as Safe
ICD	Isocitrate dehydrogenase
KPI	Key Performance Indicator
MDI	Methylene Diphenyl Diisocyanate
OD	Optical density
OTR	Oxygen Transfer Rate
PBS	Polybutylene succinate
PE	Polyethylene
PEPCk	Phosphoenolpyruvate carboxykinase
PKE	Polyketone ester
PLA	Polylactic acid
PVC	Polyvinyl chloride
PQO	Pyruvate:Quinone oxidoreductase
PTA	Phosphotransacetylase
PU	Polyurethane
rbALE	Repetitive batch Adaptive Laboratory Evolution

STY	Space Time Yield
TCA	Tricarboxylic acid cycle
v_{upt}	Specific substrate uptake rate
WT	Wild type
$Y_{P/S}$	Product yield per substrate
$Y_{X/S}$	Biomass yield per substrate
μ_{max}	Maximum specific growth rate

Table of Contents

1. Introduction

This chapter provides the motivation and background of this work. A short introduction is given to the current fossil-based economy and the concept of bioeconomy. An overview of the state of the art in bio-plastics production highlights the relevance of bio-based chemical building blocks for biopolymers. Subsequently, downstream processing strategies are briefly introduced, since efficient product recovery is crucial for the economic viability of bio-based chemical production. Afterwards, the sources of renewable carbon are presented. Finally, the use of Corynebacterium glutamicum for utilizing these sources for bio-based production is described.

1.1 The need for a sustainable economy

1.1.1 The fossil-based economy

Through industrialization, coal, gas and oil became the central components of the economic sectors of energy generation, industrial production and transport. Over the past 250 years, they have contributed significantly to the technological progress, economic growth and prosperity of industrialized nations. As a result of this development, fossil fuels have become the central component of the current (fossil-based) economic system [1, 2]. This is reflected in the fact that the demand for fossil fuels has more than tripled in the last 60 years [3, 4]. However, despite numerous technical and economic advantages, dependence on fossil fuels has considerable disadvantages. One of the most serious is climate change, which is accelerated by the massive release of CO_2 and other greenhouse gases into the atmosphere along the value chains [5, 6]. Furthermore, fossil resources are finite. With a current proven oil reserve of around 1.5×10^{12} barrels and a daily demand of around 100 10^6 barrels d^{-1}, all oil reserves would be used up in around 41 years if accessible stocks and consumption remain the same [4, 7]. Therefore, the transition to a climate-neutral economy has become one of the greatest challenges of the 21st century in order to reconcile economic growth, prosperity, and sustainability [8].

1.1.2 The bioeconomy concept

One possible solution to the challenge of transitioning to a climate-neutral economy are the concepts of bioeconomy (Figure 1). The basic idea behind these concepts is an economy that uses biological resources, processes and principles to provide sustainable products, energy

and services. The central pillars are the use of renewable carbon, the development of technological innovations in process engineering, the establishment of closed-loop systems for product and waste recycling and the substitution and supplementation of fossil resources [9-11]. The development, analysis and implementation of such bioeconomy strategies are one of the greatest political, economic and technical challenges. The evaluation of the strategies should not only be based on the sustainability of the individual national processes, but should rather consider the global impact on socio-economic and ecological aspects and the compatibility of the strategies with the sustainability development goals (SDGs) of the United Nations, which is not given for every bio-based process [8, 12, 13]. For this reason, the development of innovative and novel bioprocesses is of great importance, as they play a key role for the chemical industry within the concept of a bio-based circular bioeconomy [8].

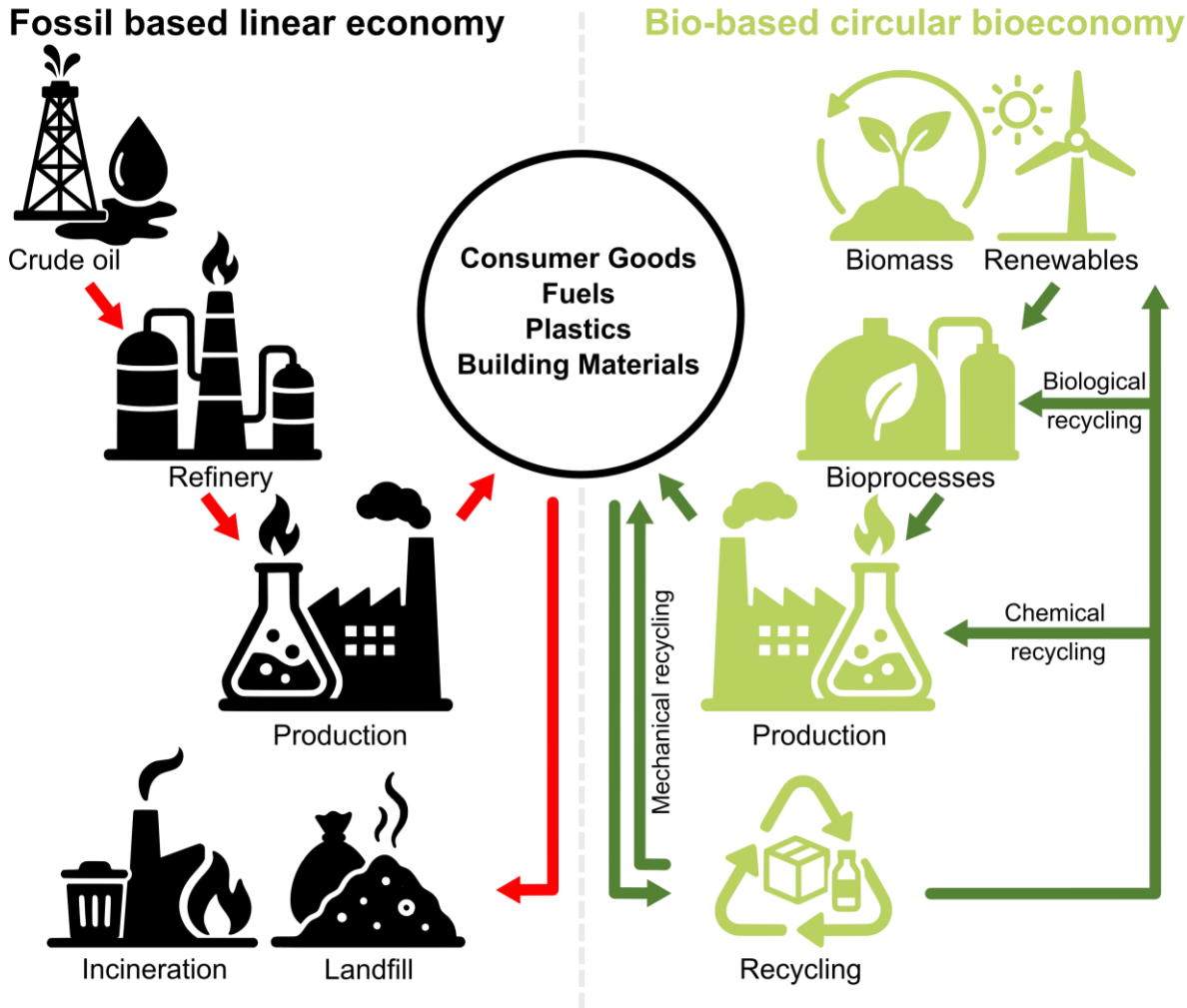

Figure 1 Bio-based value chains in the context of a circular bioeconomy. Comparison between linear, fossil-based value chains and circular, bio-based value chains. The key difference lies in the circularity enabled by the use of renewable resources and energy. Figure adapted from Bachmann et al. [14]. Icons designed with OpenAI (2025). ChatGPT, Modell: GPT-4o.

1.2 Chemical building blocks for bio-based plastics

Due to their diverse properties and applications in all areas of daily life, plastics have become one of the most important materials of our time. This is reflected by the fact, that the global annual production of plastics increased in the last 50 years from 50×10^6 t a^{-1} in 1976 to 413×10^6 t a^{-1} in 2023. However, the majority of this plastics is produced from fossil resources and ends up in landfills (46 %), is incinerated (17 %) or mismanaged (22 %). Only 15 % are collected for recycling. As of recent estimates, bio-based plastics account only for approximately 0.5 – 1 % of the total global plastic production [15-17]. But, bio-based plastics in particular, derived from renewable resources, are a key solution to the growing environmental concerns associated with fossil-based plastics and net zero-plastics strategies (Figure 2). Therefore, the market for bio-based plastics is witnessing steady growth, driven by increasing environmental awareness and regulatory pressures [18-21].

For example, polylactic acid (PLA), bio-polyethylene (Bio-PE), and polyamides (PA) are among the leading bio-based plastics, with PLA being the most commercially established and expected growth by a factor of three in the next 10 years [18, 22-24]. PLA is known for its versatility and excellent barrier properties, making it an increasingly valuable replacement for polystyrene (PS) and polypropylene (PP) in packaging and other demanding applications [25, 26]. Lactic acid, derived from fermented sugars, is the key monomer for PLA, while Bio-PE is produced from bioethanol through fermentation processes [27, 28]. The optimization of microbial fermentation processes, enzymatic catalysis, and bioengineering are crucial for enhancing the yield, selectivity, and cost-efficiency of these building blocks.

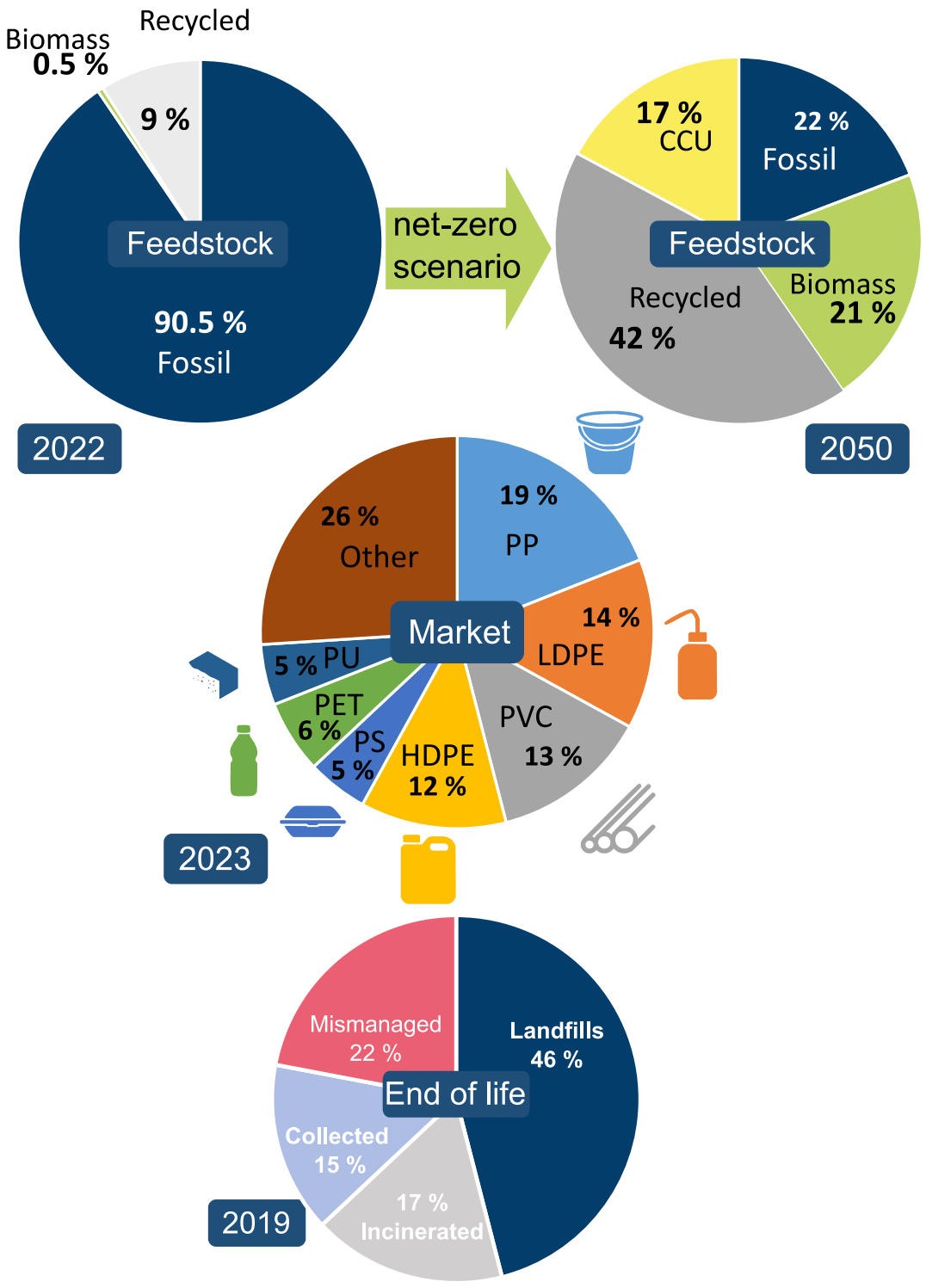

Figure 2 Global plastic production – feedstock, market distribution, and end-of-life fate. The figure illustrates the composition of feedstocks used for plastic production in 2022, with a projection for a potential net-zero CO_2 emissions scenario by 2050. It also presents the global market share of various polymer types in 2023 and the end-of-life treatment of plastic waste in 2019, including landfill, incineration, collection, and mismanagement rates. Icons designed with OpenAI (2025). ChatGPT, Modell: GPT-4o. Data adapted from [15-17].

1.2.1 Polymerization of bio-based monomers

Regardless of whether the monomer is bio-based or fossil-based, all monomers must be polymerized for plastic production. Polymerization, in polymer chemistry, is a reaction that creates a chemical bond between monomers to form polymers. There are three basic mechanisms for polymerization: chain-growth polymerization, step-growth reaction, and polyaddition reaction [29]. In chain polymerization, also known as addition polymerization, monomers with double or triple bonds join together through radical, ionic, or organometallic initiators to form long polymer chains. Examples of products from chain polymerization include polyethylene, polystyrene, and polyvinyl chloride (PVC) [27, 29]. An example of a bio-based polymer that can be obtained by chain polymerization is polylactic acid (PLA), which is derived from lactic acid and polymerized from lactide (Figure 3). Usually, PLA copolymers with various structures and biodegradable characteristics are synthesized via ring opening polymerization (ROP) [30-33].

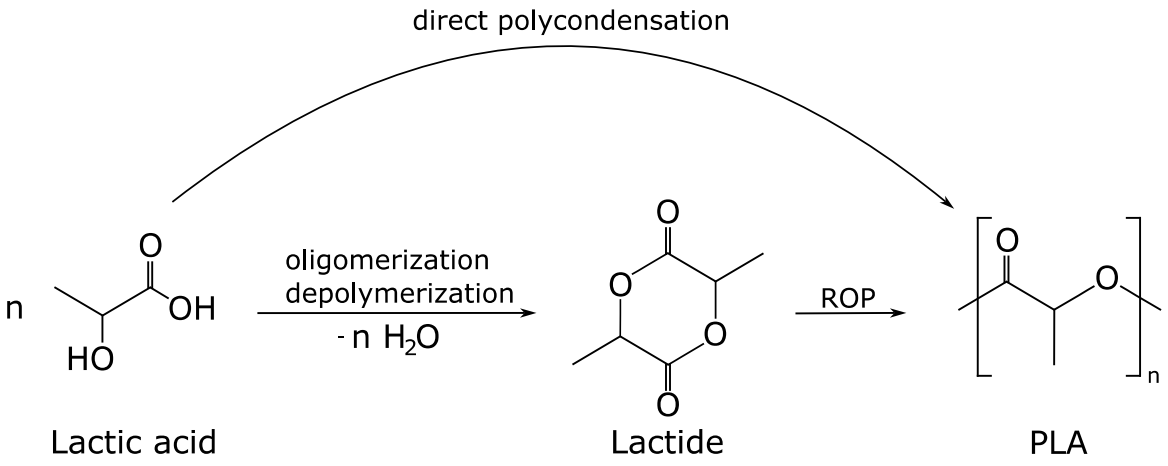

Figure 3 Chain-growth polymerization of a bio-based monomer. Lactic acid is converted into polylactic acid (PLA) via ring-opening polymerization (ROP) of lactide. Alternatively, direct polycondensation of lactic acid can also yield PLA, though with lower molecular weights.

The step-growth reaction, also known as polycondensation, is based on the stepwise linking of monomers with at least two functional groups such as hydroxyl (-OH), carboxyl (-COOH), or amine (-NH_2) [29]. During this process, small molecules such as water or methanol are released. Typical representatives of this reaction type include polyesters, polyamides (nylon), and polycarbonates [29]. An example of such a bio-based plastic is polybutylene succinate (PBS), a polyester made from succinic acid (SA) and 1,4-butanediol (1,4-BDO) (Figure 4) [34].

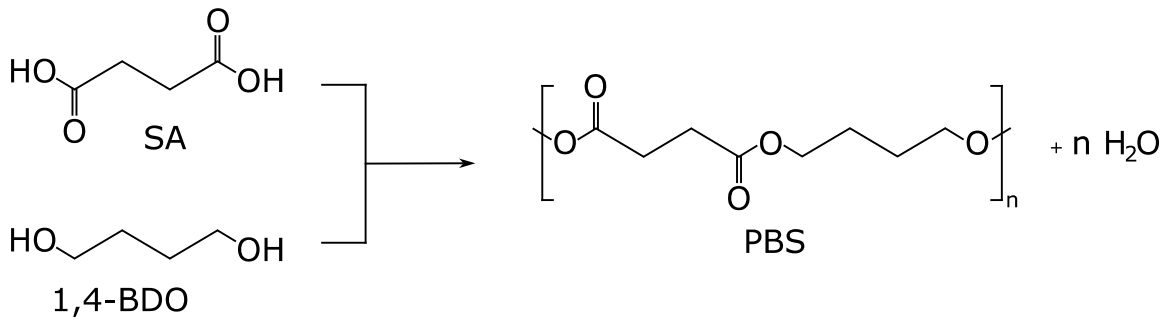

Figure 4 Step-growth polymerization (polycondensation) of bio-based monomers. Succinic acid (SA) and 1,4-butanediol (1,4-BDO) react in a condensation reaction, forming polybutylene succinate (PBS) with water as a byproduct.

In the polyaddition reaction, monomers also react stepwise with each other, but without the emission of byproducts. This reaction is for example often applied for the synthesis of polyurethanes (PU) with the characteristic urethane-group (-NH-CO-O-). One example of a bio-based PU is the bio-based production of anniline developed by the chemical company Covestro in the Bio4Pur and Bio4PURPro projects [35, 36]. In a first step, the bio-based aniline (A) is converted to methylenedianiline (MDA) in an electrophilic aromatic substitution and condensation with formaldehyde. In the second step, phosgenation to methylene diphenyl isocyanate (MDI) takes place. MDI is again converted to PU in the polyaddition reaction with a polyol like ethylene glycol (EG) (Figure 5).

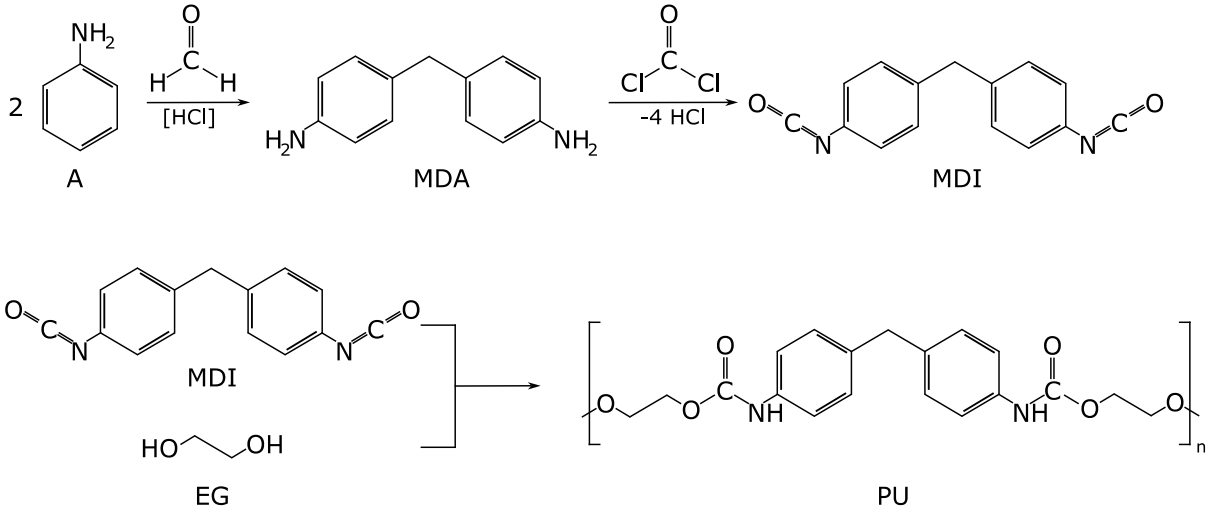

Figure 5 Polyaddition reaction using bio-based monomers. Aniline (A), derived from renewable sources, undergoes electrophilic aromatic substitution with formaldehyde to form methylenedianiline (MDA), followed by phosgenation to yield methylenediphenyl diisocyanate (MDI). MDI is subsequently polymerized with ethylene glycol (EG) in a polyaddition reaction to produce polyurethane (PU).

When two or more different monomers are combined to produce customized polymers with specific properties, the polymerization process is referred to as co-polymerization. Each of these polymerization types offers different possibilities for the production of plastics with a wide range of applications [29]. An overview of typically bio-based dicarboxylic and hydroxy acids commonly used as monomers for polyester synthesis, is given in Figure 6A.

In 2024 most of the industrially produced bioplastics are polyesters which represent more than half (around 58 %) of the global production capacities of bioplastics. Whereby one has to differentiate between bio-based polyesters that are non-biodegradable such as polyethylene (PE) and polyethylene terephthalate (PET), and biodegradable polyesters such as PBS, PLA and polyhydroxyalkanoate (PHA) (Figure 6B) [34, 37-39].

The main advantages of polyesters are the multi-stage nature of the reaction, which allows good control over the molecular weight (reaction time and conditions) and enables network-like structures for the production of thermosets. In addition, some polycondensation reactions take place at low temperatures (less energy required). However, the reactions are often slower and the polymer must be dried by splitting off water or ethanol. Compared to radical (addition) systems, the reactions are also more susceptible to impurities. This poses a further challenge for processing in biobased production by fermentation, especially when complex feedstocks such as molasses are used.

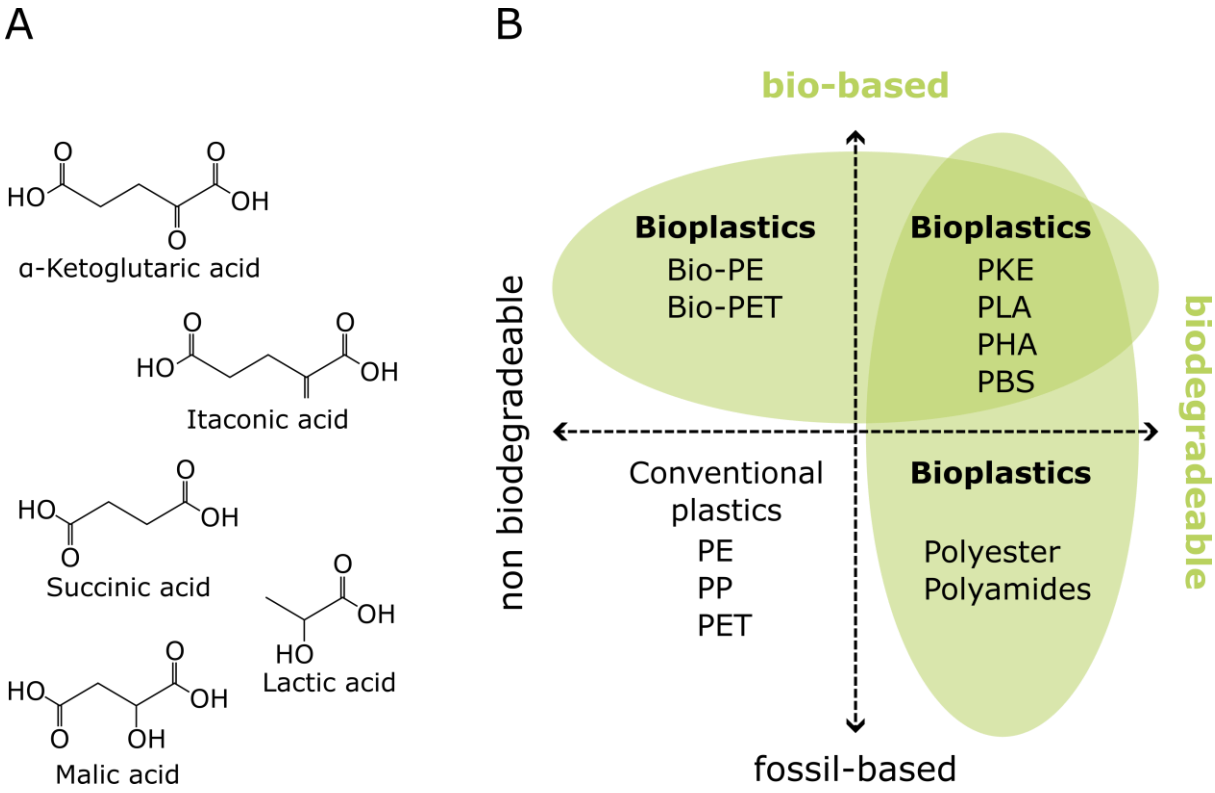

Figure 6 Overview of sustainability aspects of plastics. (A) Representative bio-based dicarboxylic and hydroxy acids commonly used as monomers for polyester synthesis. These building blocks enable the production of biodegradable and/or functional polyesters. **(B)** Classification of plastics based on their origin and end-of-life behavior. Figure adapted from [39].

1.2.2 2-oxoglutaric acid as bio-based monomer

2-oxoglutaric acid, also known as α-ketoglutaric acid, is a key metabolite in the cell metabolism of eu- and prokaryotes and belongs to the class of α-keto acids. With the chemical formula $C_5H_6O_5$, α-ketoglutaric acid is a dicarboxylic acid carrying a keto group at the α-position (Figure 6A). Its anionic form, α-ketoglutarate (AKG) plays a central role in the tricarboxylic acid cycle (TCA) and is of fundamental importance in metabolism for energy generation.

In metabolism, AKG arises as a central intermediate of the TCA cycle through the oxidative decarboxylation of isocitrate, catalyzed by isocitrate dehydrogenase (ICD). From this point, it serves as a key hub in several cellular processes. Its primary role lies in amino acid metabolism: AKG acts as a precursor for glutamate, glutamine, and proline, contributes to ammonia homeostasis and supports proline-dependent processes such as bone tissue regeneration [40-42]. In addition, AKG has secondary functions in cellular antioxidant defense. It can neutralize reactive oxygen and nitrogen species and enhance the activity of

antioxidant enzymes, including superoxide dismutase, catalase and glutathione peroxidase [43-45].

Beyond its physiological functions, AKG has particular biotechnological significance in *Corynebacterium glutamicum*. Here, the reductive amination of AKG to L-glutamate by the NAD(P)H dependent enzyme glutamate dehydrogenase (GDH) represents the central production pathway for L-glutamate and has given this organism its name.

Industrial applications of AKG are diverse. As dietary supplements, AKG salts (e.g. arginine- or creatine-AKG) are marketed to support muscle building [46, 47]. Therapeutically, AKG has been employed to promote wound healing [48] as well as an antidote in cyanide poisoning [49]. Moreover, AKG serves as a versatile starting material for the biotechnological production of valuable compounds such as ethylene or antibiotics, underlining its economic importance as a platform chemical with broad industrial application [46, 50, 51].

More recently, the suitability of AKG as a monomer for the synthesis of plastics has also been investigated. Due to its biocompatibility, reactivity and hydrolytic degradability, it represents a promising alternative for the development of new polyesters with customizable properties [52-56]. The synthesis of polyesters from AKG typically involves condensation polymerization with various polyols [53, 56]. The reaction is based on ester formation between the carboxyl groups of the 2-oxoglutaric acid and the hydroxyl groups of the polyols. This reaction produces linear or cross-linked polyesters, which have different molecular structures and properties depending on the choice of reaction conditions (temperature, catalysts, reactant ratio) [53, 56]. For example, reacting 2-oxoglutaric acid with glycerol, 1,2,4-butanetriol or 1,2,6-hexanetriol yields a series of poly(triol-α-ketoglutarates) with different mechanical and degradable properties [53].

These polymers are thermoplastics and their properties can be customized by varying the reaction conditions. Depending on the resulting properties, they are suitable for use in medical technology (e.g. bioresorbable implants and drug delivery systems, wound care materials). In addition Barret et al. showed the polycondensation of AKG with diols like 1,4-BDO (Figure 7) [57]. Building on these studies, Herman developed a branched polymer

with rubber like characteristics, one of which demonstrated strong potential for industrial application as an adhesive [55, 56, 58].

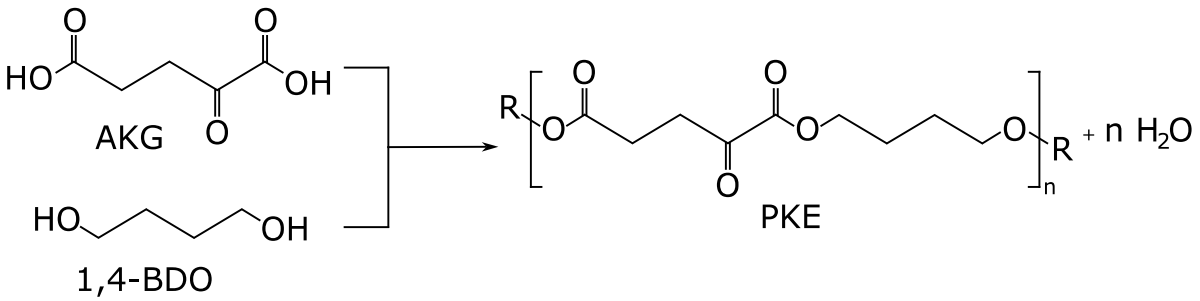

Figure 7 Novel AKG-based polymer with adhesive properties and promising biodegradability for use in debonding-on-demand applications. AKG is polymerized with 1,4-BDO via polycondensation to form a polyketone ester (PKE).

In general, the polyketone esters (PKE) synthesized from AKG are characterized by a high sensitivity to hydrolysis, which is enhanced by the adjacent ketone group. This enables rapid degradation under physiological conditions, which makes them attractive for applications in biomedicine, particularly for bioresorbable implants and drug delivery systems [53]. This property is also becoming increasingly important for materials. Biodegradable adhesives are ideal for recycling materials (e.g. car components, packaging closures) and techniques such as “debonding-on-demand technology”. In the electronics industry, for example, this makes it possible to remove high-quality components from circuit boards without leaving any residue [58, 59]. Thus, adhesive PKE from AKG would moreover be biodegradable making it a sustainable product with a circular value chain. However, the AKG currently industrially used is produced based on a multi-step chemical synthesis route starting from succinic acid and oxalic acid diethyl ester [56, 60]. Since this process causes increased costs due to toxic starting materials and by-products, has low selectivity and does not use sustainable carbon sources, the efficient biotechnological production of AKG through microbial fermentation offers economic and sustainable potential [56, 60].

Nevertheless, biotechnological production poses its own challenges in terms of the purity of the monomers, which is of great importance for the polymerization process. Fermentation broths contain salts, possibly by-products and water. All three components interfere with polycondensation. Since petrochemical-based monomers are also very inexpensive, bio-

based monomers must be produced efficiently and, above all, purified in downstream processing as efficiently and cost-effectively as possible [34, 61, 62].

1.3 Downstream process development for bio-based products

Downstream processing (DSP) is a central element of industrial bioproduction and comprises all steps downstream of biosynthesis for the isolation, purification and formulation of a target product. Typically, DSP contributes with 30 – 40 % to total production costs [63]. Especially in the case of relatively inexpensive bulk chemicals such as organic acids, an efficiently designed DSP is decisive for ensuring both the economic viability of the process and the quality of the final product.

The DSP typically consists of several process steps (Figure 8A). Depending on the localization of the target product (intra- or extra-cellular), the cells may have to be disrupted by cell disruption in the first step. Subsequent centrifugation or membrane filtration separates cells and (cell) particles, i.e. solid-liquid separation (recovery). Pre-concentration and coarse purification can be achieved by solvent extraction, precipitation or ultrafiltration (isolation). Fine purification, if necessary, relies on selective processes such as crystallization, ion exchange, adsorption or other suitable chromatography methods, depending on the physico-chemical properties of the product [64]. In the final step (polishing), the product is converted into the desired form, e.g. powder, granules or a solution. Common processes here include vacuum drying, spray drying and freeze drying. Each individual process step brings new challenges and depends on the physico-chemical properties of the respective target molecule, the ingredients of the fermentation broth and the desired product purity and property [64].

For the primary recovery step of carboxylic acids such as citric, lactic, succinic, and itaconic acid, commonly employed methods include liquid-liquid extraction, adsorption, precipitation, and conventional electrodialysis. Due to the typically neutral pH conditions during fermentation, these acids are often present in their dissociated carboxylate form rather than as free carboxylic acids. In such cases, the carboxylate must first be protonated through acidification in order to release and remove the associated cation. To minimize the formation of inorganic salt waste and to enable a more economical and sustainable process, electrodialysis or thermal processes are preferred alternatives to chemical acidification [65].

Innovative process concepts have been enabled through the coordinated application of the described and further developed separation techniques. Reactive extraction, for instance, employs a chemical extractant (such as tri-n-octylamine, TOA) to form a reversible complex with the organic acid, allowing selective phase transfer into an organic solvent, often under mild pH conditions. In the case of itaconic acid, a combination of in situ reactive extraction, pH-shift-based back extraction, and crystallization under controlled pH conditions has demonstrated both ecological and economic advantages (Figure 8B). This approach enables product recovery without relying on thermal energy input and maintains fermentation at optimal pH levels [66, 67]. Another emerging technique is electrochemical pH-shift separation, which adjusts pH via electrolysis rather than adding chemicals, thus reducing salt loads and simplifying downstream steps (Figure 8C). This method has enabled the high-purity recovery of itaconic acid (>99 %) directly from fermentation broth [68, 69]. Reducing or eliminating waste streams is a critical objective in the advancement of sustainable DSP strategies. For instance, although lactic acid is traditionally isolated via chemical precipitation, this method is associated with significant environmental concerns, particularly due to gypsum byproduct formation [70]. As a result, alternative separation technologies such as ion-exchange adsorption and membrane-based processes have received increasing attention as more sustainable options [71, 72].

These advancements illustrate how coupling classical DSP methods with innovative approaches can significantly enhance separation efficiency, reduce waste, and improve the overall sustainability of bio-based production processes.

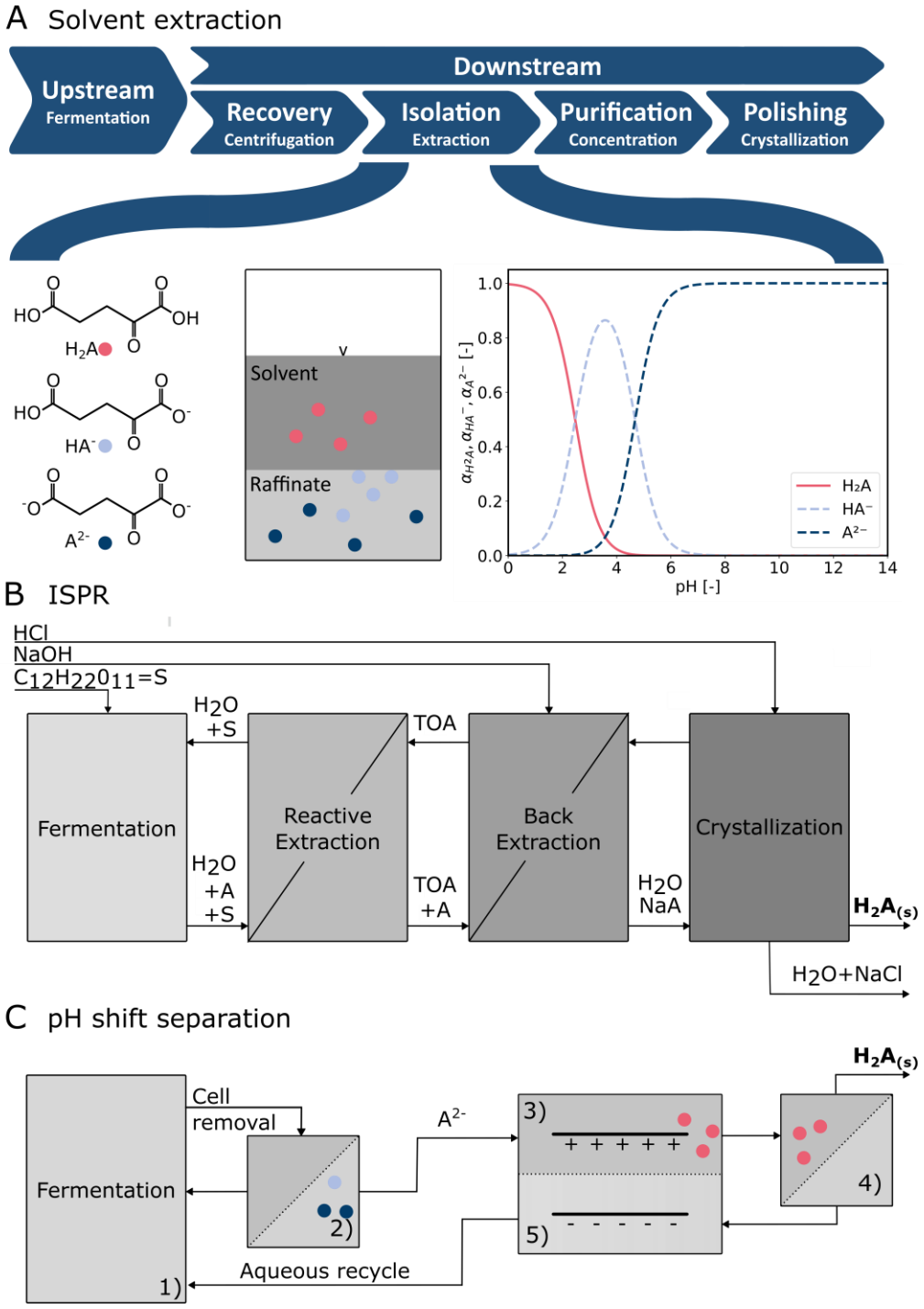

Figure 8 Downstream processing strategies and innovative separation concepts for the purification of biobased organic acids. (A) Solvent extraction (liquid-liquid extraction): Depending on the protonation state of the dicarboxylic acid (e.g. α-ketoglutaric acid), the molecule exists as H_2A, HA^-, or A^{2-} and preferentially partitions into the organic or aqueous phase. The dissociation diagram illustrates the relative abundance of each species as a function of pH. **(B)** In situ product removal (ISPR) via reactive extraction and pH-shift back extraction: Block flow diagram of an integrated process (example: AKG), comprising fermentation, reactive extraction with TOA, aqueous back-extraction, and crystallization of the acid. Adapted and adjusted from Eggert (2019) [66]. **(C)** Electrochemical "Power-to-Purity" process for the separation of biotechnologically produced carboxylic acids (example: AKG). Steps include (1) fermentation under neutral pH, (2) cell removal, (3) electrochemical acidification in the anode chamber enabling pH-shift crystallization, (4) product separation via solid-liquid separation, and (5) cathodic basification for pH regulation and aqueous recycle. Adapted and adjusted from Kocks (2019) [68].

Nonetheless, the development and selection of DSP strategies cannot rely on technical feasibility and sustainability alone. Comprehensive techno-economic assessments (TEAs) are essential to holistically evaluate the economic viability, energy requirements, material efficiency, and environmental impact of the process [62, 73]. Such analyses provide crucial decision-making tools early in development, guiding the selection of unit operations and integration strategies that align with industrial scalability and sustainability [74, 75]. Therefore, coupling innovative separation technologies with rigorous TEA provides a foundation for competitive bio-based chemical production in a market dominated by petrochemical alternatives.

1.3.1 Suitable downstream process for AKG fermentation broth

For the purification of AKG from the fermentation broth, a liquid-liquid extraction process (LLE) was conceptualized and applied in this work. In general, LLE is often used for the separation and purification of organic acids from complex matrices. The principle of LLE is based on the different solubility of a substance in two liquids that are as immiscible as possible. The distribution of an organic acid between an aqueous and an organic phase can be described by Nernst's distribution theorem (equation 1), where K_E is the distribution coefficient, c_E is the concentration of the acid in the organic phase (extract) and c_R is the concentration of the acid in the releasing aqueous phase (raffinate) [64].

$$\frac{c_E}{c_R} = K_E = const. \tag{1}$$

For organic acids, the pH value is a decisive influencing factor for the distribution, as it influences the dissociation equilibrium of the carboxyl function, either in protonated form (R-COOH) or as a deprotonated form ($R\text{-}COO^-$). Since uncharged molecules tend to have a higher affinity for the organic phase (solvent), the carboxyl functions of the acid should be as completely protonated as possible [64].

For AKG as a dicarboxylic acid, there are three fractions with regard to the protonation state depending on the pH value: i) the form A^{2-} dissociated at both carboxyl functions, ii) the form HA^- dissociated at one carboxyl function, and iii) the fully protonated form H_2A. All three

species together form the total concentration of acid c_0. Using the equilibrium equations and the pKs values of the carboxyl functions of AKG (pKs_1 = 2.47, pKs_2 = 4.68) the protonation states can be predicted as a function of pH. The protonation states and the distribution diagram for AKG determined with equations 5 – 7 is shown in Figure 8A.

$$c_0 = c(H_2A) + c(HA^-) + c(A^{2-}) \tag{2}$$

$$Ka_1 = \frac{c(H^+)\, c(HA^-)}{c(H_2A)} \; ; \; Ka_2 = \frac{c(H^+)\, c(A^{2-})}{c(HA^-)} \tag{3}$$

$$c_0 = c(H_2A)\left(1 + \frac{Ka_1}{c(H^+)} + \frac{Ka_1 Ka_2}{c(H^+)^2}\right) \tag{4}$$

$$c(H_2A) = c_0 \frac{1}{1 + 10^{(pH - pKa_1)} + 10^{(2pH - pKa_1 - pKa_2)}} \tag{5}$$

$$c(HA^-) = c_0 \frac{10^{(pH - pKa_1)}}{1 + 10^{(pH - pKa_1)} + 10^{(2pH - pKa_1 - pKa_2)}} \tag{6}$$

$$c(A^{2-}) = c_0 \frac{10^{(2pH - pKa_1 - pKa_2)}}{1 + 10^{(pH - pKa_1)} + 10^{(2pH - pKa_1 - pKa_2)}} \tag{7}$$

In addition to the pH value, the equilibrium distribution depends on the solubility in the solvent and the influence of temperature on the solubility. Zeng et al. have already described a separation process for the purification of AKG and pyruvate from fermentation broth [76]. Since ethyl acetate proved to be suitable here, this solvent was also used for the extraction in this work.

Especially for cost-sensitive bio-based products such as bulk chemicals or bioplastics, an efficient and economically viable downstream process is crucial. At the same time, the choice of feedstocks plays an important role, as their sustainability and economic value must be carefully assessed and integrated into a comprehensive life cycle analysis.

1.4 Utilization of renewable carbon feedstocks with microbial hosts

1.4.1 Agricultural biomass

Autotrophic organisms such as plants and some bacteria can rebuild energy-rich biomass from inorganic substances and an energy source. The agriculturally produced biomass is primarily used as food for animals and humans (94 %), as a material (3 %) or for energy production (3 %) [77]. In terms of the bioeconomy, this biomass can and should also be used as an extension and substitution of petrol-based chemistry for the production of valuable materials. The biomass feedstocks used are divided and classified into three generations. First generation (1st gen.) feedstock refers to biomass that is also used as food (e.g. glucose, sucrose, starch) for animals or humans and is therefore in competition with this use. Second generation (2nd gen.), on the other hand, refers to biomass feedstocks (e.g. 2nd gen. lignocellulosic feedstock) and the products produced with them (e.g. 2nd gen. biofuels). These are characterized by the fact that, as non-food biomass, they are not in competition with human or animal nutrition. Biomass that is not generated by plants but by algae is referred to as third generation feedstock (3rd gen.).

Currently, most established bio-based processes are carried out on the basis of 1st gen. feedstocks [78, 79]. The use of 2nd gen. lignocellulosic feedstocks is being intensively promoted and researched, as is the use of 3rd gen. feedstocks [79, 80]. However, all three generations of biomass feedstocks have in common that for their production an enormous amount of cultivable land is necessary. In addition, investment costs, e.g. for raw materials, must be low, especially for cheap mass-produced products such as bioplastics. In order not to increase land competition even further and to reduce investment costs, one approach is to utilize waste streams from these value chains, such as wood manufacturing residuals or side streams from sugar beet production like molasses [81, 82]. The latter, a viscous concentrated sugar beet residue consist largely of sucrose, additional sources of nitrogen, organic acids and particles (Figure 9A), making it interesting for direct use in bioprocesses. The salts contained in molasses can be found in Table S1 in the Appendix. Since molasses already has a wide range of applications in the animal feed industry, it should be classified as a 1st gen. feedstock, even though it is a waste stream.

In the context of 2nd gen. lignocellulosic feedstocks, the utilization of hardwood residuals is of particular interest. However, these materials require pretreatment before further processing can occur. The company Fibenol, for example, produces hemicellulosic hydrolysates from hardwoods (Figure 9B). Using a proprietary pretreatment process, the C5 sugar xylose is first released. Subsequently, the C6 sugars are liberated through a biological enzymatic process. The resulting product is a syrup-like fluid primarily composed of xylose and glucose, which can be directly employed in fermentation processes. Importantly, its origin does not compete with food or feed resources for humans or animals. An overview of the composition of the hydrolyzed hardwood residuals from Fibenol used in this work is provided in the appendix (Table S2).

Nevertheless, a growing world population and the continued shift from a fossil-based to a bio-based economy will further increase the demand for food production and agriculturally available land. Therefore, another promising approach to avoid further fueling the feed and land use competition in the use of renewable carbon feedstocks is the fixation of CO_2 by means of novel carbon capture and utilization technologies.

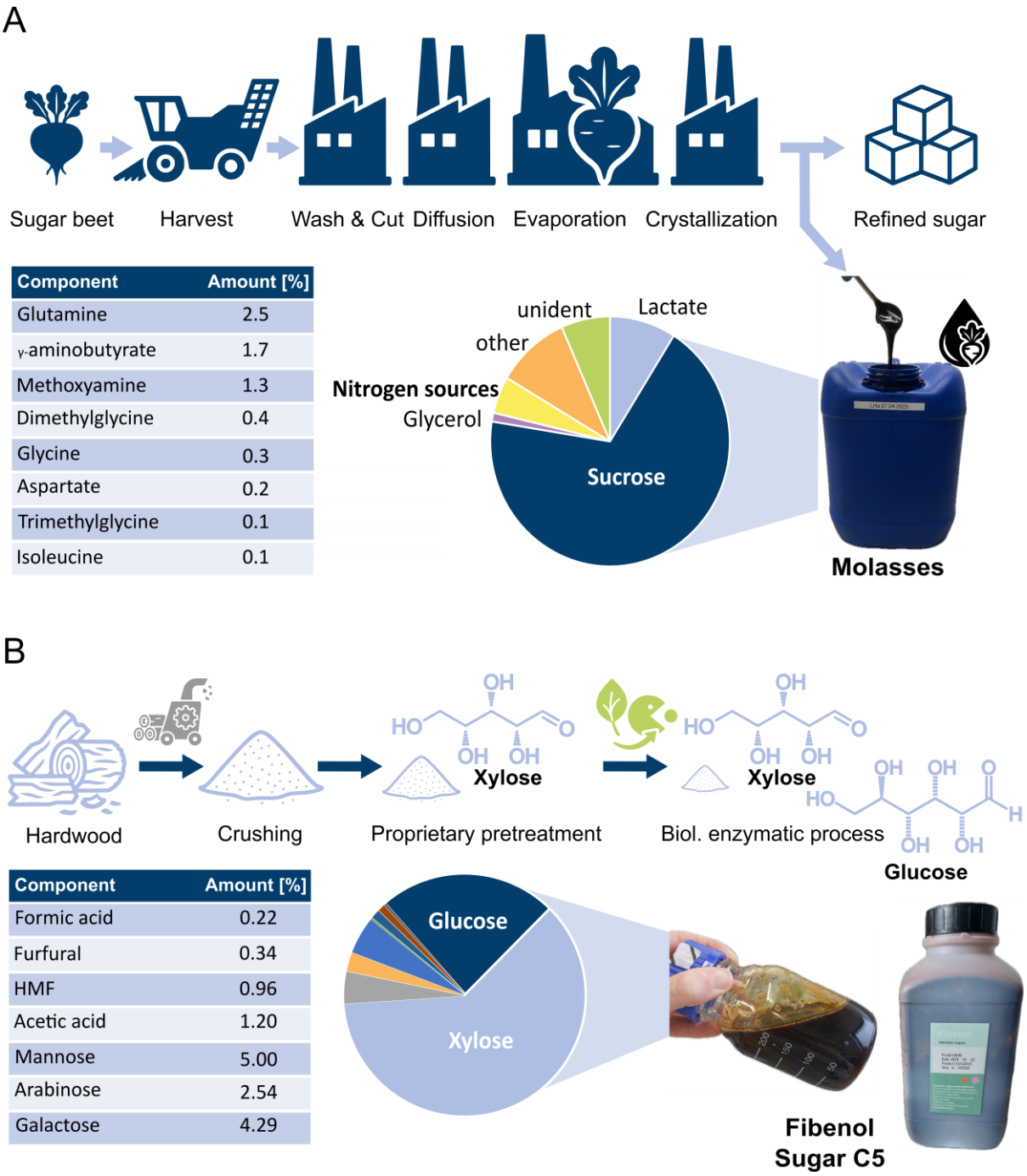

Figure 9 Renewable carbon feedstocks from industrial waste streams. (A) Schematic overview of industrial sugar production from sugar beet, highlighting the generation and composition of the side stream molasses (1st gen. feedstock). The composition of molasses was analyzed using untargeted GC-ToF-MS [81]. (B) Shematic overview of the hydrolysis process of hardwood, highlighting the generation of xylose and glucose-rich hydrolysates. The shown lignocellulosic hydrolysate and information about its composition was kindly provided by the company Fibenol (Tallinn, ET). Icons designed with OpenAI (2025). ChatGPT, Modell: GPT-4o.

1.4.2 Carbon capture and utilization

Carbon capture (CC) technologies are methods for capturing CO_2. Originally, these were used for enhanced oil recovery in order to extract more oil from the reservoirs during production and have existed in their basic form since the 1970s [83, 84]. The first large-scale trial was

carried out in the Sleipner project in 1996 to store CO_2 from a natural gas extraction plant as carbon capture and storage concept [85]. Since the 2000s, these technologies have been further developed to make additional use of the captured CO_2 in carbon capture and utilization (CCU) concepts [86, 87]. Today, CO_2 is already being captured in innovative and increasingly efficient CC processes from point sources, such as fossil fuel-based power generation, fermentation off gas or even from air (direct air capture) [88-91]. The latter technology is well suited for Power-to-X concepts, which covers all processes that convert green electricity into chemical energy carriers for electricity storage, electricity-based fuels or raw materials for the chemical industry. However, it should be noted that a lot of electrical energy is required for CC processes compared to biomass utilization. The latest technology developments in CC integrate the separation process into synthesis routes for energy-rich alcohols such as methanol (C1) and ethanol (C2) [91, 92]. These developments pave the way for economical and sustainable production of biofuels like CC-methanol and CC-ethanol for combustion and as potential feedstock for sustainable (bio-)processes in the chemical industry. With the goal of reducing CO_2, using it as a solid chemical raw material offers a longer-term reduction in emissions than using it as a fuel that is ultimately oxidized again [91, 93]. These technologies are currently transferred in large scale and are being commercialized. For example, in collaboration with Linde, Heidelberg Materials is building a large-scale CCU plant at its Lengfurt cement plant, which is scheduled to go into operation in 2025. According to the company, it will be the first of its kind. The project is called Capture-to-Use (CAP2U) and will capture 70,000 tons of CO_2 per year [94]. Another example is the start-up Air Company, which secured USD 69 million in financing in September 2024 under the leadership of aviation fuel supplier Avfuel.

Beside this electrochemical capture and conversion technologies, biological technologies were applied in hybrid processes [95, 96]. For example in Evoniks and Siemens Rheticus project with funding from Germany's Federal Ministry of Education and Research (BMBF). Here CO_2 is captured and converted to CO. The latter is than used in a fermentation process to produce a variety of chemicals [96, 97]. Another application example is given with the company LanzaTech. LanzaTech was the first company to successfully commercialize a gas fermentation process using CO and H_2 for ethanol production. Beyond ethanol, LanzaTech is also advancing fermentation technologies to produce other chemicals from industrial waste

gases containing CO, CO_2, and H_2 [98]. In the future, these developments could lead to even greater availability of sustainable energy sources such as methanol and ethanol as feedstock for chemical production routes.

Biotechnological production processes offer the opportunity to utilize both renewable carbon feedstocks from CC technologies and agricultural biomass. These processes are well-suited to handle a wide range of substrates, including biological feedstocks as well as C1 and C2 compounds, and typically operate under relatively mild process conditions [99]. In this way, they lay the foundation for a CO_2-based circular value chain in the context of a bioeconomy (Figure 10). The establishment of such a circular value-added cycle for AKG based on renewable feedstocks (molasses (1^{st} gen.) and ethanol (CCU) is part of this work.

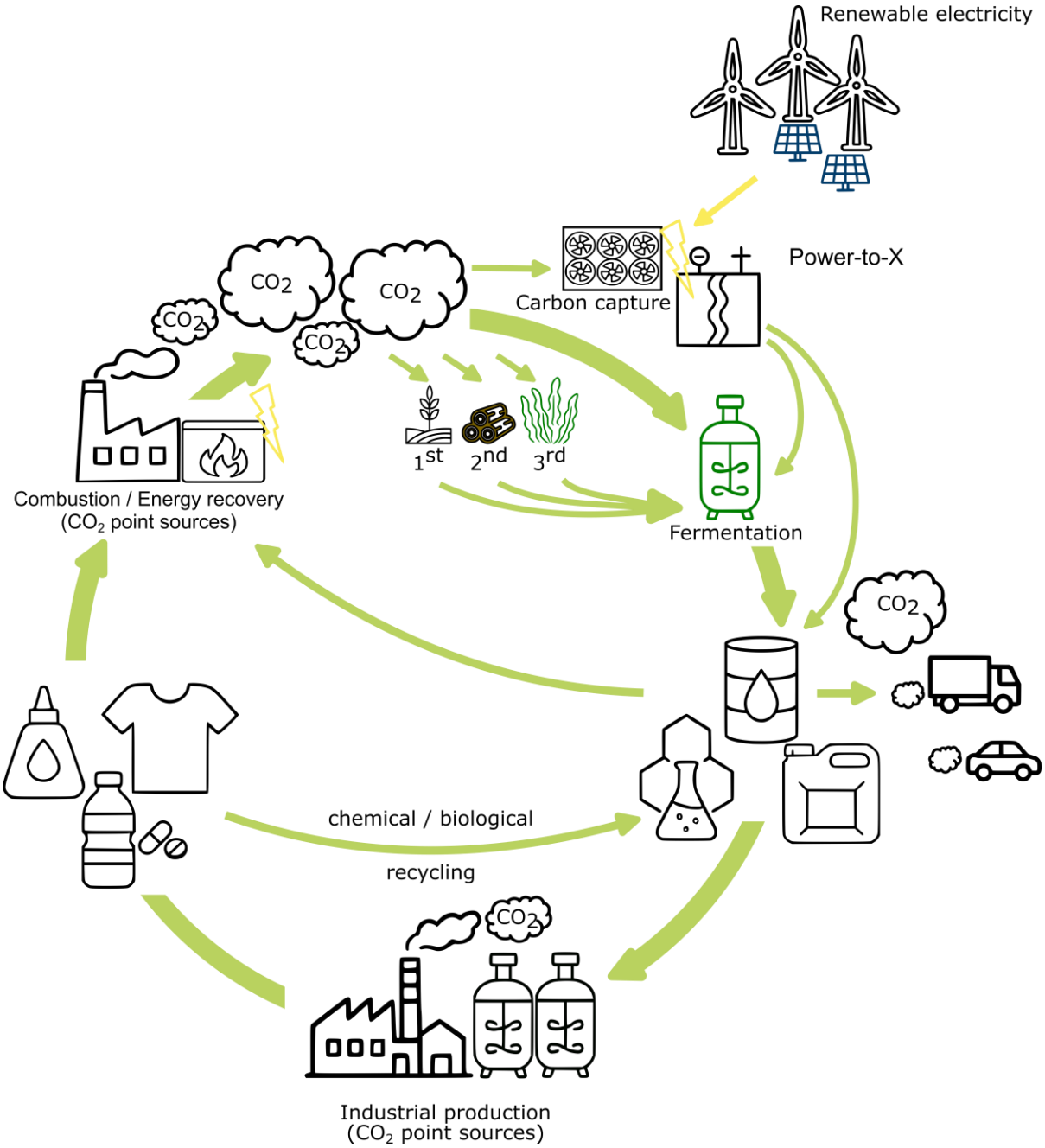

Figure 10 CO_2-based circular value chains integrating renewable carbon sources from biomass and carbon capture, combined with fermentation and recycling technologies. The scheme illustrates both photosynthetic CO_2 fixation into biomass feedstocks and physicochemical fixation via carbon capture, powered by renewable electricity (Power-to-X). The resulting energy-rich molecules are used for energy recovery (e.g., combustion for transport or heat) and for the production of value-added products in the (bio)chemical industry.

1.5 Upstream process development for bio-based production

1.5.1 *Corynebacterium glutamicum* as production host

During a screening project for the isolation of L-glutamate producing microogranisms, the soil bacterium *Corynebacterium glutamicum* (*C. glutamicum*) was discovered in 1957 by Kinoshita [100]. The Gram-positive, aerobic to facultative anaerobic, non-pathogenic bacterium belongs to the *Corynebacteriaceae* family. Typically for Gram-positive bacteria, *C. glutamicum* has a thick peptidoglycan layer on the outside of the cell membrane. This natural barrier can protect the cell from the entry of toxic substances, including antibiotics, and from mechanical stress, which makes it interesting for large-scale production [101, 102]. Since its discovery, *C. glutamicum* has been intensively analyzed. The 3.3 million base-pair long genome is fully sequenced and well-studied [103]. Today, *C. glutamicum* is widely used in industry, for example in the production of the amino acids L-glutamate and L-lysine on a scale of millions of tons (e.g. L-glutamate: 2,160,000 $t\,a^{-1}$ and L-lysine: 1,330,000 $t\,a^{-1}$) [102, 104, 105]. Beyond amino acid production the microbe has shown its potential in the production of organic acids, alcohols, carotenoids and polyphenols [106-109]. The organism is naturally able to utilize a variety of different carbon sources and can be cultivated to high cell densities. The carbon utilization capability includes sugars such as glucose or sucrose, organic acids such as acetate, pyruvate and lactate, and alcohols such as ethanol [102, 110, 111]. *C. glutamicum* is classified as GRAS ("generally regarded as safe") by the United States Food and Drug Administration (FDA). Furthermore, since *C. glutamicum* has proven itself in various industrial applications as a stress-tolerant production organism for a wide range of products, it could also be suitable for utilization and conversion of CCU derived ethanol with an industrial relevant perspective [110, 112-114].

When exploring the biotechnological use of second-generation lignocellulosic feedstocks that contain xylose, it is important to note that *C. glutamicum* can not naturally utilize xylose as a carbon source. Through targeted metabolic engineering, however, two distinct metabolic routes have been introduced to enable xylose assimilation.

The first option is the isomerase pathway, which operates in two steps. Xylose is initially converted to xylulose by a heterologous xylose isomerase, typically sourced from *Escherichia coli* or *Xanthomonas campestris*. The resulting xylulose is then phosphorylated by the

endogenous xylulokinase to form xylulose-5-phosphate, which subsequently enters central metabolism via the pentose phosphate pathway [115]. Application of the isomerase pathway has enabled *C. glutamicum* to produce a wide range of value-added products from xylose, including succinate, lysine, glutamate, ornithine, putrescine, 1,5-diaminopentane, and anthranilate [116-118].

The second option is the oxidative Weimberg pathway, which consists of five enzymatic steps: i) xylose is first oxidized by xylose dehydrogenase (XylB) to produce xylonolactone, ii) which is then hydrolyzed to xylonate either spontaneously or through the action of xylonolactonase (XylC), iii) through two successive dehydration reactions catalyzed by xylonate dehydratase (XylD) and 2-keto-3-deoxyxylonate dehydratase (XylX), iv) xylonate is further processed via 2-keto-3-deoxyxylonate to α-ketoglutarate semialdehyde, v) in the final step, α-ketoglutarate semialdehyde dehydrogenase (XylA) oxidizes the semialdehyde to AKG and directs the carbon flow into the TCA cycle [119].

The latter pathway has been identified in a variety of bacteria and archaea and is most thoroughly characterized in the freshwater bacterium *Caulobacter crescentus*, where the relevant genes are organized within the pentacistronic operon *xylXABCD* [120]. In comparison to the isomerase pathway, the Weimberg pathway presents several notable advantages for the microbial conversion of hemicellulose-derived xylose into valuable products. All steps proceed with favorable thermodynamics, the pathway maintains metabolic linearity without diversions into side routes, and ATP consumption is not required for phosphorylation or sugar activation [121]. Furthermore, especially for AKG production the full carbon skeleton is retained, since there is no loss of carbon as CO_2.

Functional implementation of the complete Weimberg pathway has been demonstrated in various hosts, including *Escherichia coli*, *Saccharomyces cerevisiae*, *Pseudomonas putida*, and *C. glutamicum* [122-125]. In *C. glutamicum*, the introduction of the heterologous *xylXABCD* operon from *C. crescentus* on a plasmid enabled the engineered strain to grow in defined medium with xylose as the sole carbon source, achieving a maximum specific growth rate of $0.07 \pm 0.01\ h^{-1}$ [125, 126]. Through subsequent codon optimization of the Weimberg genes and adaptive laboratory evolution, the evolved strain *C. glutamicum* WMB2evo exhibited an improved growth rate of $0.26 \pm 0.02\ h^{-1}$ when cultivated on xylose [126]. Genome analysis of

this variant revealed a deregulation of the *myo*-inositol/proton symporter gene *iolT1*, which was shown to facilitate xylose uptake in *C. glutamicum*. By rationally engineering the promoter region of *iolT1*, this deregulation could be deliberately reproduced, resulting in the strain *C. glutamicum* P_{O6}-*iolT1* pEKEx3-*xylXABCD*$_{opt}$, which displayed a specific growth rate of 0.24 ± 0.01 h^{-1} on xylose in defined medium [127].

1.5.2 Targeted metabolic engineering for AKG production

For the production of desired substances (e.g. drugs, fine chemicals or proteins) in microorganisms such as *C. glutamicum*, metabolic pathways can be specifically modified using directed genetic engineering methods. Depending on the identified target molecule, the metabolic pathway from the carbon source to the target product and the enzymes responsible for the respective reactions are analyzed [128]. Genetic tools allow the cloning, expression, disruption, and replacement of microbial genes (homologous and heterologous) and the investigation of metabolic pathways, which are relevant for product accumulation. Since *C. glutamicum* belongs to the Gram-positive bacteria, standard DNA transfer methods established for Gram-negative bacteria such as *Escherichia coli* are not generally applicable. For *C. glutamicum*, the most efficient transfer techniques include (electro-)transformation, transduction and conjugation [129, 130]. Interesting targets are the improvement of substrate uptake, the enhancement of key reactions, the control of carbon flow by eliminating reactions to by-products, and the improvement of export. For accumulation of native substances, such as metabolic intermediates like AKG, prevention of further reaction of the target molecule by deletion of specific genes is a common strategy. In *C. glutamicum*, targeted gene deletions are commonly achieved via two-step homologous recombination, for example using the pK19*mobsacB* system, which enables markerless chromosomal modifications (Figure 11A) [131].

1.5.3 Untargeted metabolic engineering by adaptive laboratory evolution

In addition to targeted strategies for metabolic engineering, for which knowledge of specific genes and their regulation is essential, there is a powerful tool for untargeted metabolic engineering called adaptive laboratory evolution (ALE). In addition, ALE enables multiple mutations and alteration of regulation for adaptation [132]. The ALE method is based on the evolutionary adaptation of microorganisms to changing environmental conditions (selection

pressure). Due to their rapid division rate and the resulting high number of generations, beneficial mutations can accumulate, leading to increased fitness (Figure 11B). ALE experiments are increasingly utilized to harness this adaptive potential for non-targeted strain optimization and, when combined with genome sequencing, provide valuable insights into genomic research [126, 133-136].

ALE experiments are typically performed in two different operational modes (repetitive batch or chemostat), at varying scales (laboratory or micro-scale), and with different levels of technical complexity (manual or automated). A comprehensive comparison of operational modes at the laboratory scale is provided by Dragosits et al. and Gresham et al. [134, 137]. In summary, it can be stated that continuous operation in chemostat or turbidostat enables a constant growth rate and cell density. The environmental conditions such as power input, pH value and oxygen availability can be well controlled. In addition, these approaches are less labor-intensive once they are in operation. One disadvantage of continuous operation, however, is the process costs. The setup for continuous process control is technically more complex and contamination is a common problem with long cultivation times. Therefore, due to its low cost and simple implementation, the repetitive batch ALE (rbALE) mode is widely used across various applications, regardless of scale or automation level [135]. The typical procedure of a rbALE is based on the over-inoculation of an aliquot of a growing culture (usually in a shake flask) into fresh medium. The transfer is performed after a defined time interval, which depends on the growth rate of the organism and can range from a few hours to several days or even weeks (Figure 11C) [134]. Typical mutations in ALE experiments include single nucleotide variations, such as insertion, substitutions or deletions in genes or promoter regions, as well as the amplification or deletion of entire genes. Such changes are often associated with altered protein expression or enzyme activity (Figure 11D). In contrast to continuous process control, the cell density (X), pH and dissolved oxygen (DO) vary in the batch and the manual work of the inoculation process is high [134]. Moreover, due to the fact that an operator is required, who is adapted to day-night rhythm, the cells may be transferred in different cell phases, which may result in fluctuation of metabolites.

Therefore automated and miniaturized rbALE approaches have been developed in recent years [126, 138, 139]. These approaches enable higher parallelization, precise control of selection conditions, improved reproducibility and reduce manual work to a minimum. By

combining microbioreactors and liquid handling systems, e.g. as for the Mini Pilot Plant technology, batch online data can be recorded for precise process control and the over-inoculation processes can be carried out in a targeted, reproducible, and automated manner (Figure 11E) [126].

However, one bottleneck that exists when using the Mini Pilot Plant technology is the limited number of possible batches. With a standard, moderately used 48 well FlowerPlate, a maximum of 48 consecutive batches are possible [126]. Resolving this limitation in the duration of the automated ALE application was part of this work.

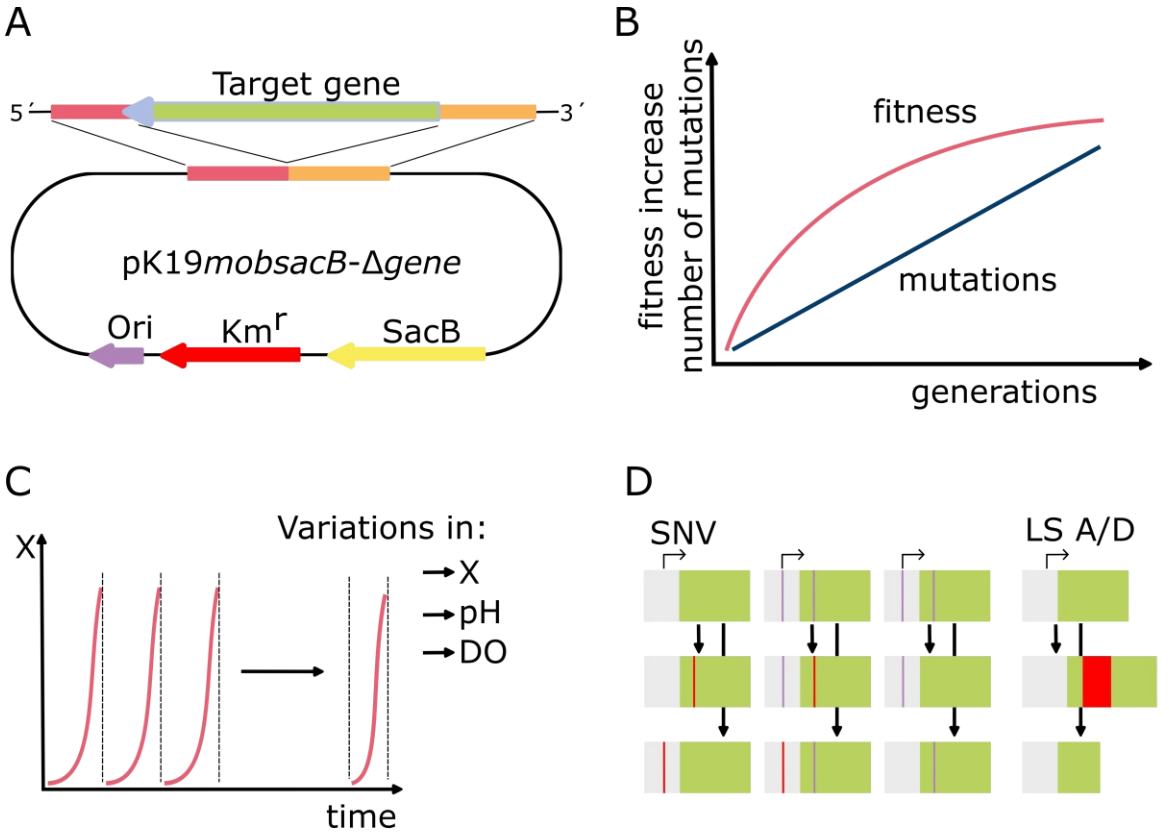

Figure 11 Overview of targeted and untargeted metabolic engineering concepts. (A) Targeted metabolic engineering. Schematic overview of a gene deletion strategy using pK19*mobsacB*. The plasmid carries only the flanking regions of the target gene. By homologous recombination, the target gene is deleted. **(B) Adaptive Laboratory Evolution (ALE)**. Illustration of the dependence of strain fitness and the number of mutations on the number of generations under selection pressure in an ALE experiment. With increasing number of generations the number of potential beneficial mutations for adaption and so the fitness increases. **(C) Repetitive batch ALE (rbALE) operation**. Observation of the cell density (X) in a rbALE experiment. The cultivation time of the rbALE is extended by several consecutive batches. The nutrient supply is not limited, but cell density, pH and dissolved oxygen (DO) can fluctuate. **(D) Types of mutations in ALE experiments**. Single nucleotide variants (SNV), e.g. insertion, substitution or deletion (in genes and promotors) and large scale (LS) amplifications and deletions of whole genes are typical mutations that occur during selection for increased fitness. **(E) Mini Pilot Plant technology**. The Mini Pilot Plant combines a liquid handling system and a microbioreactor. This combination enables, among other things, the miniaturized, parallelized and automated execution of state of the art rbALE in high throughput.

2. Objective of this thesis

2.1 Aim of this thesis

This thesis was conducted within the framework of the Bioeconomy Science Center project "BioPlastiCycle – Transitioning bioplastics to the circular economy". The overarching aim of this thesis was the development of a microbial production platform for AKG. To achieve this, the work integrates metabolic engineering, process development, DSP, and systems-level analyses to address key challenges in the sustainable biotechnological production of organic acids (Figure 12). The envisioned process aims to rely on renewable feedstocks, including sugar-based biomass, lignocellulosic hydrolysates, and ethanol.

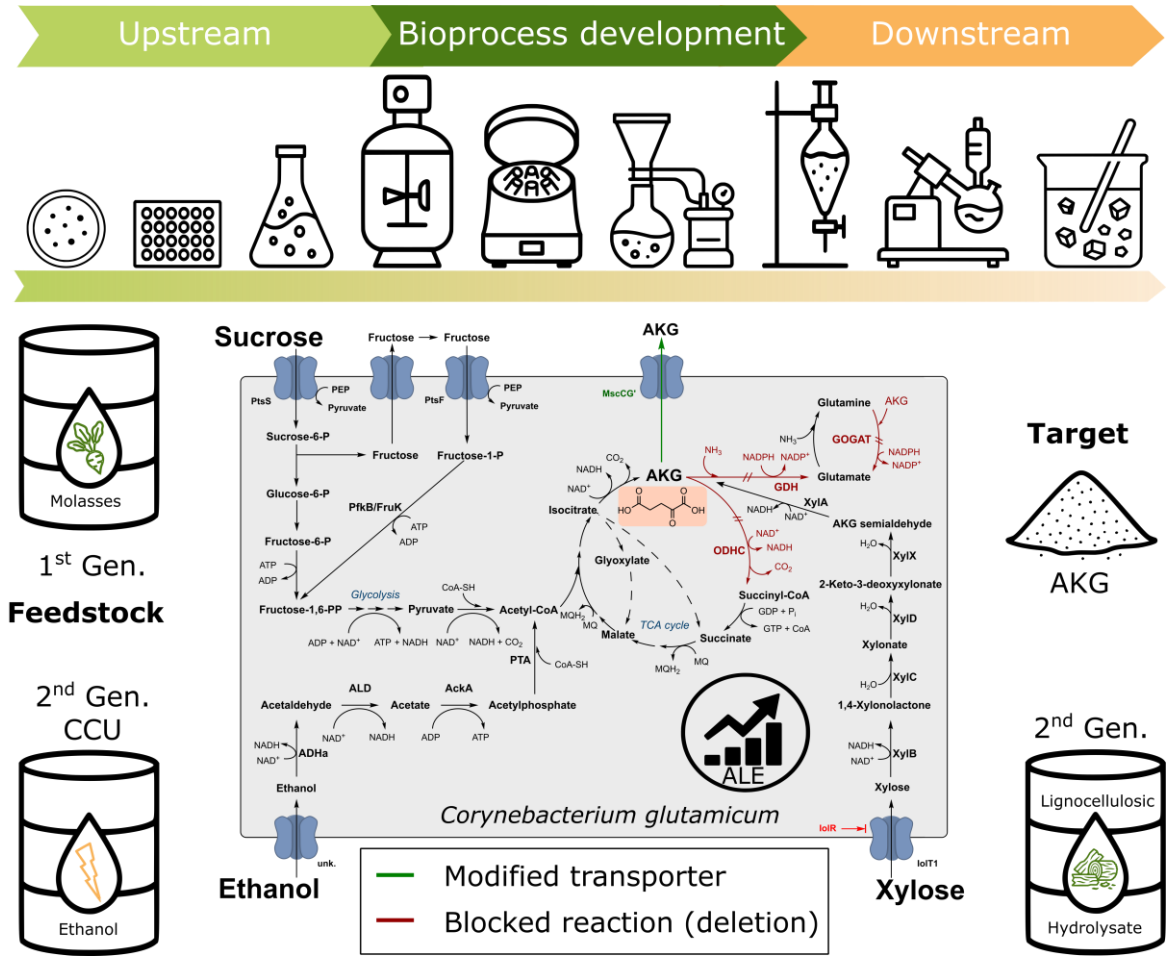

Figure 12 Graphical abstract illustrating the objective of this thesis. Development of a bioprocess for the microbial production of AKG using *C. glutamicum*. The process integrates upstream and downstream operations with renewable carbon sources, including first-generation feedstock such as molasses and ethanol. The latter serves as a model substrate representing potential CCU feedstocks. Strain improvement was achieved through targeted metabolic engineering and ALE. High-throughput cultivation systems enabled efficient screening of strains and substrates. Promising candidates were scaled up in stirred-tank bioreactors, followed by downstream processing involving centrifugation, filtration, liquid-liquid extraction, evaporation, and crystallization for product recovery.

2.2 Structure of this thesis

The experimental work presented in this thesis covers the development of a microbial production platform for AKG by combining metabolic engineering, ALE, scalable fermentation strategies, and downstream process development. The following structure outlines the key research components:

1. **Rational strain engineering**

   AKG accumulation in *C. glutamicum* was enhanced by targeted genetic modifications. These included deletion of native enzymatic reactions consuming AKG and the enhancement of its transport out of the cell (see Chapter 3.1).

2. **Automated strain screening and characterization**

   Engineered strains were cultivated in miniaturized and automated batch systems (Mini Pilot Plant) using different carbon sources (glucose, sucrose, and molasses). Online process analytics and automated sampling enabled high-throughput phenotypic comparison (Chapter 3.2).

3. **Proteome analysis**

   To gain insight into metabolic regulation and strain behavior on different carbon sources, proteomic analyses were conducted during microbial growth and product formation (Chapter 3.3).

4. **Process scale-up and fermentation in stirred-tank bioreactors**

   The most promising strain and medium combinations were scaled up to bench-scale fermenters for controlled fed-batch cultivation. The focus was placed on yield, productivity, and carbon source utilization (Chapter 3.4).

5. **Development of a downstream process**

   A tailored purification protocol involving liquid-liquid extraction, concentration, and crystallization was developed to isolate AKG from complex fermentation broths (Chapter 3.5).

6. **Lignocellulosic hydrolysates as a carbon source**

   The potential of lignocellulosic feedstocks as second-generation substrates was assessed. AKG production strains were engineered for xylose utilization and evaluated on different carbon sources (glucose, xylose, and lignocellulosic hydrolysates).

In addition, scale-up experiments and inhibitory tests were performed (Chapter 4.1 – 4.4).

7. **Ethanol as a carbon source**

   In parallel, the scope was extended to evaluate ethanol as a sustainable substrate derived from carbon capture. An automated long-term ALE workflow was developed and applied to evolve *C. glutamicum* for ethanol utilization. The resulting strain (WT_EtOH-Evo) was characterized in terms of physiology, genetics, and proteome (Chapter 5.1 – 5.6).

8. **AKG production from ethanol**

   The evolved ethanol strain was finally tested for its capacity to produce AKG using ethanol as sole carbon and energy source (Chapter 5.7).

3. Production of 2-oxoglutaric acid from 1st gen. biomass

This chapter centers on the biosynthesis of 2-oxoglutaric acid (AKG) from renewable biomass, with a particular focus on molasses as a substrate, and the subsequent downstream purification process. Metabolic engineering of the production strains was carried out by Daniela Höppner from the 'Synthetic Cell Factories' research group at IBG-1, Forschungszentrum Jülich. Strain characterization experiments were supported by Marvin Doser during the course of his master's thesis. Proteome samples were analyzed by Bianca Klein from the research group 'Quantitative Microbial Phenotyping' at IBG-1 Forschungszentrum Jülich.

The production strain and cultivation conditions identified during the screening phase were successfully transferred to a fed-batch process using molasses, which was then thoroughly analyzed at scale. The resulting AKG-containing fermentation broths served as the basis for the development and optimization of a suitable downstream processing strategy. The upconcentration of AKG in the solvent were supported by Heike Offermann from the 'Biocatalysis' research group at IBG-1 Forschungszentrum Jülich.

3.1 Targeted metabolic engineering for AKG production strains

In order to improve *C. glutamicum* specifically for the production of AKG, the already modified variant *C. glutamicum* P_{O6}-*iolT1* was used as a starting point [127]. This strain has two point mutations in the regulatory region of the *iolT1* promoter, which increases the expression of the *myo*-inositol/proton symporter IolT1. While IolT1 is primarily known to transport *myo*-inositol, it has also been shown to import various sugars such as glucose, fructose and xylose [127, 140-142].

To initiate AKG synthesis, the metabolic pathway of glutamate formation was specifically interrupted. For this purpose, the gene for glutamate dehydrogenase (*gdh*) was deleted, resulting in the strain *C. glutamicum* AKG-1. Glutamate dehydrogenase catalyzes the formation of glutamate by reductive amination of AKG under ammonia-rich conditions using NADPH as cofactor (cf. Figure 13).

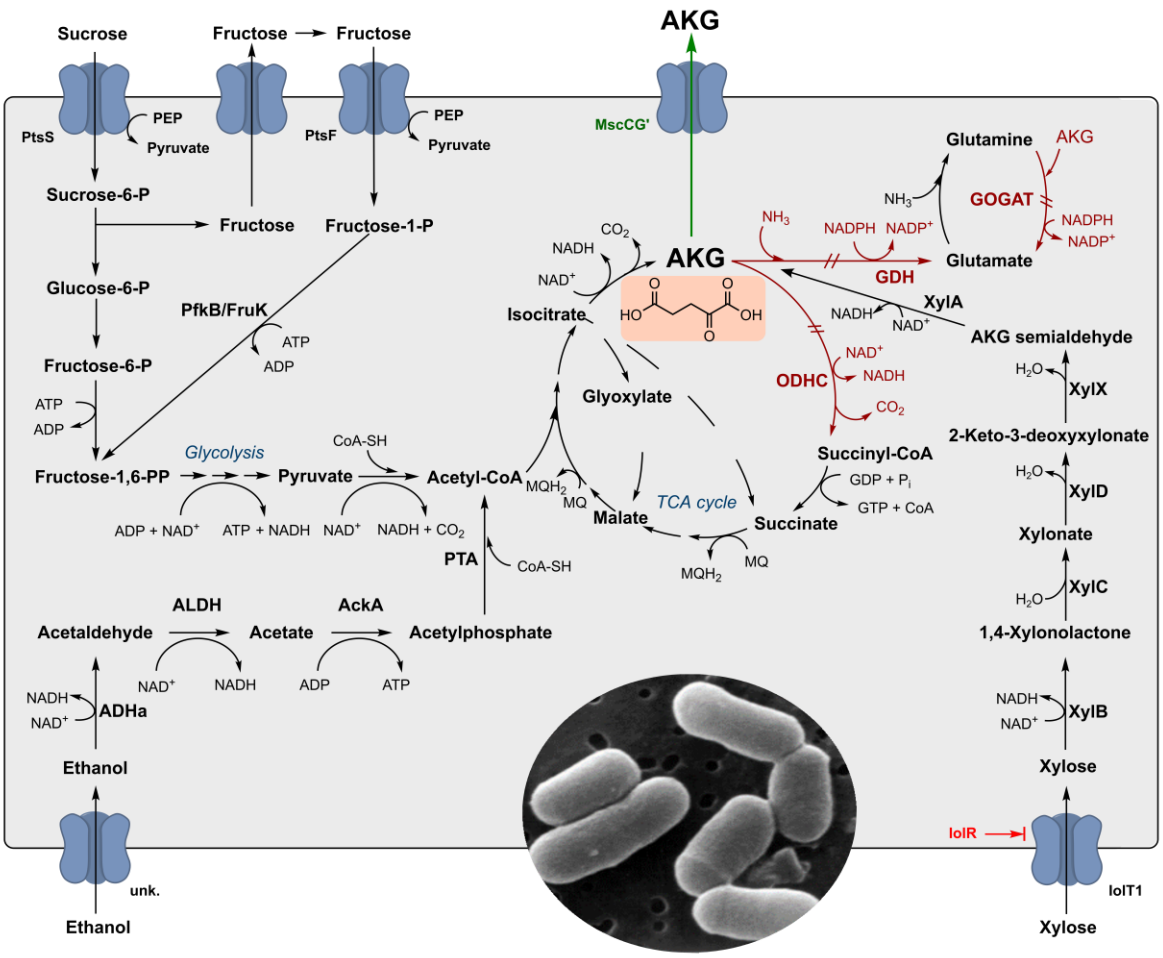

Figure 13 Schematic overview of the metabolic pathways in *C. glutamicum* for AKG production from sucrose-, xylose-, and ethanol-containing feedstocks. ADHa: alcohol dehydrogenase; ALDH: aldehyde dehydrogenase; AckA: acetate kinase, GDH: glutamate dehydrogenase; GOGAT: glutamine-2-oxoglutarate aminotransferase/ glutamate synthase; IolT1: *myo*-inositol/proton symporter; MscCG: mechanosensitive glutamate transporter; ODHC: 2-oxoglutarate dehydrogenase complex; PfkB/ FruK: 1-phosphofructokinase; PTA: phosphotrans-acetylase; PtsF: fructose-specific phosphotransferase system; PtsG: glucose-specific phosphotransferase system; PtsS: sucrose-specific phosphotransferase system; XylA: semialdehyde dehydrogenase; XylB: xylose dehydrogenase; XylC: xylonolactonase; XylD: xylonate dehydratase; XylX: 2-keto-3-deoxyxylonate dehydratase.

The next step focused on improving the AKG export. Several non-specific dicarboxylate transporters have already been identified in *C. glutamicum*, but no specific export mechanism for AKG is known to date [143]. The mechanosensitive glutamate transporter MscCG (Ncgl1221, also known as YggB) has been intensively studied over decades. Various conditions have been discovered that promote its glutamate secretion, including limiting biotin availability, the addition of β-lactam antibiotics and certain detergents [144]. It has also been shown that C-terminal truncations of the *mscCG* gene lead to increased glutamate release without the need for additional induction. Recent studies have also shown that MscCG partially transports 2-hydroxyglutarate, a derivative of AKG [145]. Therefore, in this thesis,

the *mscCG* gene was specifically truncated to test whether this modified transporter enables continuous export of AKG in the engineered *C. glutamicum* AKG-2 variant. In addition, to prevent further consumption of AKG by native pathways, the gene encoding the large subunit of GOGAT was deleted in AKG-2. In *C. glutamicum*, several transaminases use AKG as an amino acceptor thereby channeling it into glutamate biosynthesis [146]. For instance, glutamine 2-oxoglutarate aminotransferase (GOGAT) transfers an amino group from glutamine to AKG producing glutamate in concert with glutamine synthetase (GS) in the GS/GOGAT cycle. The GS/GOGAT system plays a minor role in glutamate formation under standard culture conditions, i.e. sufficient access to nitrogen, but it has been described to be activated in *C. gutamiucm* in response to deletion of *gdh* [147]. Therefore, the gene encoding the large subunit of GOGAT was deleted, resulting in strain AKG-3. Finally, the gene *odhA* was deleted, which encodes the OdhA subunit of the 2-oxoglutarate dehydrogenase complex (ODHC). This enzyme catalyzes the conversion of AKG to succinyl-CoA in the TCA cycle. The resulting strain AKG-4 therefore has an interrupted TCA cycle.

3.2 Miniaturized and parallelized strain characterization

3.2.1 AKG production from defined glucose

The designed AKG-producing strains were characterized on the Mini Pilot Plant for their performance in defined CGXII media using glucose as sole carbon and energy source (Figure 14). As expected, the base strain *C. glutamicum* P_{O6}-*iolT1* exhibited wild-type-like growth on glucose and did not accumulate AKG (Figure 14A). The introduction of the *gdh* deletion (AKG-1) resulted in a reduced growth performance. However, AKG accumulated in the supernatant of glucose-grown cells, reaching a concentration of 1.92 mM. The additional truncation of MscCG (AKG-2) further impaired growth performance. At the same time, the AKG titer and yield increased by 67 %. The subsequent deletion of *gltB* (AKG-3) continued this trend, i.e. further reduction in growth performance and increase in the AKG concentration to 3.5 mM. Finally, the strain AKG-4, in which the TCA cycle was interrupted by the deletion of *odhA*, failed to grow under glucose conditions. The AKG concentration decreased to 1.5 mM, indicating only basal metabolic activity.

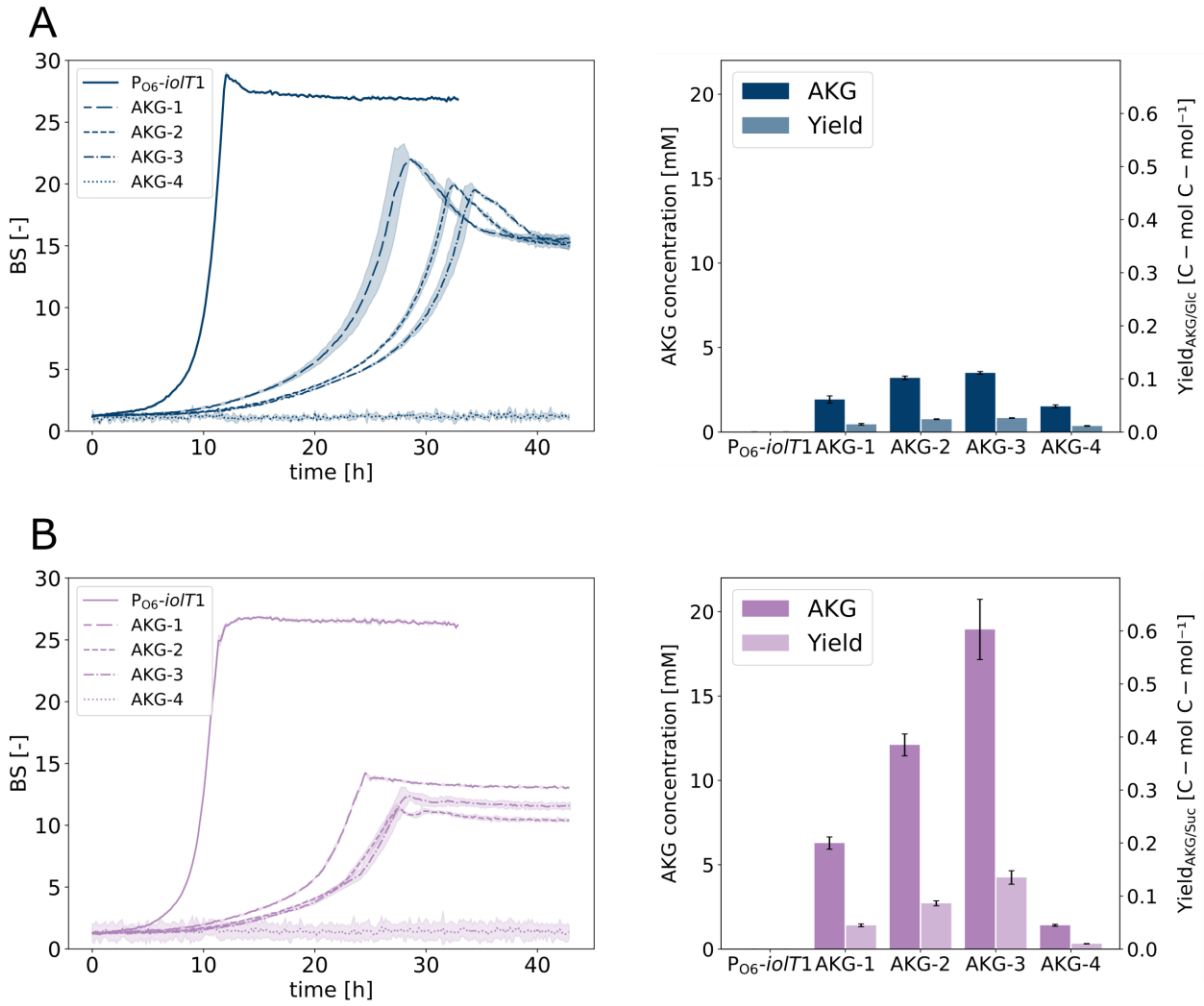

Figure 14 Growth behavior and AKG production performance of engineered *C. glutamicum* strains cultivated in defined CGXII medium. **(A)** Cultivation using glucose (20 g L^{-1}) as the sole carbon and energy source. **(B)** Cultivation using sucrose (20 g L^{-1}) as the sole carbon and energy source. All strains were grown in a microbioreactor system (BioLector) using 48-well FlowerPlates with a working volume of 1 mL per well. The shaking speed was set to 1,400 rpm with a backscatter (BS) gain of 3. Biomass formation was monitored online via BS signal , and AKG concentrations were determined from endpoint samples via HPLC measurement. Data represent mean values ± standard deviation from biological triplicates.

3.2.2 AKG production from defined sucrose

It is important to note that the deregulated promoter P_{O6}-*iolT1* of the *myo*-inositol permease is not expected to enhance sucrose uptake and is therefore not required for AKG production from this carbon source. However, to ensure comparability between the tested carbon sources and to eliminate other potential influencing factors, identical strains were used, and the main cultures were inoculated in parallel from the same preculture.

In defined sucrose medium, the base strain *C. glutamicum* P_{O6}-*iolT1* exhibited a growth phenotype similar to that observed on glucose, with no detectable AKG accumulation

(Figure 14B). In contrast, the modified strains AKG-1 to AKG-3 produced significantly higher AKG concentrations, ranging from 6.3 to 22.0 mM. As expected, this increase in AKG titers was accompanied by a proportional decrease in final biomass, which was reduced by 16.1 to 24.7 % compared to glucose-grown cultures. In line with the characterization on glucose, *C. glutamicum* AKG-4, which lacks ODHC activity, was unable to grow on sucrose, and its AKG production remained low at 1.4 mM (cf. Figure 14B).

The observed differences in carbon flux between biomass formation and AKG production can be attributed to the specific utilization pathway of sucrose. Inside the cell, sucrose is transported via the sucrose-specific phosphotransferase system (PtsS) and simultaneously phosphorylated to sucrose-6-phosphate (Chapter 3.1, cf. Figure 13) [148]. This intermediate spontaneously hydrolyzes into glucose-6-phosphate and fructose. While glucose-6-phosphate is directly funneled into glycolysis, fructose requires export and re-import through PtsF before being activated via phosphorylation to fructose-1-phosphate. Subsequently, fructose-1-phosphate enters glycolysis after ATP-dependent phosphorylation to fructose-1,6-bisphosphate by 1-phosphofructokinase (PfkB/FruK). Since the oxidative pentose phosphate pathway (oxPPP) is initiated by glucose-6-phosphate, its activity is considerably lower when cells are grown on fructose [148]. Furthermore, fructose-6-phosphate and glyceraldehyde-3-phosphate are necessary for the operation of the reductive PPP in reverse via transketolase. Krahn et al. determined the significantly reduced oxPPP flux on fructose with ∼10 % compared to glucose with ∼60 % [148]. However, the availability of fructose-6-phosphate may be further constrained by the activity of fructose-1,6-bisphosphatase, a gluconeogenic enzyme upregulated under fructose conditions [149]. As a result, metabolic pathways supplying NADPH, erythrose-4-phosphate, and ribose-5-phosphate are diminished, leading to reduced biomass formation. On the other hand, the conversion of fructose to fructose-1,6-bisphosphate enhances carbon flux through lower glycolysis and into the oxidative TCA cycle, thereby promoting AKG accumulation.

3.2.3 AKG production from complex sugar beet side stream molasses

The molasses-based feedstock used in this study has a sucrose content exceeding 60 % and provides multiple nitrogen sources (Chapter 1.4.1, Figure 9A) and trace elements (Table S1). Due to these characteristics, it serves as a suitable substrate for *C. glutamicum*. Furthermore,

the phenotypic analysis on defined sucrose media confirmed the potential of sucrose in molasses for efficient AKG production. Interestingly, unlike on defined media, the reference strain *C. glutamicum* P_{O6}-*iolT1* and the engineered producer strains AKG-1 – AKG-3 exhibited comparable growth when cultivated on molasses (Figure 15). Moreover, AKG production was significantly lower than on pure sucrose, with the highest concentration observed in strain AKG-3 reaching only 3.9 mM. This suggests that the available carbon and essential nutrients in molasses were preferentially allocated toward biomass formation rather than product synthesis.

In contrast, the highly engineered strain AKG-4, which was incapable of growing on defined glucose or sucrose media, also displayed limited growth on molasses. Unexpectedly, AKG accumulation reached 82.7 ± 1.2 mM, with a yield of $Y_{P/S} = 0.59\ C_{mol}\ C_{mol}^{-1}$, representing a more than 325 % increase compared to the highest AKG production observed on sucrose-based media. The genetic alterations in AKG-4 (Δ*gdh*, Δ*gltB*, Δ*odhA*) affect ammonium assimilation and metabolic fluxes through the TCA cycle. It is conceivable that alternative nitrogen sources present in molasses (e.g., amino acids, NO_3^-) compensated for these deficiencies.

Since for all AKG-strains a glutamate limitation or even an auxotrophy was expected, all experiments were additionally carried out with supplementation of glutamate to the cultivation media. Surprisingly, no compensation of the growth deficit could be observed (Figure S1).

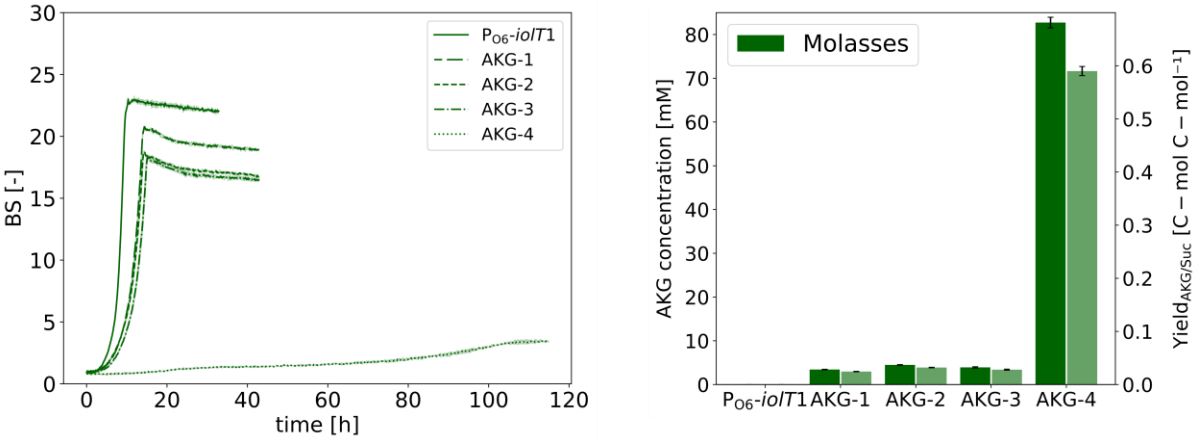

Figure 15 Batch cultivation and AKG production of engineered *C. glutamicum* strains in molasses-based medium. Strains were cultivated in biological triplicates using a BioLector microbioreactor system with 48-well FlowerPlates. Each well contained 1 mL of CGXII medium supplemented with molasses, corresponding to a sucrose concentration of 20 g L^{-1}. Cultivations were conducted at 1,400 rpm with a backscatter (BS) gain of 3 for online biomass monitoring. Final AKG concentrations were determined from endpoint samples. Data are presented as mean values ± standard deviation from triplicate experiments.

3.3 Proteomics reveals regulation of metabolic pathways on molasses

3.3.1 Proteome comparison between sucrose and glucose

To gain deeper insights into the effects of the applied metabolic engineering steps, the strains P_{O6}-*iolT1* and AKG-3 were analyzed by untargeted proteomics on all three different carbon sources. The growth phenotyping of AKG-3 on sucrose and glucose (Chapter 3.2.2) has shown that growth on both conditions is similar, but that the biomass and AKG formed differ significantly (four times higher AKG titer on sucrose condition). A direct proteome comparison of the production strain AKG-3 grown on sucrose with AKG-3 grown on glucose revealed 32 differentially expressed proteins (Table 1).

As expected, the four most strongly up-regulated proteins are the sugar-specific PTS system (PtsF), the sucrose-specific enzyme II component (PtsS), L-lactate dehydrogenase (LdhA), and 1-phosphofructokinase (PfkB). This pattern reflects the shift in carbon source and the corresponding regulatory adjustment in response to sucrose as carbon source and is in accordance with literature and my expectations. Notably, there is a decreased expression of the glyoxylate shunt genes encoding malate synthase (AceB) and isocitrate lyase (AceA), indicating down-regulation of the glyoxylate shunt under sucrose conditions [150]. This is accompanied by a further down-regulation of SdhCD, suggesting a lower flux from succinate to fumarate within the following part of the TCA cycle. In contrast, the expression of pyruvate

carboxylase (PCx), which is essential as an anaplerotic enzyme for growth on lactate but not on glucose or acetate as carbon sources [151], is significantly up-regulated on sucrose.

Taken together, these results support the predicted carbon source differences in carbon flux between sucrose and glucose metabolism. The stronger routing of the fructose moiety of sucrose into the TCA cycle [148], combined with the redirection of glucose metabolism through the glyoxylate shunt, offers a clear mechanistic explanation for the up to fourfold higher accumulation of AKG observed under sucrose conditions.

Table 1 Proteomic comparison of AKG-3 on defined media. Significantly regulated proteins in the direct comparison of *C. glutamicum* AKG-3 grown on sucrose versus glucose. Proteins specifically involved in sucrose metabolism are strongly upregulated when grown on sucrose. The protein ratios are represented by the fold changes (FC).

Protein	FC	Gene	Locus	Regulated by
Sugar specific PTS system	4.42	*ptsF*	cg2120	FruR, GlxR, LldR, SigA, SugR
Enzyme II sucrose protein	3.53	*ptsS*	cg2925	GntR1, GntR2, RamB, SigA, SugR
L-lactate dehydrogenase	3.33	*ldh*	cg3219	GlxR, LldR, RamA, SigA, SugR
1-phosphofructokinase	2.7	*pfkB*	cg2119	FruR, GlxR, LldR, SigA, SugR
Rhodanese-related sulfurtransferase	2.45	*sseA2*	cg1613	-
Permease	2.43	-	cg0683	-
Putative secreted protein	2.26	-	cg1604	-
Methylcitrate synthase	2.25	*prpC2*	cg0762	GlxR, PrpR, RamA, SigA
Probable methylisocitric acid lyase	2.22	*prpB2*	cg0760	GlxR, PrpR, RamA, SigA
Penicillin tolerance protein	2.09	*lytB*	cg1164	-
Predicted Fe-S-cluster redox enzyme	2.04	-	cg2214	SigH
Pyruvate carboxylase	2.02	*pyc*	cg0791	GlxR, RamB, SigA
Succinate dehydrogenase CD	0.48	*sdhCD*	cg0445	DtxR, GlxR, RamA, RamB, RipA, SigA
ABC-type cobalamin/Fe3+-siderophores transport system, ATPase component	0.48	-	cg0928	DtxR
Putative molybdopterin converting factor	0.45	-	cg0264	-
Malic enzyme	0.45	*mez*	cg3335	AmtR, MalR, RamA, RamB, SigA
DTXR/Iron regulated lipoprotein precursor	0.45	*irp1*	cg0771	DtxR, SigA
Thiamine biosynthesis protein	0.44	*thiC*	cg1476	-

Malate synthase	0.44	*aceB*	cg2559	CspA2, GlxR, RamA, RamB, SigA
Mg/Co/Ni transporter MgtE (contains CBS domain)	0.43	*mgtE1*	cg1276	-
Alkanal monooxygenase alpha chain	0.43	-	cg3085	DtxR, RosR
Isocitrate lyase	0.41	*aceA*	cg2560	GlxR, RamA, RamB, SigA
Catechol-1,2-dioxygenase	0.41	*catA1*	cg2636	BenR, GlxR, RipA
Putative carboxymuconolactone decarboxylase subunit	0.41	-	cg3212	-
ABC-type cobalamin/Fe3+-siderophores transport system, secreted component	0.4	-	cg3404	DtxR
Flavin-containing monooxygenase (FMO)	0.4	-	cg3195	GlxR, IpsA
Zn-dependent alcohol dehydrogenase	0.34	*adhA*	cg3107	AtlR, GlxR, RamA, RamB, SigA
Aldehyde dehydrogenase	0.34	-	cg3096	GlxR, RamA, RamB, SigA
Imidazolglycerol-phosphate synthase / Amidotransferase	0.32	*hisH*	cg2300	-
ABC-type cobalamin/Fe3+-siderophores transport sys	0.31	-	cg0924	DtxR
Superfamily II DNA/RNA helicases, SNF2 family	0.31	-	cg1316	-
Protecatechuate dioxygenase beta subunit	0.29	*pcaH*	cg2631	GlxR, PcaO, PcaR

3.3.2 Proteome comparison between molasses and sucrose

The characterization of strains in Chapter 3.2 revealed that the genetic engineering interventions had a growth-delaying effect under defined glucose and sucrose conditions, with strain AKG-4 exhibiting a complete growth arrest. In contrast, when cultivated on molasses, strains AKG-1 – AKG-3 showed only minor growth delays compared to the defined media. Direct proteome comparisons of AKG-3 between molasses and sucrose identified 48 significantly regulated proteins (Table S3).

Out of this 48 proteins 17 were upregulated on molasses. The most strongly upregulated proteins included alcohol dehydrogenase (AdhE), a putative lactate dehydrogenase (LldA), glyceraldehyde-3-phosphate dehydrogenase (GAPDH), sulfite reductase (CysI), aldehyde dehydrogenase (MsmA), and the nitrate reductase subunit NarG. These enzymes reflect metabolic activity related to the constituents of molasses such as alcohols, lactate, sulfate,

and nitrate [152-155]. Notably, seven out of these ten upregulated proteins are oxidoreductases that generate reducing equivalents like NADH, NADPH, or MQH2, indicating an increased cellular energy supply.

3.3.3 Proteome response to metabolic engineering

A direct comparison between AKG-3 and P_{O6}-*iolT1* revealed 153 significantly altered proteins on glucose, 93 on sucrose, and 72 on molasses. A detailed overview of all significantly regulated proteins can be found in the Appendix (Table S4 – S6). In order to further limit this large number of proteins to a metabolic engineering specific response independent of the carbon source, intersection operations were performed (Figure 16).

By intersecting the three datasets (glucose, sucrose, molasses), 23 proteins (Table 2) were identified which can be classified as a specific response to the genetic modifications in AKG-3 (*Δgdh*, *ΔgltB*, and *mscCG* truncation). Among these proteins, the most strongly upregulated are the nitrogen regulatory protein PII (GlnK) and glutamine synthetase (GS). This corresponds to the expectation of impaired nitrogen assimilation as GInK plays an essential role in nitrogen control [156]. In addition, AKG-3 compensates for the loss of GDH by switching to GS for ammonia fixation, a pathway that consumes ATP instead of NADPH, and that is normally activated when ammonia concentrations are lower than 0.1 mM [157]. Since GOGAT is not present, the subsequent conversion of glutamine to glutamate requires alternative NADPH-dependent routes. Compared to the canonical GS/GOGAT cycle, this would result in even higher energy expenditure, reducing the overall efficiency of ammonia assimilation and leading to poor growth.

Considering the increased energy availability observed as a consequence of the regulatory differences identified in the comparison between molasses and sucrose (Chapter 3.3.2), this may provide an explanation for the improved growth on molasses.

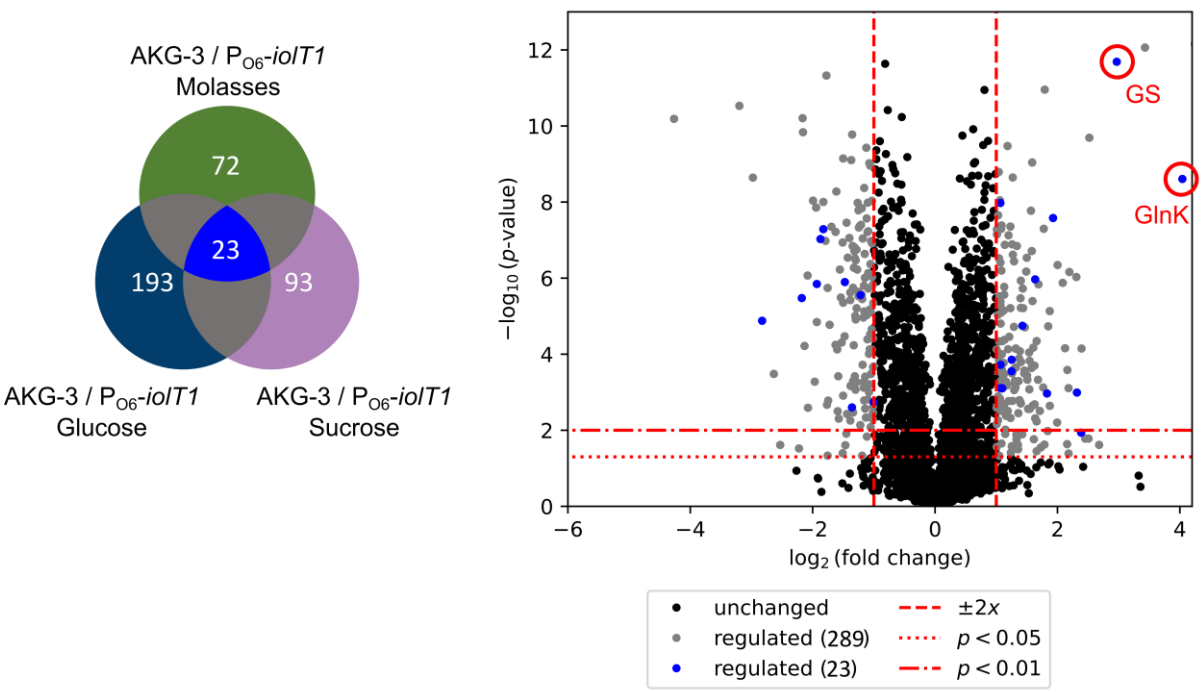

Figure 16 Proteomic analysis of engineered *C. glutamicum* strains. Comparison between the engineered and wild-type strains across the three carbon sources glucose, sucrose, and molasses. The intersection of significantly changed proteins revealed 23 common proteins.

In general, the analysis revealed that a considerable fraction of the regulated proteins responding to both the variation of carbon source and the applied metabolic engineering are under the control of the global regulator GlxR. This observation highlights the central role of GlxR in coordinating carbon metabolism in *C. glutamicum* [158].

However, the fundamental question remains how *C. glutamicum* AKG-3 is able to synthesize L-glutamate de novo after deletion of both *gdh* and *gltB*, given that no alternative pathway is currently known that utilizes either inorganic nitrogen or glutamine-derived amide groups for the amination of AKG. Addressing this question will require further detailed metabolic studies potentially involving metabolic flux analyses and the construction of additional deletion mutants to clarify the mechanisms underlying glutamate biosynthesis in these highly engineered strains.

Table 2 Proteomic response to genetic engineering. Significantly regulated proteins in response to metabolic engineering *in C. glutamicum* strain AKG 3 (Δ*gdh*, Δ*gltB*, truncated msCCG-channel) compared to the parental strain P_{O6}-*iolT1*. Differential proteomic analyses were conducted across three carbon sources (glucose, sucrose, and molasses). The overlap of significantly regulated proteins under all three conditions resulted in a set of 23 proteins, which are interpreted as a specific response to the applied genetic modifications.

Protein	FC_glc	FC_suc	FC_mol	Gene	Locus	Regulated by
Nitrogen regulatory protein PII	16.46	18.94	13.91	*glnK*	cg2260	AmtR, GlxR
Glutamine synthetase I	7.83	10.78	6.88	*glnA*	cg2429	AmtR, GlxR, SigA
Starvation-induced DNA protecting protein	5.23	4.95	3.16	*dps*	cg3327	DtxR, OxyR
Uncharacterized enzyme involved in biosynthesis of extracellular polysaccharides	4.99	2.41	2.1	-	cg2962	-
Aconitase	3.81	4.49	3.46	*acn*	cg1737	AcnR, GlxR, RamA, RipA, SigA
Ferritin-like protein	3.55	2.41	3	*ftn*	cg2782	DtxR, OxyR, SigA
Aldehyde dehydrogenase	3.11	0.39	0.11	-	cg3096	GlxR, RamA, RamB, SigA
Tetrahydrodipicolinate succinylase	2.69	2.11	2.96	*dapD*	cg1256	AmtR, SigA
Cyclomaltodextrinase	2.38	2.13	2.11	-	cg1012	SigA
Succinate dehydrogenase CD	2.38	2.52	2.19	*sdhCD*	cg0445	DtxR, GlxR, RamA, RamB, RipA, SigA
ABC-type cobalamin/Fe^{3+}-siderophores transport system protein	2.14	0.5	0.47	-	cg0924	DtxR
Phosphoenolpyruvate carboxylase	2.1	2.27	2.06	*ppc*	cg1787	GlxR, SigA, SigB
CTP synthetase	2.1	2.41	2.77	*pyrG*	cg1606	-
Transcriptional regulator, TetR family	2.1	2.63	2.61	-	cg1738	AcnR, GlxR, RamA, RipA, SigA
Putative integral membrane protein	0.5	0.35	0.28	-	cg0952	RamA, RamB
3-isopropylmalate dehydratase (large subunit)	0.43	0.45	0.4	*leuC*	cg1487	LtbR, RipA, SigA
NADP-specific glutamate dehydrogenase	0.39	0.45	0.24	*gdh*	cg2280	AmtR, ArgR, FarR, GlxR, SigA
Ribosomal protein L36	0.36	0.45	0.48	-	cg2791	-
3-isopropylmalate dehydratase (small subunit)	0.28	0.39	0.43	*leuD*	cg1488	LtbR, RipA, SigA
Cold-shock protein CspA	0.27	0.44	0.35	*cspA*	cg0215	-
Conserved hypothetical protein	0.26	0.4	0.37		cg0895	-
Universal stress protein UspA or related nucleotide-binding protein	0.22	0.24	0.26	*uspA2*	cg1595	GlxR
Rhodanese-related sulfurtransferase	0.14	0.5	0.48	*sseA2*	cg1613	-

3.4 Scale-up of the molasses AKG-4 process in 1 L STR

To validate the strain characterization results obtained in the microbioreactor and to investigate the potential for high-yield AKG production, a scale-up was conducted. The transition from the shaken micro-liter scale to the stirred 1-liter scale was primarily guided by the oxygen transfer rate (OTR) and specific power input. These parameters were chosen to ensure complete mixing and sufficient oxygen availability throughout the cultivation process. These two factors are critical for aerobic organisms such as *C. glutamicum*. By maintaining comparable OTR conditions between the BioLector and the laboratory-scale stirred-tank reactor (STR), physiological consistency in growth and production performance was targeted. This approach also enabled a more accurate assessment of the strain's suitability under industrially relevant conditions.

For this aim, the top-performing strain AKG-4 was cultivated in a 1 L laboratory-scale STR bioreactor under fed-batch conditions, using molasses exclusively as the carbon and energy source throughout the process. During the initial batch phase, the supplied 40 g L^{-1} of molasses was converted into 2.5 g L^{-1} of biomass and 131 mM (19.1 g L^{-1}) of AKG (Figure 17A). The relatively slow biomass formation, coupled with high growth-associated AKG production, was consistent with the results observed in microbioreactor experiments for this engineered strain (cf. Figure 15).

Approximately 80 hours into cultivation, the DO level began to rise, indicating depletion of available carbon sources from molasses. Unlike the sharp, rapid DO spikes (up to 90 – 100 %) typically seen within minutes in defined glucose media, DO increased gradually over 15 hours, reaching around 80 % (Figure 17B). This suggests that the cells remained metabolically active, further supported by the fact that sucrose had not yet been completely consumed at the time of the DO peak. This could indicate limitation by a secondary substrate or nutrient (e.g. nitrogen or phosphate), where cells remain metabolically active but are unable to sustain growth and production at the previous rate.

Upon initiating feed addition, the DO level dropped immediately, accompanied by renewed cell growth and continued AKG accumulation. The initial accumulation of sucrose points to moderate overfeeding at the beginning of the feeding phase, until the culture transitioned

back into substrate-limited conditions approximately 42 hours later. Notably, the DO peak observed during this phase was steeper than that at the end of the batch phase, likely due to the increased cell density and consequently higher oxygen demand. Following this sudden rise, DO levels quickly decreased again, indicating ongoing metabolic activity in the absence of further substrate supply. At the start of the second feeding phase, DO once more dropped sharply below 30 %, and cell growth along with AKG production resumed over the next 20 hours, mirroring the pattern of the first feeding phase.

In total, 659 mmol (96.2 g) of AKG was produced in a single reactor, corresponding to a carbon yield of 0.63 $C_{mol}\,C_{mol}^{-1}$ (0.64 $g\,g^{-1}$). The resulting space-time yield was 2.7 $mmol\,L^{-1}\,h^{-1}$. When compared to previously reported processes utilizing *E. coli*, which achieved a maximum space-time yield of 3.7 $mmol\,L^{-1}\,h^{-1}$ and a product yield of 0.32 $g\,g^{-1}$ [159], productivity with strain AKG-4 was 27 % lower; however, the product yield was doubled. To the best of my knowledge, this represents the highest AKG titer and yield reported for *C. glutamicum*, and marks the first documented production of AKG from the waste stream molasses.

Further improvement of the process could be achieved by increasing the inoculum density, potentially accelerating substrate conversion at a nearly constant specific production rate of 1.2 $mmol\,g_{CDW}^{-1}\,h^{-1}$. Given the inherently slow cell growth, this approach appears promising for enhancing the current space-time yield of 2.7 $mmol\,L^{-1}\,h^{-1}$. Additionally, the batch phase could be shortened by approximately 25 hours, as only 2.1 g of sucrose was consumed between 70 and 95 hours, indicating minimal substrate uptake during that period.

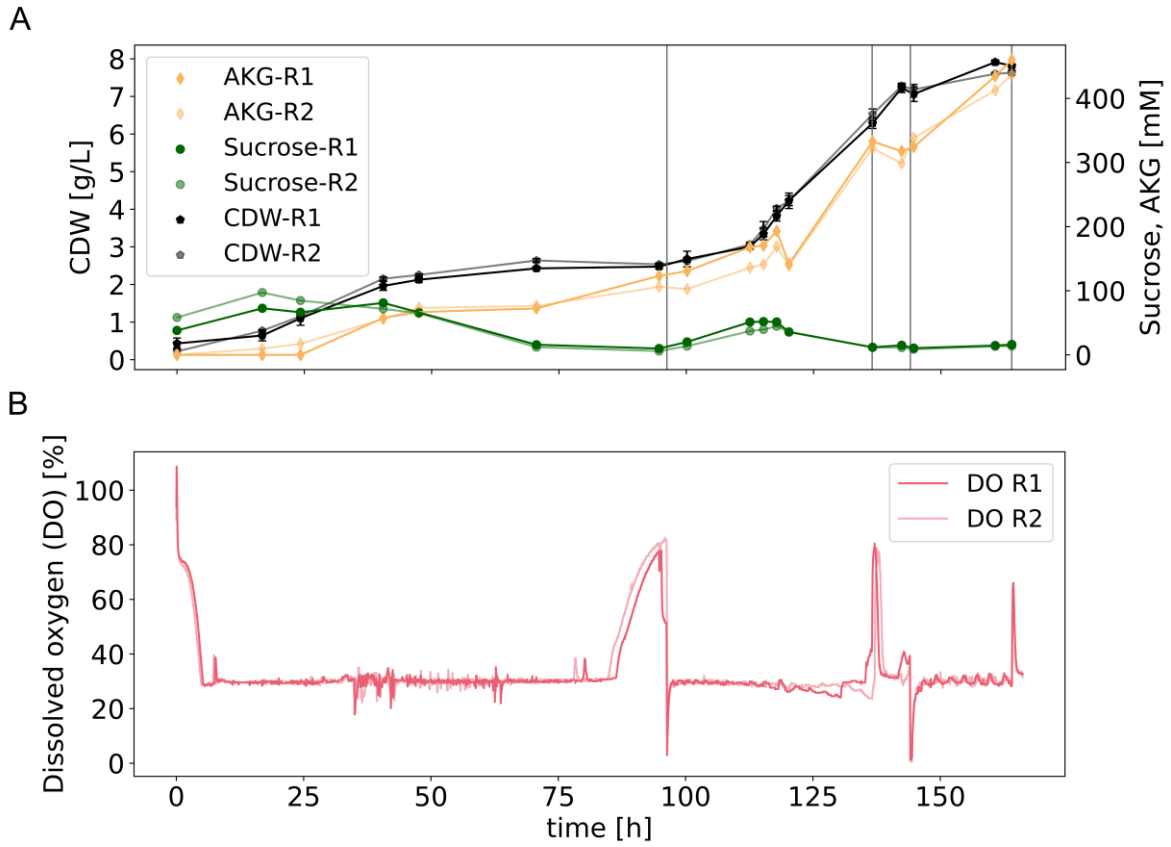

Figure 17 Fed-batch bioreactor cultivation of *C. glutamicum* P_{06}-*iolT1* Δ*gdh* Δ*gltB* Δ*odhA* mscCG' (AKG-4). Cells were grown in two parallel 1 L bioreactors (R1, R2) using CGXII medium with molasses as the carbon source. The initial sucrose concentration at the start of cultivation was 40 g L^{-1}. The feed solution consisted of molasses with a sucrose concentration of 300 g L^{-1} and did not contain additional CGXII salts.

3.5 Purification of 2-oxogluataric acid from fermentation broth

To recover AKG from the molasses-based fermentation broth, a liquid-liquid extraction (LLE) process utilizing ethyl acetate was developed as described in Chapter 1.5.1 (Figure 18A). The fermentation broth was initially subjected to solid-liquid separation via centrifugation, followed by microfiltration to remove cells and suspended particles. The clarified supernatant was then acidified to approximately pH 1 using hydrochloric acid, effectively shifting the equilibrium below the second pKa of AKG (2.47). This protonation of over 97 % of AKG's dicarboxylic acid groups significantly increased its partitioning into the organic phase. In the extraction step, ethyl acetate was added to the acidified aqueous phase at solvent-to-raffinate ratios up to 5:1. The mixture was vigorously agitated in a separatory funnel to enhance mass transfer. Upon phase separation, a triphasic system was observed, with a viscous interfacial layer discarded. The aqueous phase underwent two additional extraction cycles with fresh solvent to maximize recovery. The pooled organic phases containing

solubilized AKG were concentrated via rotary evaporation, and the recovered solvent condensed and recycled, contributing to process sustainability. Final AKG crystallization was induced by cooling the concentrated extract to 4 °C. Systematic variation of extraction parameters demonstrated that multiple extractions with fresh solvent significantly enhanced overall recovery efficiency (Figure 18B). The optimized protocol achieved an extraction efficiency of 87.1 %, corresponding to an overall process yield of 0.55 $C_{mol}\,C_{mol}^{-1}$ (0.56 g g^{-1}) based on the initial sucrose content in molasses. GC-ToF-MS analysis of the crystallized product revealed an AKG purity of 93.2 % (Figure 18C), with residual impurities primarily succinate and glycerol, alongside a few unidentified minor compounds. This LLE method offers a relatively straightforward and scalable approach for AKG purification from *C. glutamicum* AKG-4 fed-batch cultures.

However, higher purity requirements for specific applications may necessitate further refinements. For example, selective removal of succinate (∼2.7 %) via back-extraction is feasible by adjusting the pH to ∼3 and remixing the organic phase with water. Given the lower pKa values of AKG (2.47 and 4.68) compared to succinate (4.16 and 5.61), AKG preferentially re-partitions into the aqueous phase, while succinate and other neutral or hydrophobic impurities remain in the organic phase. This strategy can enhance product purity but carries risks of yield losses and increased solvent consumption, which may affect process economics and environmental footprint.

A notable limitation of the current batch extraction process is the high solvent demand, requiring approximately eight volumes of ethyl acetate per volume of fermentation broth. This presents scale-up challenges related to solvent handling, safety, cost, and waste management. Continuous counter-current liquid-liquid extraction systems represent a promising industrial alternative, allowing efficient mass transfer and significant solvent savings. In such a setup, the organic solvent is introduced at the base of a packed extraction column and flows counter currently to the downward-moving fermentation broth. The enriched solvent phase is then concentrated and crystallized to recover AKG.

Beyond classical LLE, integrating in-situ product recovery (ISPR) techniques can further improve process sustainability and productivity. As introduced earlier, reactive extraction coupled with pH-shift-controlled back-extraction and crystallization (as demonstrated for

itaconic acid) can mitigate product inhibition during fermentation and reduce DSP burden. Specifically, an electrochemically controlled pH shift (“Power-to-Purity” concept) could be applied, where mild acidification via electrochemical means induces AKG crystallization directly in the fermentation broth without adding acid. This avoids salt accumulation, lowers waste generation, and enhances environmental compatibility.

In summary, the developed LLE process constitutes a robust foundation for AKG recovery. Future efforts should focus on minimizing solvent consumption through continuous extraction and ISPR integration, alongside novel pH control strategies. These advancements aim to improve yield, purity, and process economics while aligning with green chemistry principles. A thorough techno-economic analysis (TEA) of these process intensification strategies will be essential to identify optimal trade-offs and guide industrial implementation.

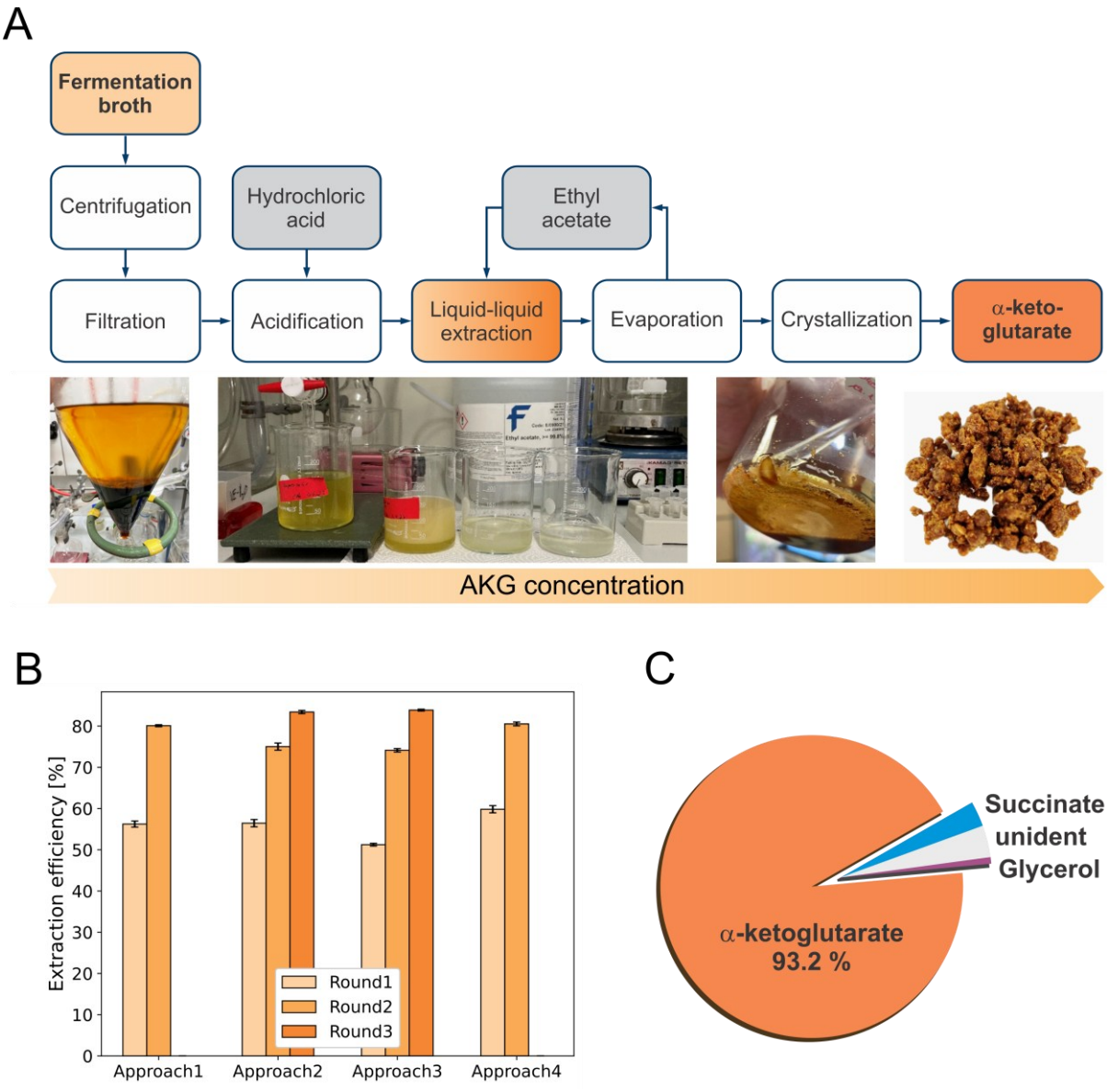

Figure 18 Purification of bio-based α-ketoglutarate (AKG) from molasses fermentation broth using multistep liquid-liquid extraction with ethyl acetate. (A) Flowchart of the purification process, from AKG-containing fermentation broth to the final crystallization of the dicarboxylic acid. **(B)** Extraction efficiency of four different cross-current liquid-liquid extraction approaches. Approaches 1 and 4 each used two extraction steps (sample-to-solvent ratios 1:4, 1:4 and 1:5, 1:3, respectively), while approaches 2 and 3 used three extraction steps (1:4, 1:2, 1:2 and 1:3, 1:3, 1:2, respectively). In all cases, the total amount of ethyl acetate used was eight times the sample volume. **(C)** Composition of the purified precipitate as determined by GC-ToF-MS.

For 1st gen. feedstocks such as molasses, both economic feasibility and sustainability considerations must be taken into account when evaluating their role in bio-based value chains. A detailed conclusion on the advantages and limitations of molasses as a carbon source is provided in Chapter 7.1.

4. Production of 2-oxoglutaric acid from 2nd gen. biomass

This chapter centers on the biosynthesis of AKG from renewable biomass of 2nd generation, with a particular focus on lignocellulosic hydrolysate as a substrate. Metabolic engineering of the production strains was carried out by Daniela Höppner from the 'Synthetic Cell Factories' research group at IBG-1, Forschungszentrum Jülich. Strain characterization experiments on defined xylose-glucose mixtures were conducted by Daniela Höppner. Strain characterization experiments on complex lignocellulosic hydrolysate were performed by Daniela Höppner and Lars Halle. Determination of substrate and (by-)product concentrations were supported by Astrid Wirtz from the 'Genomics and Expression' research group at IBG-1.

4.1 Targeted metabolic engineering for AKG production strains

For the valorization of lignocellulosic biomass, the ability to metabolize both glucose (released from cellulose) and xylose (released from hemicellulose) is essential. As described in Chapter 1.3.1, *C. glutamicum* cannot naturally utilize xylose. To overcome this limitation, the codon-optimized Weimberg operon from *Caulobacter crescentus* (Chapter 1.5.1) was introduced into the production strains developed in Chapter 3.1 via the plasmid pEKEx3-*xylXABCD*$_{opt}$. The base strain P$_{O6}$-*iolT1* and the AKG production strains AKG-1, AKG-2, AKG-3, and AKG-4 already contained the genetic modifications, including the deletions of *gdh, gltB* and *odhA* to block glutamate and succinate formation from AKG and glutamine, and truncation of MscCG for an improved export of AKG. The resulting xylose-utilizing AKG production strains were designated P$_{O6}$-*iolT1* pEKEx3-*xylXABCD*$_{opt}$ (P$_{O6}$-*iolT1*-xyl), AKG-1 pEKEx3-*xylXABCD*$_{opt}$ (AKG-1-xyl), AKG-2 pEKEx3-*xylXABCD*$_{opt}$ (AKG-2-xyl), AKG-3 pEKEx3-*xylXABCD*$_{opt}$ (AKG-3-xyl), and AKG-4 pEKEx3-*xylXABCD*$_{opt}$ (AKG-4-xyl).

4.2 Parallelized strain characterization

4.2.1 AKG production from defined xylose-glucose mixtures

The AKG-xyl production strains were evaluated in shake flask cultivations using defined CGXII medium supplemented with a glucose-xylose mixture (1:3 ratio: 10 g L^{-1} glucose, 30 g L^{-1} xylose). As expected, comparison of P$_{O6}$-*iolT1*-empty (empty plasmid as control) with P$_{O6}$-*iolT1*-xyl confirmed that the Weimberg operon was successfully expressed in the parental

strain, enabling xylose utilization for biomass formation (Figure 19). P_{O6}-*iolT1*-empty reached a final optical density (OD) of 13.9 ± 1.3 after 72 h, whereas P_{O6}-*iolT1*-xyl achieved a final OD of 62.1 ± 1.1, corresponding to the theoretical 1:3 ratio based on the supplied carbon sources. In both strains, no AKG was detected in the final supernatants, as anticipated.

Similar to observations on glucose and sucrose, deletion of *gdh* in AKG-1-xyl resulted in reduced growth performance. A maximum AKG concentration of 1.79 ± 0.22 mM was measured after 30 h, while no AKG was detectable at the end of cultivation (72 h). The double-deletion strain AKG-2-xyl (Δ*gdh* and Δ*gltB*) exhibited nearly identical growth and production behavior, reaching a maximum titer of 2.03 ± 0.25 mM at 30 h and no detectable AKG at 72 h.

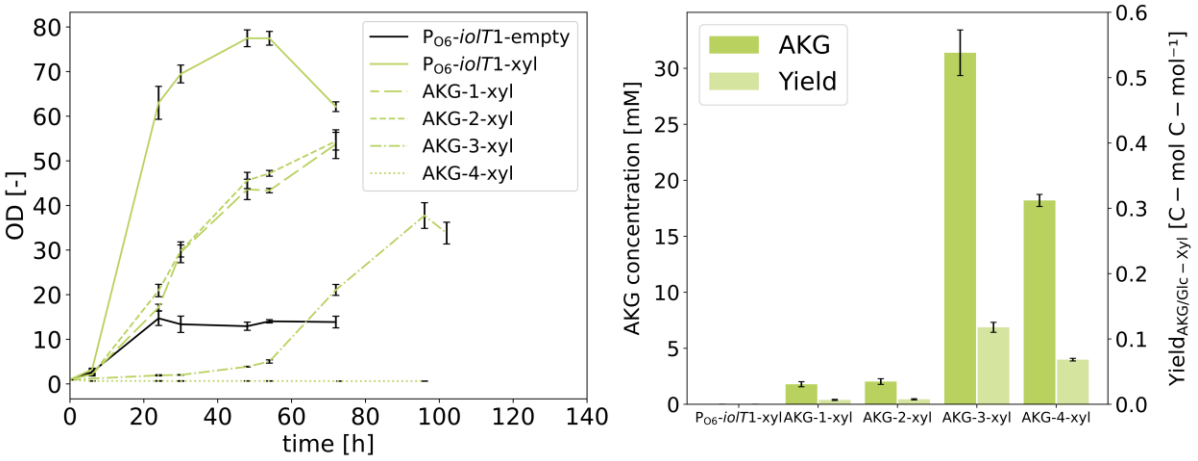

Figure 19 Growth behavior and AKG production performance of engineered *C. glutamicum* strains cultivated in defined CGXII medium. Cultivation using glucose (10 g L^{-1}) and xylose (30 g L^{-1}) as the sole carbon and energy sources. All strains were grown in 500 mL shaking-flasks with a working volume of 50 mL. The shaking speed was set to 130 rpm. Biomass formation was observed by OD measurements, and AKG concentrations were determined from endpoint samples via HPLC measurement. Data represent mean values ± standard deviation from technical triplicates.

Truncation of the mechanosensitive channel in AKG-3-xyl had the strongest effect on both growth and AKG accumulation under these conditions. The final supernatant contained 31.4 ± 2.03 mM AKG, with a product-substrate yield of 0.12 ± 0.01 C-mol C-mol^{-1}, which is in the same range as the highest yield measured for AKG-3 on sucrose in defined medium (0.14 ± 0.01 C-mol C-mol^{-1}).

As observed previously on glucose and sucrose, deletion of *odhA* in AKG-4-xyl completely abolished cell growth. Nevertheless, the final AKG titer measured for this strain was

18.2 ± 0.5 mM. This concentration is higher than that obtained on sucrose or glucose, which again suggests residual metabolic activity. These findings indicate that the deletion of *odhA* effectively blocks the carbon flux downstream of the Weimberg pathway at the level of AKG, thereby causing its accumulation.

4.2.2 AKG production from complex lignocellulosic hydrolysate

As an example of a second-generation feedstock with high relevance for the bioeconomy, this work investigated the utilization of a lignocellulose-containing waste stream. The feedstock, kindly provided by the company Fibenol, consisted primarily of glucose and xylose in a ratio of 1:3. In addition to these major components, the hydrolysate contained further monosaccharides such as mannose and galactose, as well as organic acids including formic acid and acetic acid. Furfural and hydroxymethylfurfural (HMF), which are typically formed during the thermal degradation of sugars and carbohydrates, were also detected. A detailed compositional analysis of the Fibenol feedstock is provided in Table S2.

To evaluate the capacity of the engineered strains to utilize the carbon sources present in the Fibenol feedstock, strains P_{O6}-*iolT1*-xyl to AKG-4-xyl were cultivated in CGXII medium supplemented with this substrate. Cultivation of P_{O6}-*iolT1*-xyl demonstrated growth on the Fibenol feedstock (Figure 20A). However, growth initiation was delayed by approximately 60 h, and reproducibility among triplicates was poor, with two replicates initiating growth only after more than 80 h (Figure 20B). AKG-1-xyl displayed an identical growth delay and variability, with one replicate failing to initiate growth even after 140 h of cultivation. Strains AKG-2-xyl through AKG-4-xyl exhibited no detectable growth.

The observed growth delay and non-reproducibility between replicates indicate inhibition of cell growth. Given the known sensitivity of *C. glutamicum* to furfural, it is likely that furfural toxicity was responsible for the delayed or absent growth. Occasional onset of growth after prolonged lag phases may therefore indicate adaptive evolution in some replicates due to the selection pressure of the inhibitory compound. Verification of this hypothesis would require physiological characterization and whole-genome sequencing of the late-growing cultures.

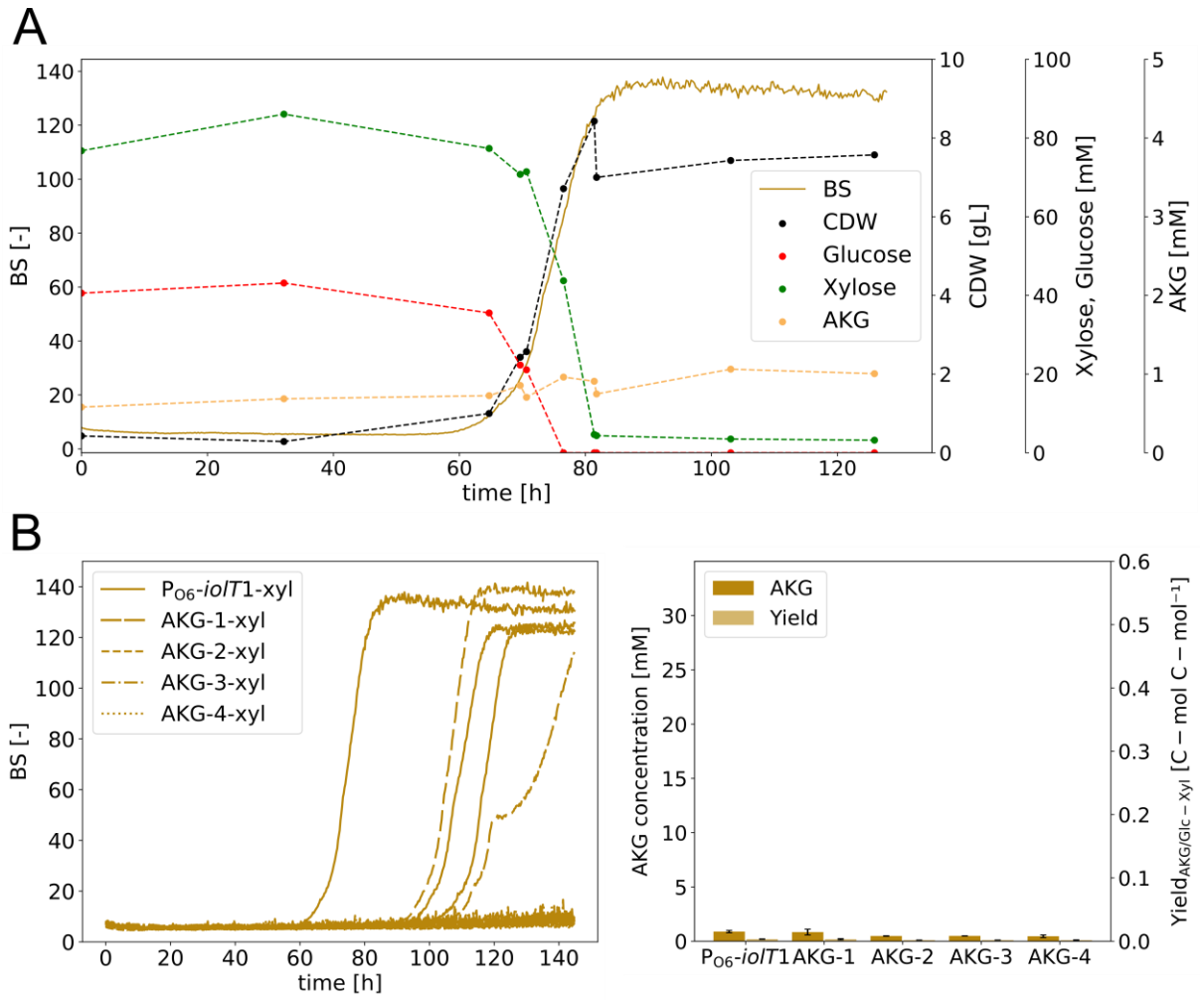

Figure 20 Batch cultivation and AKG production of engineered *C. glutamicum* strains in lignocellulosic hydrolysate based medium. **(A)** Cultivation of *C. glutamicum* P_{O6}-*iolT1*-xyl on hydrocellulosic hydrolysate. **(B)** Parallelized strain characterization of strains P_{O6}-*iolT1*-xyl to AKG-4-xyl on lignocellulosic hydrolysate. Strains were cultivated in biological triplicates (each individual culture of the triplicates are shown) using a BioLector microbioreactor system with 48-well FlowerPlates. Each well contained 1 mL of CGXII medium supplemented with lignocellulosic hydrolysate, corresponding to a glucose concentration of 10 g L^{-1} and a xylose concentration of 30 g L^{-1}. Cultivations were conducted at 1,400 rpm with a backscatter (BS) gain of 20 for online biomass monitoring. Final AKG concentrations were determined from endpoint samples. Data are presented as mean values ± standard deviation from triplicate experiments.

In order to systematically evaluate the inhibitory effect of individual compounds, targeted inhibition tests with furfural and HMF were performed in the next step.

4.3 Inhibitory effect of lignocellulosic hydrolysate components

Sakai et al. have previously described the inhibitory effects of furfural and HMF on *C. glutamicum* growth performance [160]. To test this hypothesis for the Fibenol feedstock, both a feedstock concentration assay (Figure 21A) and specific furfural and HMF inhibition tests (Figures 21B and 21C) were performed. The feedstock concentration assay revealed the inhibitory effect associated with increasing concentrations of the Fibenol feedstock. At a xylose concentration equivalent to 0.5 % (33 mM) from the Fibenol hydrolysate, no inhibition was observed. Cells initiated growth immediately after inoculation without a detectable lag-phase, and a second growth phase, analogous to that observed in the glucose-xylose mixture experiments, was clearly discernible. Doubling the xylose concentration to 1 % (66 mM) resulted in a growth delay of more than 40 h, indicating the onset of inhibition. Nevertheless, the final biomass concentration was approximately twice as high as at 0.5 %, consistent with expectations, suggesting efficient utilization of the carbon source despite the delayed onset of growth. Further increasing the xylose concentration led to an even longer lag phase of more than 60 h, while the final biomass again doubled upon substrate doubling. At a concentration corresponding to 3 % and 4 % xylose in the Fibenol feedstock, no growth was observed within the 190 h cultivation period.

The furfural and HMF inhibition tests showed a similar relationship between inhibitor concentration and lag-phase extension. At 40 mM furfural, the lag phase extended beyond 80 h, while 30 mM HMF prolonged the lag phase to over 40 h. Growth was completely inhibited at 40 mM HMF. It should be noted that at a feedstock concentration corresponding to 2 % xylose, the furfural and HMF levels in the Fibenol hydrolysate were 1.13 mM and 2.46 mM, respectively. This is below the thresholds determined in the inhibition tests, suggesting that synergistic effects between the inhibitors may contribute to the stronger inhibition observed in hydrolysate fermentations.

Nevertheless, the results indicate that components of the lignocellulosic hydrolysate exert an inhibitory effect on *C. glutamicum*. A detailed investigation of degradation processes during the lag-phase and further compositional analyses of this feedstock were beyond the scope of this work but are recommended for future process development for lignocellulosic hydrolysates, particularly to optimize targeted detoxification of inhibitory compounds.

Among these, the heterocyclic aldehyde furfural is considered one of the most toxic inhibitors [161, 162]. *C. glutamicum* has been shown to detoxify furfural by converting it into the less toxic products furfuryl alcohol and 2-furoic acid, with an enzyme encoded by *cg0408* (designated as FudC) playing a major role in furfural reduction to furfuryl alcohol [162]. Building on these insights, future strategies may exploit metabolic engineering to enhance or redirect these endogenous detoxification routes, thereby increasing the robustness of AKG production from lignocellulosic substrates.

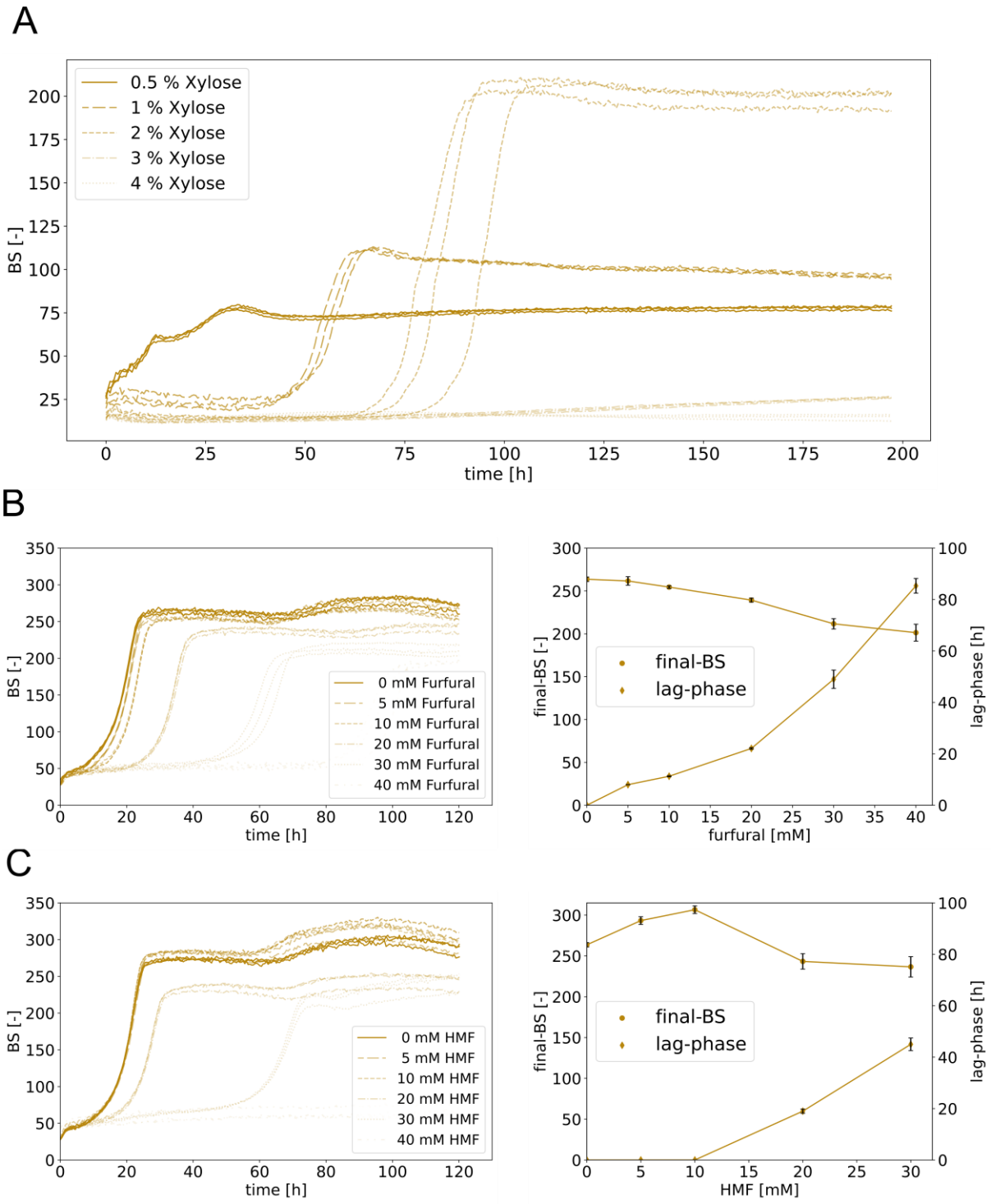

Figure 21 Feedstock, furfural, and HMF inhibition test on *C. glutamicum* P_{O6}-*iolT1*-xyl. **(A)** Cultivation of P_{O6}-*iolT1*-xyl on different concentrations of lignocellulosic hydrolysate. Corresponding to a xylose concentration of 0.5 % – 4 %. **(B)** Cultivation of P_{O6}-*iolT1*-xyl on different concentrations of furfural (0 – 40 mM). Final backscatter (BS) and culture lag-phases shown as function of time. **(C)** Cultivation of P_{O6}-*iolT1*-xyl on different concentrations of hydroxymethylfurfural (0 – 40 mM). Final BS and culture lag-phases shown as function of time. Strains were cultivated in biological triplicates using a BioLector microbioreactor system with 48-well FlowerPlates. Each well contained 0.8 mL of CGXII medium supplemented either with lignocellulosic hydrolysate or 2 % xylose and furfural/hydroxymethylfurfural. Cultivations were conducted at 900 rpm with a BS gain of 3 for online biomass monitoring.

4.4 Scale-up of the glucose-xylose AKG-3-xyl process in 1 L STR

Since AKG-3-xyl had proven to be the most promising production strain for AKG synthesis from glucose-xylose mixtures in the shake flask screenings (Chapter 4.2.1), a first scale-up to a 1 L bioreactor was performed in parallel to the investigations on the Fibenol feedstock (Figure 22). The initial batch phase of the cultivation was successful, and the feed was initiated based on the detection of a DO peak. Post-run analysis, however, revealed that in this particular case the DO peak corresponded to the depletion of glucose rather than complete consumption of all carbon sources. At the time of feeding, xylose had not yet been utilized and only 20.9 ± 0.4 mM AKG had been produced from glucose.

Following the onset of feeding, both glucose and xylose accumulated in the fermentation broth. It should be noted that growth on glucose-xylose mixtures in shake flasks exhibited a bi-phasic growth pattern, suggesting a sequential substrate utilization, and consistent with previous reports in the literature [125]. This sequential metabolism likely contributed to the unsuccessful fed-batch process. With a continuous feeding strategy, glucose remained available at all times, preventing the activation of xylose metabolism during the feeding phase. As a result, xylose accumulated, exposing the cells to osmotic stress and inhibition, ultimately impairing glucose consumption as well.

The utilization of lignocellulose-derived feedstocks represents a promising strategy to integrate second-generation carbon sources into value-added production chains. However, the challenges associated with growth inhibition and the metabolism of mixed substrates need to be specifically addressed through metabolic engineering and tailored process design. An initial manual ALE experiment with the strain P_{O6}-*iolT1*-xyl on xylose (data not shown) already highlighted these challenges: due to repeated over-inoculation during the glucose consumption phase, the strain lost the plasmid part with the Weimberg operon, retaining only the antibiotic resistance marker. This outcome underlines the importance of precisely controlling the transfer phase during ALE. Automated strategies that enforce transfers specifically during the xylose consumption phase would represent a first step toward repeating this untargeted engineering experiment more effectively.

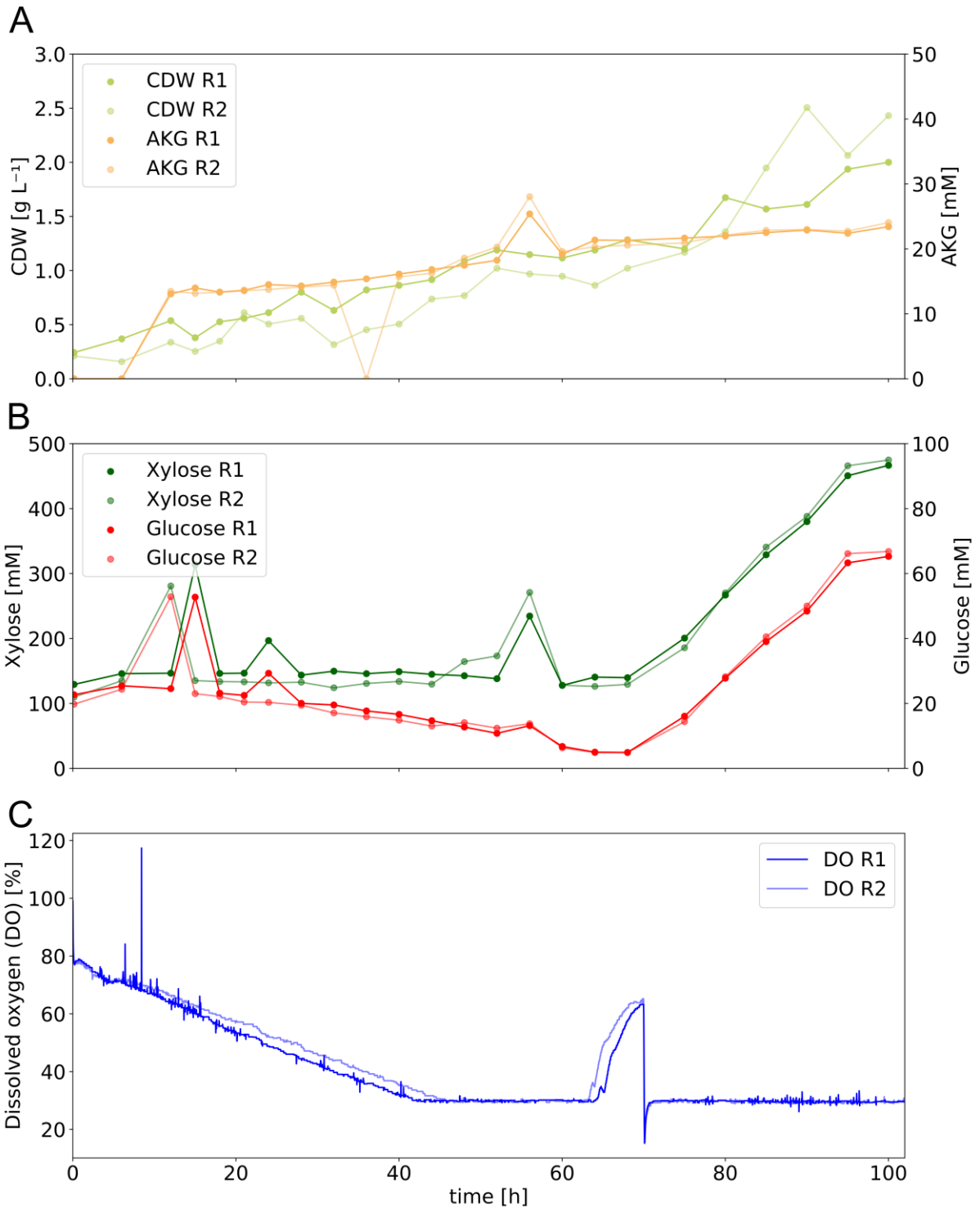

Figure 22 Fed-batch bioreactor cultivation of *C. glutamicum* P_{O6}-*iolT1* Δ*gdh* Δ*gltB* mscCG' pEKEx3-*xylXABCD*$_{opt}$ (AKG-3-xyl). Cells were grown in two parallel 1 L bioreactors (R1, R2) using CGXII medium with glucose-xylose mixtures as the sole energy and carbon sources. The initial glucose-xylose concentration at the start of cultivation was 10 g L^{-1} and 30 g L^{-1}. The feed solution consisted of glucose-xylose mixture with a glucose concentration of 100 g L^{-1} and 300 g L^{-1} xylose and did not contain additional CGXII salts.

5. Production of 2-oxoglutaric acid from ethanol

The utilization of ethanol as a carbon source opens new perspectives for sustainable biotechnological production processes, especially when derived from renewable sources such as CCU technologies. While microbial production of AKG from molasses was demonstrated in the previous chapter, specific challenges in ethanol metabolism remain to be addressed. Emphasis is placed on the development of an automated long-term ALE workflow and the untargeted optimization of *C. glutamicum* for improved ethanol assimilation using this method. Bioprocess modeling of the ALE experiments was supported by Niels Hollmann during his master's thesis. Proteomic analysis and whole-genome sequencing of the evolved ALE strain identified a beneficial mutation underlying the improved phenotype. The proteomic work was conducted in collaboration with Bianca Klein from the "Quantitative Microbial Phenotyping" research group at IBG-1, Forschungszentrum Jülich. Genomic sequencing was supported by Tino Polen and Ursula Degner from the "Genomics and Expression" research group at IBG-1, Forschungszentrum Jülich.

5.1 Utilizing ethanol with *C. glutamicum*

C. glutamicum possesses the native ability to metabolize ethanol as a sole carbon and energy source; however, this capability is limited by substrate toxicity and metabolic constraints at higher ethanol concentrations. In this study, growth experiments were conducted using defined medium supplemented with increasing initial ethanol concentrations (34 mM, 86 mM, 171 mM, and 342 mM) to evaluate tolerance and substrate utilization (Figure 23). The data reveals a clear negative correlation between ethanol concentration and growth performance. At 342 mM ethanol, no detectable growth occurred within 90 hours of cultivation. These findings align with previous studies, including Arndt et al. (2008), who demonstrated that *C. glutamicum* can utilize ethanol but experiences growth inhibition beyond certain concentration thresholds [110]. Arndt's work mainly focused on concentrations up to approximately 100 mM ethanol, highlighting the strain's limited tolerance at elevated substrate levels. The inhibitory effect at higher ethanol concentrations can be attributed to membrane damage and cellular stress responses caused by ethanol's solvent properties. Additionally, prolonged lag phases observed at elevated ethanol levels likely reflect the time required for cells to adapt metabolically and physiologically to this stress. Interestingly, extended cultivation beyond 90 hours often results in eventual growth

recovery, which is hypothesized to result from ethanol evaporation, reducing effective substrate concentration to more tolerable levels.

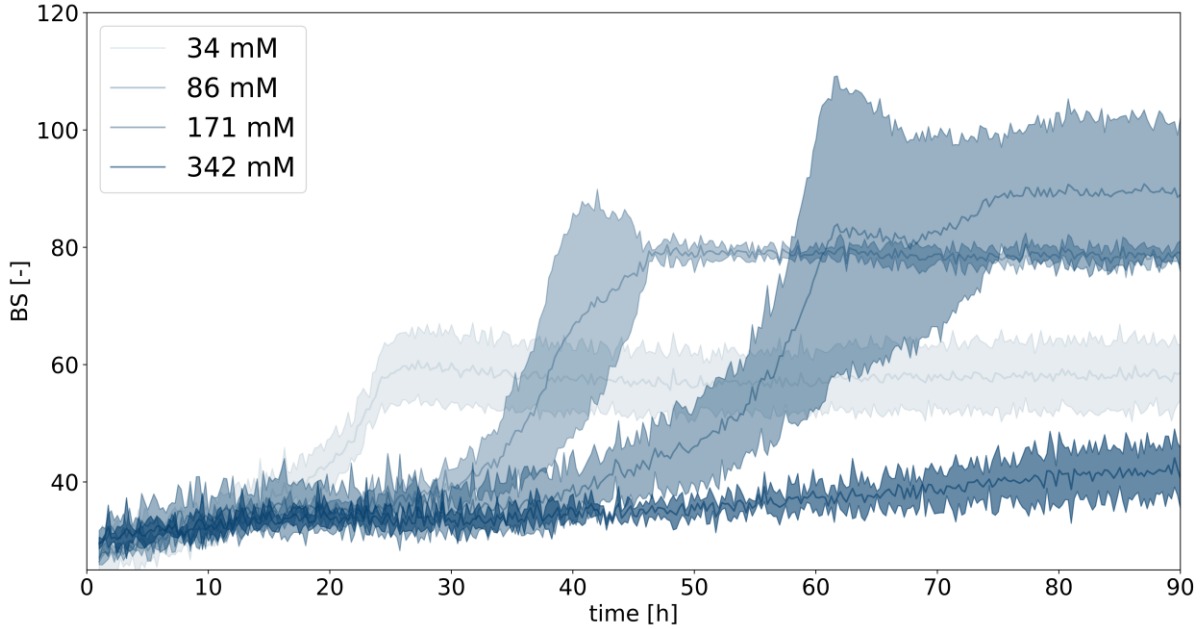

Figure 23 Growth of *C. glutamicum* ATCC 13032 at different ethanol concentrations (34 mM, 86 mM, 171 mM, and 342 mM) as the sole carbon and energy source. Cultivations were performed in a BioLector microbioreactor system using 1 mL working volume per well and a shaking speed of 1,400 rpm. Biomass formation was monitored online via backscatter (BS) signal. Data represent means ± standard deviation from biological triplicates. No growth was observed at 342 mM ethanol within 90 hours.

The volatilization effect underscores the challenge of maintaining stable substrate concentrations during batch cultivation. The native ethanol catabolic pathway in *C. glutamicum* involves sequential oxidation steps from ethanol to acetaldehyde and acetate, which subsequently enters central metabolism via the glyoxylate shunt and TCA cycle (cf. Figure 13). Key enzymatic activities include alcohol dehydrogenase, acetaldehyde dehydrogenase, phosphotransacetylase, isocitrate lyase and malate synthase [110]. While these pathways enable ethanol metabolism, their activity levels and regulatory control limit efficient substrate conversion, especially at higher ethanol concentrations. Given these physiological constraints, improving ethanol utilization is essential for enhancing strain performance and process robustness. The following chapter presents a miniaturized and automated ALE approach aimed at selecting *C. glutamicum* variants with increased ethanol tolerance and improved metabolic capacity for ethanol assimilation.

5.2 Development of an automated long-term ALE workflow

ALE is a powerful strategy to enhance microbial traits such as substrate utilization, stress tolerance, and production efficiency through iterative identification of beneficial mutations. In the context of improving *C. glutamicum*'s ethanol metabolism, ALE provides a promising route to overcome native physiological limitations at elevated substrate concentrations. However, rbALE workflows based on microtiter plate cultivation remain constrained by the limited number of wells per plate, restricting both experimental throughput and total number of generations. Radek et al. (2017), introduced repetitive batch ALE using 48-well plates with automated sampling and media exchange, but the overall experiment duration and evolutionary depth were still limited by the plate format [126].

To address these bottlenecks, we developed an expanded and automated long-term rbALE workflow that incorporates a well-recycling strategy. The following section details the experimental design and validation of this automated workflow, including the plate layout, media handling, inoculation procedure, and online monitoring protocols.

The enhanced Mini Pilot Plant based rbALE setup used a 48-well FlowerPlate B (without optodes), organized into six evolution groups (rows A – F), each consisting of eight wells (Figure 24A). This layout supported up to six parallel adaptive evolution runs per experiment. Fresh cultivation medium, pre-distributed into 96-deep-well plates and sealed with perforated plastic foil, was stored on a temperature-controlled deck at 4 °C prior to use. Maintaining low temperatures significantly stabilized media components over time compared to ambient conditions, as previously reported [126].

For inoculation, a seed culture of the target strain was grown in CGXII medium supplemented with 111 mM glucose, washed twice with sterile 0.9 % NaCl, and diluted to achieve an initial OD of 0.2. The first well of each evolution group received 800 µL of medium and 50 µL of inoculum. Throughout the process (Figure 24B), backscatter (BS) was monitored at 15-minute intervals. Once a predefined threshold (60 % of the expected final biomass signal based on prior calibrations) was reached, the automated system initiated the repetitive batch sequence:

1. **Pre-tempering**: 800 µL of fresh medium was aspirated from the storage plate and dispensed into the next available well within the same ALE group. This well was allowed to equilibrate at 30 °C for one measurement cycle (15 min) to prevent cold-shock during inoculation.
2. **Harvesting**: The culture in the triggering well was completely aspirated and transferred to a sterile intermediate plate. This ensured precise inoculum handling and minimized pipetting variability.
3. **Inoculation**: A 50 µL aliquot from the harvested culture was transferred to the pre-tempered well containing fresh medium.
4. **Well recycling**: The previously used well underwent a two-step washing procedure using 900 µL sterile water per step, followed by a final aspiration step to remove residual liquid. Due to the fixed aspiration height of 1 mm above the well bottom, a residual volume of approximately 50 µL remained. However, this volume typically evaporated during the minimum 40-hour interval before the well's next use.

Even if trace amounts of residual fluid were retained, they posed negligible risk to experimental performance. CGXII medium is nutrient-rich, and minor dilution effects would not alter growth kinetics. Moreover, any cells surviving in the residual volume would likely be displaced by fresh and vital cells in their exponential phase during the next inoculation. In fact, these harsher conditions could even impose additional selective pressure, potentially accelerating adaptive responses. Following washing and evaporation, the recycled well was reintroduced into the batch cycle. Once the final well in a group (column 8) was used, the system returned to the first well, enabling theoretically unlimited batch cycles within each ALE group. This closed-loop workflow decouples the number of achievable generations from both the physical limitations of the plate and the organism's specific growth rate. Instead, the generation count per batch is governed solely by the inoculum size and the set BS threshold. In the current setup, approximately three generations occur per batch (BS_start ≈ 8, BS_threshold = 60). Without well recycling, a maximum of 144 generations is achievable (6 groups × 8 wells × 3 generations).

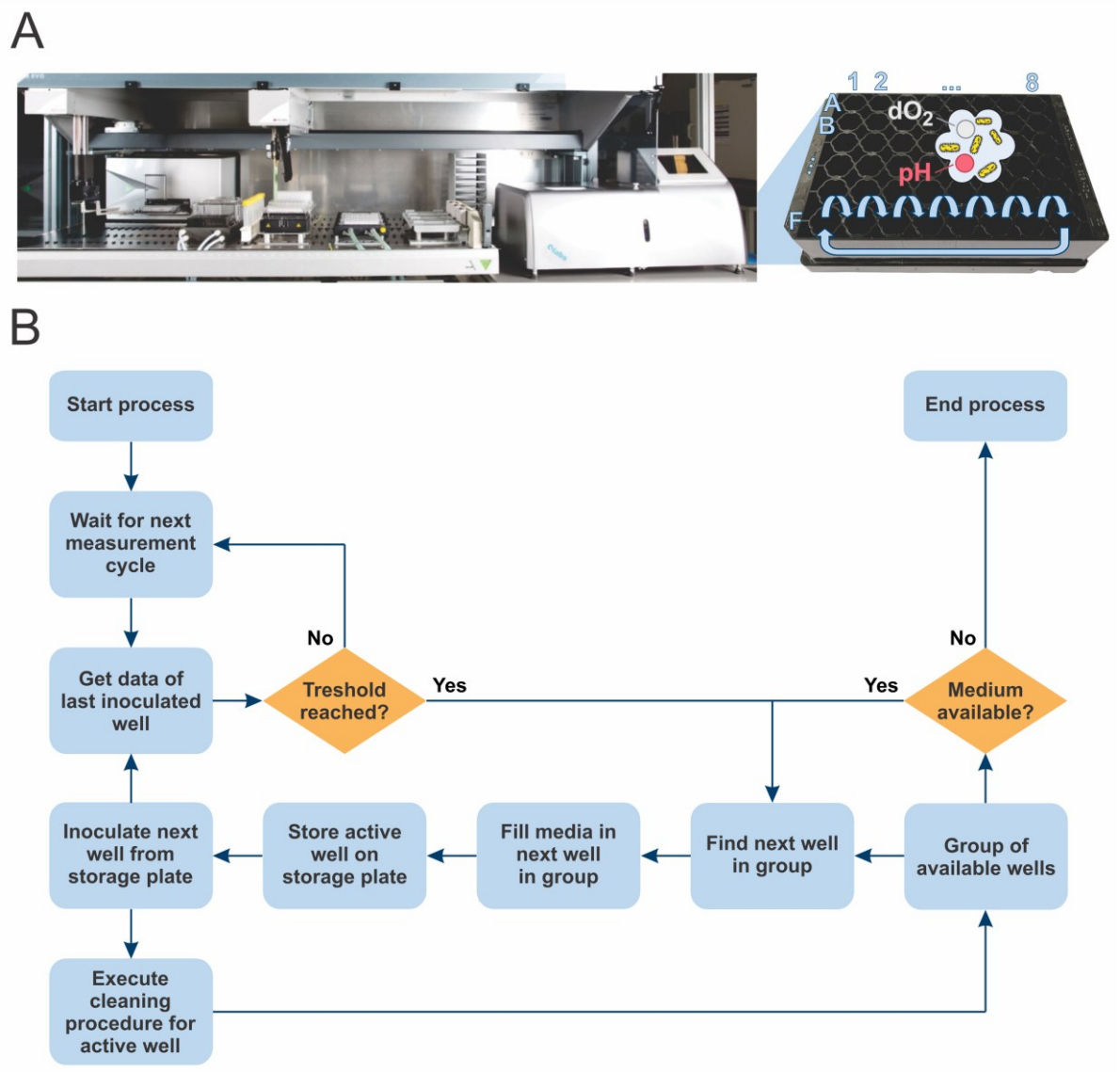

Figure 24 Overview of the robotic workflow for automated long-term rbALE experiments. (A) Mini Pilot Plant technology integrating the BioLector microbioreactor into a liquid handling system. On the right, a typical microtiter plate used for cultivation in the microbioreactor is shown, divided into six groups (rows) of eight wells each. The repetitive batch scheme is indicated by blue arrows. **(B)** Flowchart of the long-term rbALE process with well reuse. The process starts with the backscatter (BS) measurement cycle. After each cycle, measurement data are evaluated, and when the BS threshold is reached, the system triggers inoculation of the next batch and execution of the washing procedure.

This method enables repeated use of the same wells by automating the emptying, washing, and drying of wells between batches. These procedures restore optimal cultivation conditions and ensure consistent and reliable BS monitoring over extended periods.

Using the expanded protocol, over 288 generations have been performed in a single run, which was only interrupted by experimenter´s intervention. To further increase generations per batch, one might consider reducing the inoculation density or increasing the substrate

concentration. However, the latter risks oxygen limitation in aerobic systems, and the former reduces the population size per generation, which would lower the statistical probability of capturing beneficial mutations. A major advantage of this improved design is its scalability and parallelization. The current setup supports six evolution replicates with unlimited batch cycles, allowing for comparative selection strategies or evolutionary trajectories. Further parallelization could be realized by subdividing the rbALE groups even more (e.g., using four or more smaller groups).

5.3 Validation of the well-recycling concept

As a proof of concept for the newly developed long-term rbALE workflow, it was evaluated whether the repeated reuse of cultivation wells affects growth performance under non-selective conditions. To this end, an rbALE experiment was conducted with *C. glutamicum* ATCC 13032 (wild-type strain, hereafter referred to as WT) cultivated in CGXII medium containing 111 mM glucose as the sole carbon and energy source. Online BS measurements were recorded throughout the cultivation, and fitted biomass trajectories along with growth rate estimates for one representative replicate (R1) are presented in Figure 25A. Over the course of 96 individual batches performed within five days, the WT strain exhibited consistent and stable growth across all batches, indicating that well recycling and the associated automated procedures did not impose detectable physiological stress or limit culture viability. Furthermore, analysis of six independent rbALE runs revealed that the specific growth rates remained nearly constant throughout the successive batches (Figure 25B). The maximum specific growth rate of $\mu_{max} = 0.41 \pm 0.05\ h^{-1}$ aligns well with previously reported values for *C. glutamicum* WT under similar cultivation conditions [102], confirming that the automated well-recycling protocol preserves the native growth characteristics of the strain. These results validate the robustness and reliability of the well-recycling approach, demonstrating its suitability for prolonged ALE experiments without detrimental effects on microbial growth. This methodological advancement thus enables extended evolutionary cultivation campaigns while maintaining experimental reproducibility and throughput.

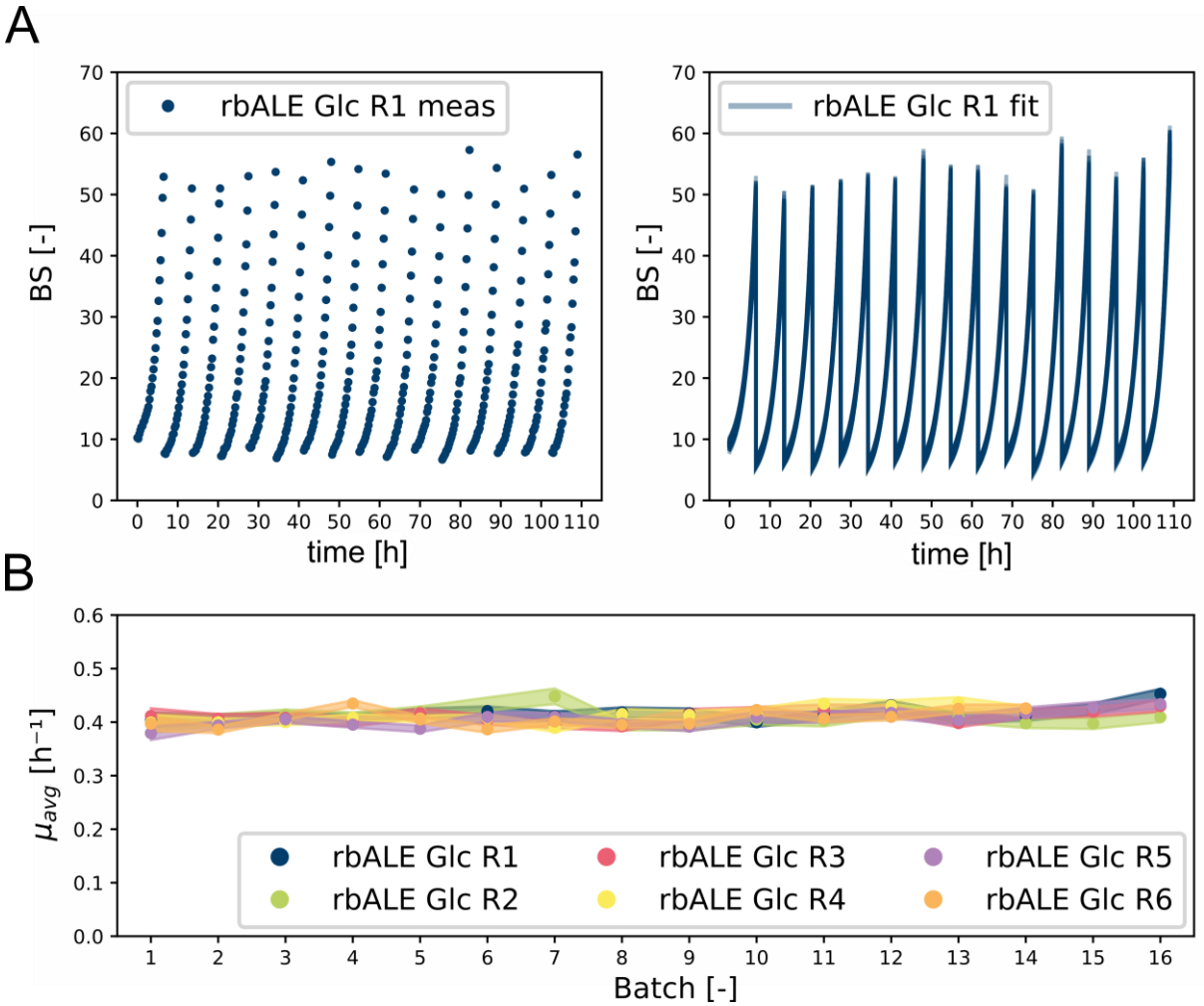

Figure 25 Validation of the long-term rbALE workflow. (A) Example dataset (rbALE Glc R1) from one of six independent ALE experiments performed using the Mini Pilot Plant technology. *C. glutamicum* WT was cultivated for 16 consecutive batches in a FlowerPlate with defined CGXII medium containing 111 mM glucose as the sole carbon and energy source. Online backscatter (BS) measurements were used for process model fitting. **(B)** Estimated specific growth rates across the individual batches for all six rbALE runs.

5.4 Untargeted metabolic engineering for ethanol utilization with *C. glutamicum*

To enhance the ethanol utilization capabilities of *C. glutamicum* WT, a long-term rbALE experiment was conducted using ethanol as the selective pressure. An inhibitory ethanol concentration of 428 mM was chosen, based on the preliminary screening data (cf. Figure 23). Alongside pure ethanol, additional conditions involving ethanol-glucose mixtures were initially evaluated. However, only the approaches cultivated solely on ethanol demonstrated adaptive improvement, and thus only those results are discussed herein. The rbALE process was executed using one 48-well FlowerPlate, divided into six ALE groups (three per condition), and was run continuously over approximately 10 days, comprising more than 100 individual batch cycles. Among the six total runs, the three ethanol-only conditions resulted in successful

adaptation of *C. glutamicum* WT. A representative example of an ALE approach (EtOH R3) is shown in Figure 26 (with replicates presented in Appendix Figure S2).

The first batch cycle displayed irregular growth kinetics, probably due to insufficient washing following pre-cultivation in glucose-containing medium (Figure 26A). This likely resulted in residual carbon carryover, which could have temporarily masked ethanol-specific selection pressure. As such, the initial batch was excluded from specific growth rate analysis. To avoid similar artifacts in future workflows, it is recommended to perform at least two saline wash steps when transitioning between carbon sources. In batch two of EtOH R3, the wild-type strain exhibited a specific growth rate of $\mu_{max} = 0.085 \pm 0.003\ h^{-1}$, consistent with previous experiments and reported values from literature (Figure 26B). Starting from this batch, a progressive increase in growth rate was observed, suggesting the emergence of beneficial mutations. By batch five, the strain had reached $\mu_{max} = 0.16 \pm 0.01\ h^{-1}$, culminating in a maximum rate of $\mu_{max} = 0.21 \pm 0.01\ h^{-1}$. This steady but non-linear improvement is characteristic of population-level competition between evolving and ancestral subpopulations. During batch nine, a malfunction in the liquid-handling robot's control unit resulted in unintended extended cultivation, pushing the culture into stationary phase. Subsequent inoculation from these late-phase cells resume to normal growth, indicating that the process can recover under these conditions. To mitigate such disruptions, it is advisable to implement real-time system monitoring with fail-safe mechanisms, such as automated alerts and continuous logging to allow process recovery.

The gradual nature of fitness improvement across successive batches can be attributed to the stochastic emergence and slow enrichment of advantageous mutations. Initially, such mutations are carried by only a few individuals within the population. As the beneficial mutants ($\mu_{evo} > \mu_{wt}$) slowly displace the parental strain, the overall culture growth rate increases over time. This fact is one of the main reasons for the need of evolution campaigns with a longer duration. Similar evolutionary dynamics were observed in the other ethanol-only replicates, reflecting heterogeneous mutation events and intra-population competition (Appendix Figure S 2).

To confirm ethanol adaptation, final strains from all three successful evolution lines were characterized alongside the wild type in single-batch experiments under identical conditions,

each in triplicate (Figure 26C). All evolved variants demonstrated superior growth performance on ethanol compared to the wild type. Additional online data to this characterization can be found in the Appendix (Figure S3). Nonetheless, significant differences in lag phase duration and specific growth rates among the evolved strains indicate divergent evolutionary paths, likely shaped by differences in the nature, timing, and combination of genetic or regulatory adaptations acquired during rbALE. The best-performing isolate, designated *C. glutamicum* WT_EtOH-Evo, exhibited markedly improved growth on ethanol in microscale cultivation.

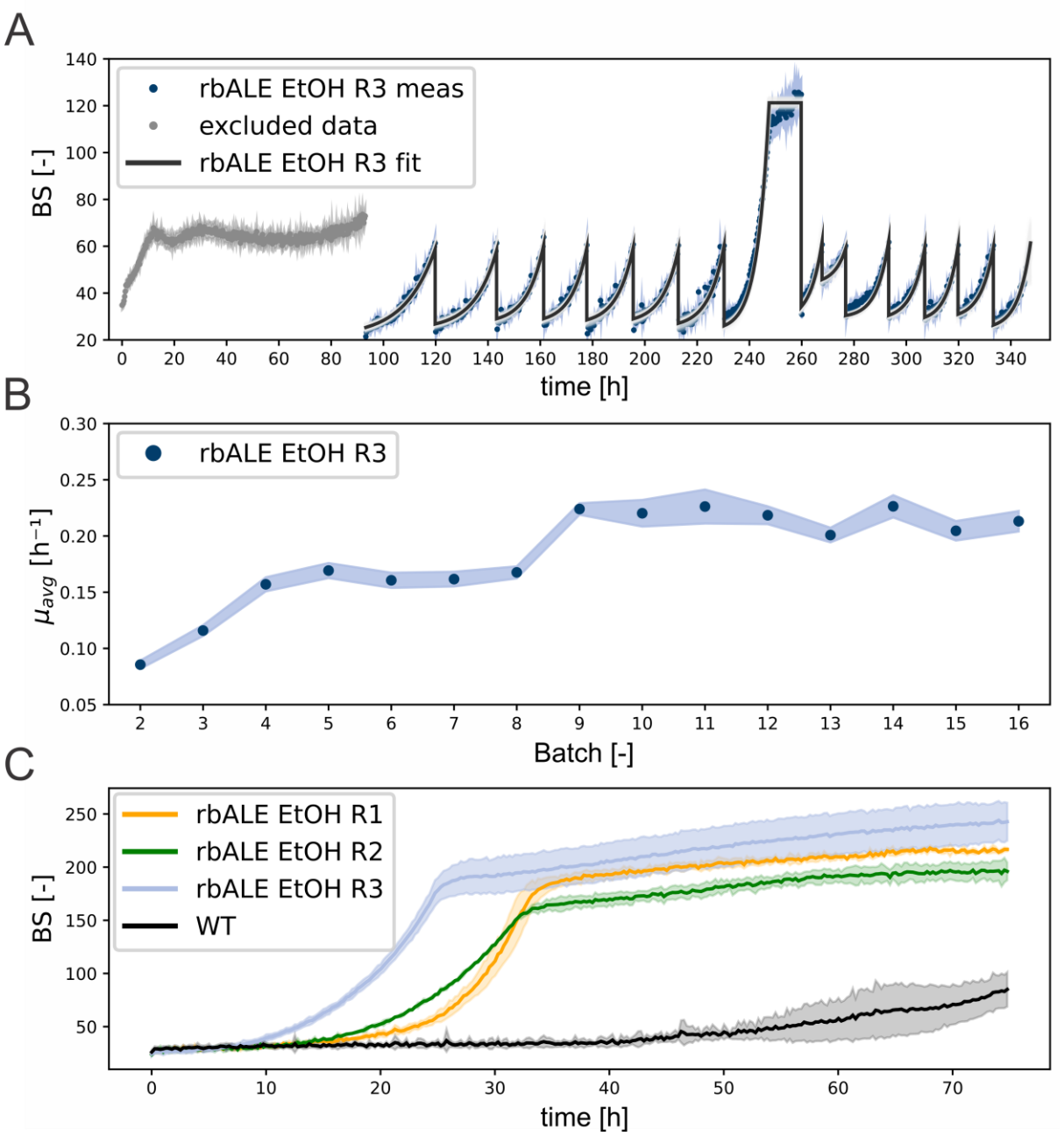

Figure 26 Improving ethanol utilization of *C. glutamicum* WT through long-term rbALE. (A) Example dataset (rbALE EtOH R3) from one of three replicate experiments. *C. glutamicum* WT was cultivated in a FlowerPlate using defined CGXII medium with 428 mM ethanol as the sole carbon and energy source over 16 repetitive batches. Online backscatter (BS) measurements were used for process model fitting. **(B)** Estimated specific growth rates across the individual batches of rbALE EtOH R3. **(C)** Growth performance of the three evolved mutants compared to *C. glutamicum* WT. Microscale batch experiments were performed under rbALE-equivalent conditions in triplicates for each mutant strain. Mean values and standard deviations are presented as lines and shaded areas, respectively.

5.5 Verification and evaluation of the evolved *C. glutamicum* strain

5.5.1 Testing the phenotypical stability of WT_EtOH-Evo

To validate the enhanced growth phenotype and assess the genetic stability of the evolved mutant strain during ethanol utilization, a modified version of the previously established rbALE protocol was applied [26]. In this adapted approach, cells from a pre-culture grown on 111 mM glucose in shake flasks were used to inoculate the first column (A1 – F1) of a FlowerPlate (Figure 27A). Alternating rows were filled with different carbon sources: rows A, C, and E contained CGXII medium supplemented with 55.5 mM glucose, while rows B, D, and F contained CGXII medium with 428 mM ethanol as the sole carbon and energy source.

The experimental design included repeated sequential cultivations, where each glucose batch was followed by an ethanol batch. Specifically, once the BS of a glucose well reached 60 % of the known final BS value, both the next glucose well and the ethanol well located directly below were inoculated using the culture from the triggering glucose well. This enabled consistent pre-conditioning of the cells on glucose before each ethanol exposure, establishing a robust framework for phenotype verification across multiple batch cycles (Figure 27B).

The evolved strain, *C. glutamicum* WT_EtOH-Evo, consistently exhibited high specific growth rates on ethanol (μ_{max} = 0.19 ± 0.01 h^{-1}), demonstrating stable inheritance of ethanol adaptation traits over time (Figure 27C). Although no washing step was included during the transitions between glucose and ethanol media, and thus traces of residual glucose may have remained during ethanol inoculation, this had no apparent influence on the observed phenotypic stability. Nevertheless, to improve accuracy and eliminate potential carryover effects in future experiments, it is advisable to incorporate a cell washing step between carbon source changes.

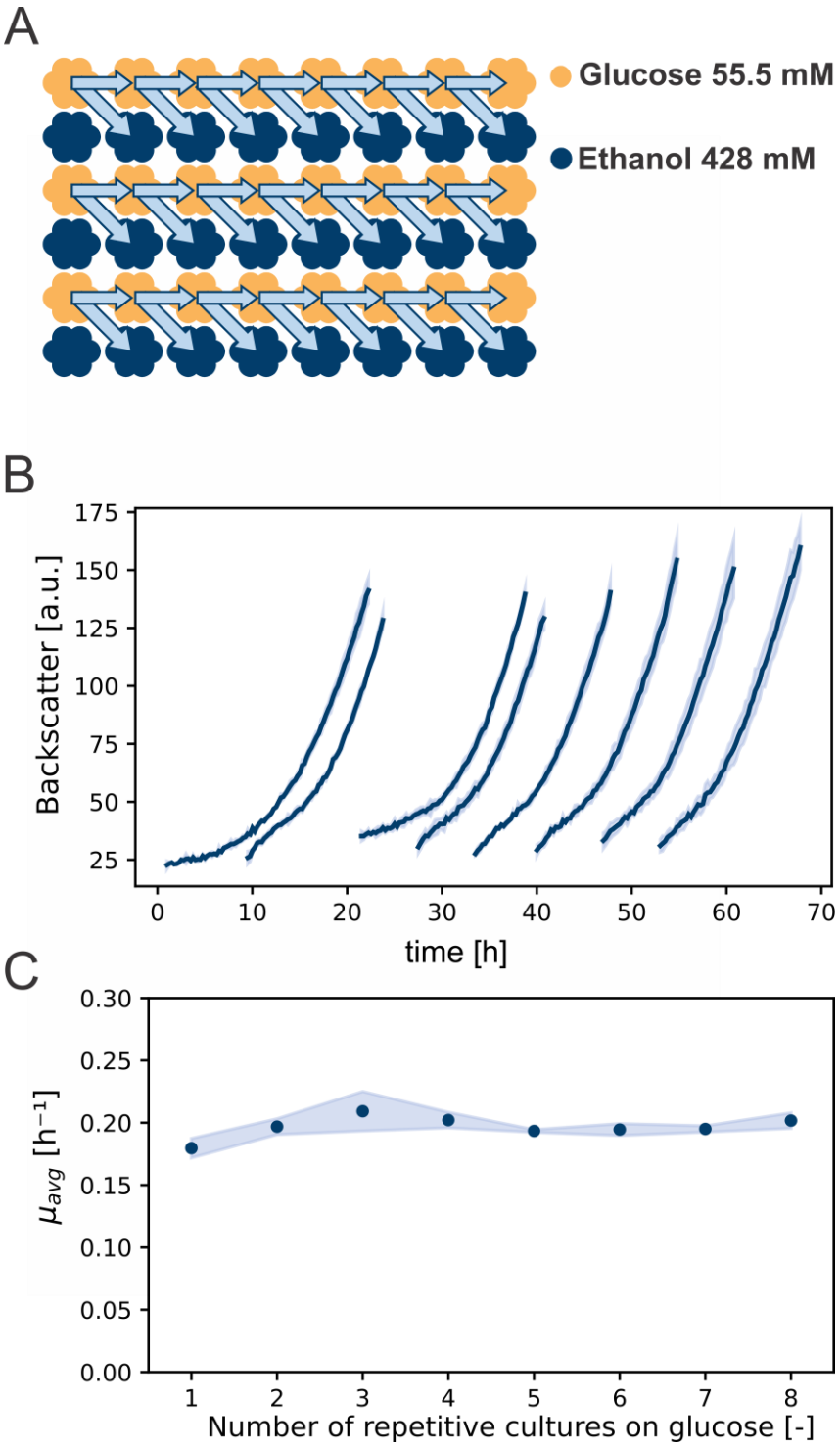

Figure 27 Verification of the evolved strain *C. glutamicum* WT_EtOH-Evo. (A) Experimental setup for automated microscale cultivation using one FlowerPlate and defined CGXII medium with either 55 mM glucose or 428 mM ethanol as the sole carbon and energy source, respectively. Repetitive cultures were performed in triplicate on glucose; after each glucose batch, a characterization on ethanol was conducted. **(B)** Growth performance of *C. glutamicum* WT_EtOH-Evo in 24 consecutive batch cultures on ethanol. Mean values and standard deviations from the three parallel cultures are shown as lines and shaded areas, respectively. **(C)** Estimated specific growth rates across the batch cultures on ethanol.

5.5.2 Proteomics shows increased amount of ALDH

To investigate the molecular basis of improved ethanol utilization in the evolved strain *C. glutamicum* WT_EtOH-Evo, proteomic analysis was conducted comparing the evolved strain to the wild type under ethanol growth conditions. The results revealed a notable fourfold increase in the abundance of the NAD-dependent aldehyde dehydrogenase (ALDH) protein, encoded by the *ald* gene (NCgl2698 / cg3096) (Figure 28A). This enzyme catalyzes the conversion of acetaldehyde to acetate, a critical step in ethanol metabolism. In addition to ALDH, key enzymes involved in ethanol assimilation such as phosphotransacetylase (PTA) and phosphoenolpyruvate carboxykinase (PEPCk) were significantly upregulated (Table S7). Conversely, enzymes like pyruvate carboxylase (PCx) and pyruvate:quinone oxidoreductase (PQO) were downregulated, suggesting a shift in metabolic flux towards gluconeogenesis.

The extent of proteomic remodeling in response to ethanol was unexpectedly large compared to glucose growth, indicating a complex adaptive mechanism. In wild-type *C. glutamicum*, ALDH activity is known to be approximately half that of alcohol dehydrogenase (ADHa) [110], implying that the acetaldehyde-to-acetate conversion may represent a rate-limiting step in ethanol assimilation. Given acetaldehyde's reactivity and toxicity, the increased ALDH levels likely facilitate rapid detoxification, enhancing metabolic flux and reducing aldehyde-associated inhibition.

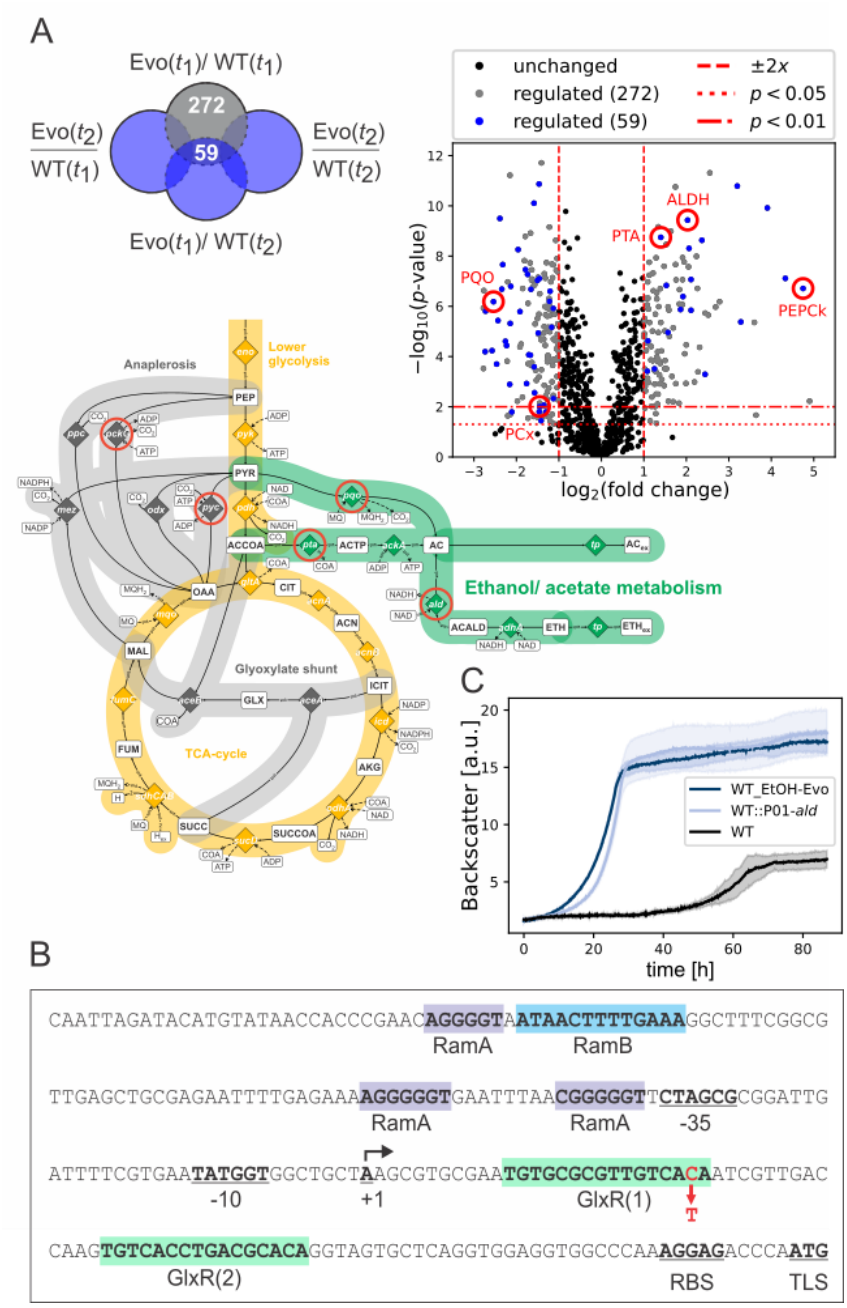

Figure 28 Key mutation of *C. glutamicum* WT_EtOH-Evo identified by genomics and proteomics. **(A)** Differentially expressed proteins in *C. glutamicum* WT_EtOH-Evo compared to the control strain WT during cultivation in defined CGXII medium with 428 mM ethanol as the sole carbon and energy source. Each culture was sampled at two time points: during exponential growth (EVO(*t1*), WT(*t1*)) and stationary phase (EVO(*t2*), WT(*t2*)). Left: Proteins showing significant changes in all four conditions. Right: Volcano plot depicting relative protein abundances between WT_EtOH-Evo and WT at the first sampling point *t1*. Proteins significantly up- or downregulated and associated with ethanol metabolism in *C. glutamicum* are highlighted in red. **(B)** Overview of the *ald* (cg3096) promoter and its regulatory elements. The transcriptional start site (TSS) is indicated by a black arrow and "+1" [163]. The −10 and −35 regions, ribosome binding site (RBS), and translational start site (TLS) are underlined and shown in bold. Regulator binding sites are depicted as colored boxes. The mutation identified in the WT_EtOH-Evo strain is indicated by a red arrow. **(C)** Growth performance of the reengineered strain WT::P01-*ald* compared to WT_EtOH-Evo and the parental wild type. Microscale cultivations were conducted in a FlowerPlate with defined CGXII medium containing 428 mM ethanol as the sole carbon and energy source. Mean values and standard deviations from six replicates are shown as lines and shaded areas, respectively.

5.5.3 Genomics reveals small nucleotide variations

To elucidate the genetic changes underlying the increased ALDH abundance and improved ethanol utilization, genomic DNA of WT_EtOH-Evo was sequenced using Illumina MiSeq technology. Several single nucleotide variants (SNVs) were identified (Table S8). While many mutations were synonymous or located in genes of unknown function unrelated to ethanol metabolism, one mutation of particular interest was found: a G-to-A substitution 68 base pairs upstream of the *ald* gene. The *ald* gene's promoter region, transcribed from approximately 92 – 93 base pairs upstream of the translational start site (Figure 28B), contains regulatory motifs bound by transcription factors such as GlxR, RamA, and RamB [158, 163, 164]. GlxR, the global carbon metabolism regulator, binds two predicted motifs within this region; only the first site (GlxR(1)) shows confirmed binding [158]. Chromatin immunoprecipitation studies further validate GlxR interaction at this promoter [165, 166]. Importantly, these motifs lie downstream of the transcription start site, indicating that GlxR acts as a transcriptional repressor of *ald*.

The identified SNV alters the GlxR(1) binding motif from TGTGCGCGTTGTCACA to TGTGCGCGTTGTCATA (C→T on the reverse strand, Figure 28A), likely disrupting GlxR binding and leading to derepression of *ald* transcription.

5.5.4 Reengineering of WT_EtOH-Evo

To experimentally validate the functional relevance of the identified single nucleotide variant (SNV) located in the *ald* promoter region, this mutation was precisely reintroduced into the wild-type *C. glutamicum* genome using targeted genetic engineering. The resulting strain, designated WT::P01-*ald*, was subjected to growth experiments under ethanol as the sole carbon source alongside the evolved strain WT_EtOH-Evo and the wild-type control. As shown in Figure 28C, the engineered WT::P01-*ald* strain exhibited a significantly improved growth phenotype on ethanol compared to the wild type. The growth kinetics of WT::P01-*ald* closely resembled those of the evolved WT_EtOH-Evo strain, with both strains reaching higher biomass densities and shorter lag phases relative to the parental wild type. This demonstrates that the promoter mutation alone is sufficient to confer enhanced ethanol utilization capacity. These findings confirm that the disruption of the GlxR transcriptional repressor binding site in the *ald* promoter leads to derepression and increased expression of ALDH. The

elevated ALDH abundance accelerates acetaldehyde detoxification and conversion to acetate, alleviating the metabolic bottleneck in ethanol catabolism observed in the wild type. Consequently, this regulatory mutation constitutes a key adaptive mechanism underlying the improved growth performance on ethanol. Nevertheless, while WT::P01-*ald* recapitulates much of the evolved phenotype, other minor mutations identified in the evolved strain may contribute synergistically to full optimization. Further characterization of these mutations will be necessary to comprehensively understand the molecular basis of enhanced ethanol metabolism. Overall, the successful reengineering of the SNV highlights the potential of promoter-targeted genetic modifications as a rational strategy for strain improvement, complementing the untargeted evolutionary approach employed in this study.

5.6 Validation of improved growth performance in stirred tank reactor

A scale-up batch cultivation was carried out using *C. glutamicum* WT_EtOH-Evo in 1-L stirred-tank bioreactors with defined CGXII medium containing 428 mM ethanol as the sole carbon and energy source. The time courses of ethanol and biomass concentrations exhibited the characteristic profile of batch fermentations, with biomass increasing as ethanol was consumed (Figure 29A).

The DO signal showed distinct transient peaks at approximately 6 and 9 hours, which correspond to adjustments in the cascade control system (Figure 29B). Specifically, maximum stirrer speed and gas flow rates were increased to prevent oxygen limitation and maintain aerobic conditions. After roughly 14 hours, ethanol depletion led to an abrupt metabolic shift in the culture, reflected by a prominent starvation peak in the DO signal. Interestingly, a renewed increase in respiration activity was observed after this starvation event, despite no further biomass accumulation. The underlying causes of this respiratory behavior remain unclear and warrant further investigation, potentially relating to maintenance metabolism or alternative electron acceptor utilization.

Process modeling of the STR batch cultivation data enabled extraction of the following key performance indicators:

- A maximum specific growth rate of $\mu_{max} = 0.15 \pm 0.01\ h^{-1}$, confirming the strain's growth performance under these conditions. This value is slightly lower than the previously observed rate in microscale microbioreactor experiments ($\mu_{max} = 0.19 \pm 0.01\ h^{-1}$), which may be attributed to differences in medium composition (the omission of MOPS buffer and urea) and active aeration with air instead of enriched oxygen.
- A specific biomass yield of $Y_{X/S} = 0.45 \pm 0.02\ g_{CDW}\, g_{EtOH}$, showing an efficient build-up of biomass from ethanol. This value is in the same order of magnitude as the literature values for *C. glutamicum*, which was described under aerobic conditions on glucose ($Y_{X/S} = 0.5\ g_{CDW}\, g_{Glc}$) [102].
- A specific ethanol uptake rate of $v_{upt} = 8.45 \pm 0.12\ mmol_{EtOH}\, g_{CDW}^{-1}\, h^{-1}$, reflecting efficient substrate conversion.

Overall, these results demonstrate the successful scale-up of ethanol-based cultivation for the evolved *C. glutamicum* strain, providing a foundation for further process optimization and industrial application. The observed proteomic responses and kinetic parameters contribute valuable insights into the strain's physiology under relevant bioprocess conditions.

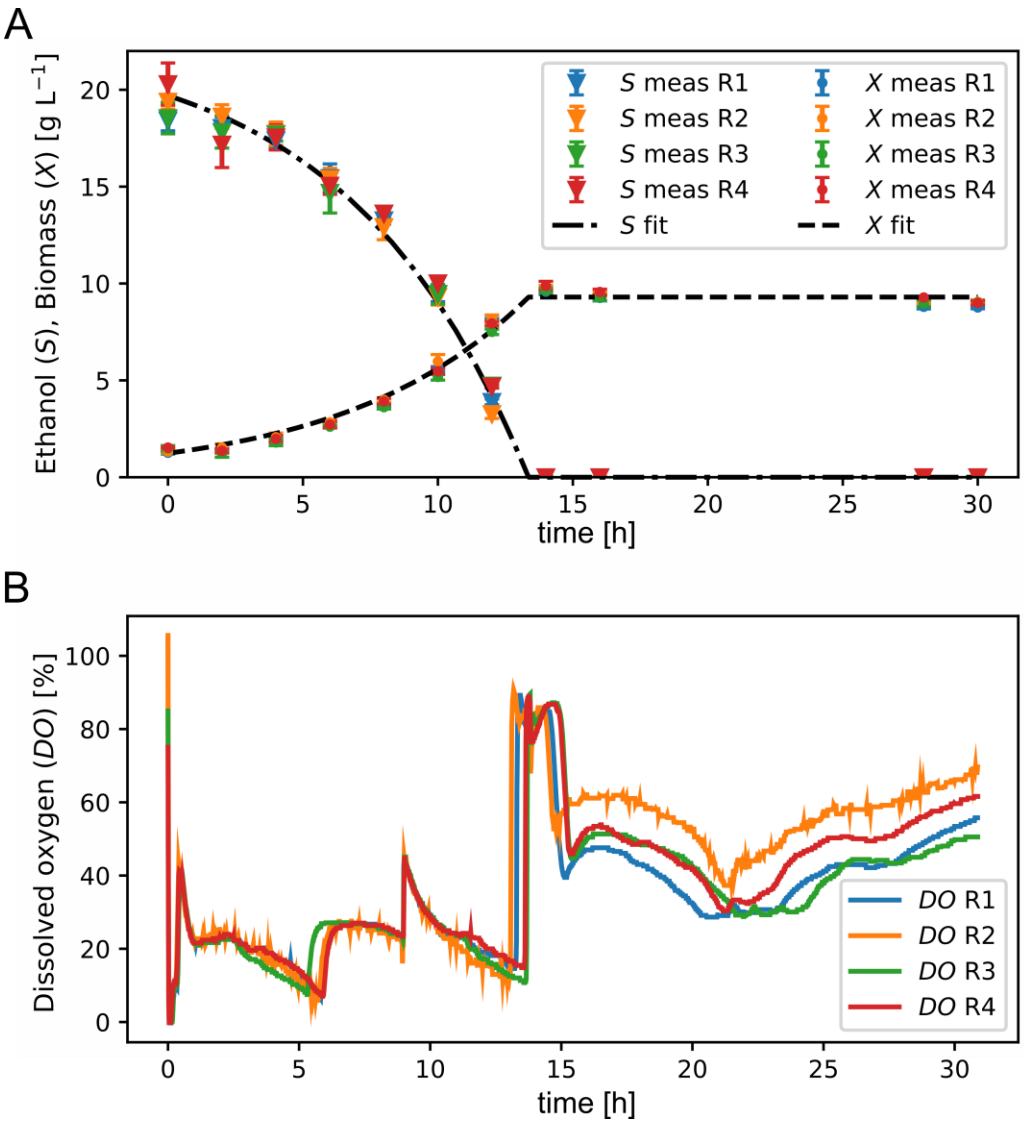

Figure 29 Batch cultivations of *C. glutamicum* WT_EtOH-Evo were carried out in four parallel lab-scale bioreactors using defined CGXII medium supplemented with 428 mM ethanol as the sole carbon and energy source. Samples were collected periodically for offline quantification of ethanol concentration and biomass. These measurements served as input data for fitting the process model.

5.7 Production of 2-oxoglutaric acid from ethanol

To explore ethanol as a sustainable feedstock for bioproduction, its use for 2-oxoglutaric acid synthesis with engineered *C. glutamicum* strains was assessed.

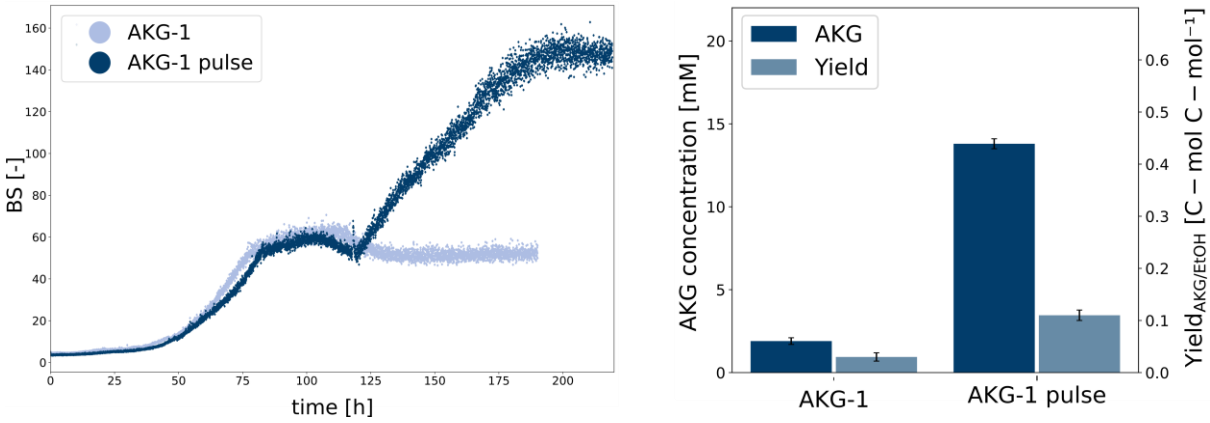

Figure 30 Ethanol-based α-ketoglutarate production in engineered *C. glutamicum*. Growth and AKG production performance of the engineered *C. glutamicum* Δ*gdh* strain (AKG-1) cultivated in defined CGXII medium with ethanol (171 mM) as the sole carbon and energy source. Cultivation was carried out in 500 mL shake flasks with a working volume of 50 mL. Biomass formation was monitored online via backscatter (BS) signal. AKG concentrations and yields were determined from endpoint samples using HPLC. In the "ethanol pulse" experiment, an additional 171 mM ethanol was added after the initial batch phase.

Although the beneficial point mutation identified in the evolved strain WT_EtOH-Evo was shown to significantly enhance ethanol metabolism, technical challenges were encountered when attempting to introduce this mutation into the AKG-1 production strain background via targeted genetic engineering. Ideally, this mutation would be introduced into all AKG-producing strains and systematically evaluated, as described in Chapter 3.2, to fully assess its impact on AKG production from ethanol.

In the absence of engineered AKG-1 derivatives carrying this mutation, the conversion of ethanol to AKG was tested using the parental AKG-1 strain at a relatively low ethanol concentration of 171 mM, similar to conditions used by Arndt et al. [110]. Because higher ethanol concentrations proved inhibitory, a pulse feeding strategy was applied in shake flask cultivations, where after the initial batch phase a second ethanol pulse of 171 mM was added to maintain substrate availability while avoiding excessive toxicity (Figure 30). The biomass signal profiles show that AKG-1 is capable of growth and ethanol metabolism under these pulsed conditions, although growth rates are lower compared to the evolved strain. Importantly, AKG production was observed and confirmed by HPLC analysis, which also

detected other minor byproducts. While productivity and ethanol tolerance remain limited in the AKG-1 strain, these findings confirm the feasibility of bioconversion of ethanol to AKG. They provide a foundation for future efforts to transfer the beneficial ALE-derived mutations into AKG and other production strains and optimize fermentation processes for improved yield and productivity using ethanol as feedstock.

6. Summary

This dissertation presents the development of an efficient microbial production process for the sustainable production of AKG from renewable carbon sources using *C. glutamicum*. The work combines process engineering, metabolic optimization, and advanced automation, leading to the establishment of a scalable AKG production processes with high yield and purity.

In the first part, a high-yield AKG production process from sugar beet molasses, a sugar-rich first-generation agro-industrial side stream, was developed. The bioprocess development, including strain engineering, automated high-throughput screening, scale-up, and DSP, resulted in an AKG titer of 460 mM and a yield of 0.59 C-mol AKG per C-mol sucrose, representing the highest values reported for *C. glutamicum* to date. The established liquid-liquid extraction and crystallization protocol enabled recovery of AKG with efficiency of 87.1 %, corresponding to an overall process yield of 0.55 $C_{mol}\,C_{mol}^{-1}$ (0.56 g g^{-1}), with a final product purity over 93 %. Project partners in the BioPlastiCycle project were able to further process and successfully polymerize this purified bio-based AKG to novel polyketone esters. These results not only demonstrate the technical suitability of molasses for industrial-scale AKG production but also the necessary interdisciplinarity for the development of sustainable products.

To further increase sustainability of bio-based AKG production, the second part explored the use of 2nd gen. lignocellulosic hydrolysate as a carbon source. Defined glucose-xylose mixtures were successfully converted into AKG with conversion yields of $Y_{P/S}$ = 0.12 ± 0.01 C-mol C-mol^{-1}. In contrast, real lignocellulosic hydrolysates posed additional challenges. It was shown that components present in the hydrolysate exert an inhibitory effect on *C. glutamicum*, leading to a pronounced extension of the lag-phase and a complete absence of AKG production.

Finally, this work explored the use of ethanol as a carbon source. Overcoming the intrinsic metabolic limitations of wild-type *C. glutamicum* on ethanol, an automated long-term rbALE workflow was developed. The application of this workflow resulted in the evolved strain WT_EtOH-Evo, which exhibited a marked improvement in ethanol utilization. This includes

tolerance of ethanol concentrations above 428 mM, a more than threefold increase in specific growth rate compared to the parental strain, and robust performance in laboratory-scale bioreactors with a maximum specific growth rate μ of 0.15 h^{-1} and a biomass yield of 0.45 $g\,g^{-1}$. Proteomic and genomic analyses as well as reengineering confirmed that a key regulatory mutation in the *ald* promoter increased ALDH expression, underpinning the improved phenotype.

Initial proof-of-concept experiments established the feasibility of producing AKG from ethanol, highlighting the broader potential for improved valoration of CCU-derived feedstocks through metabolic evolution.

Overall, this work demonstrates the flexibility and robustness of *C. glutamicum* as a cell factory for the sustainable production of AKG and paves the way for the broader biotechnological utilization of both traditional and next-generation renewable feedstocks. The workflows and strategies established here can contribute directly to the realization of a circular, resource-efficient bioeconomy.

7. Outlook

7.1 AKG production from sugar beet molasses

The process developed in this work demonstrated promising titers and established a straightforward purification concept for AKG production from sugar beet molasses. However, several areas require further optimization before an industrial application can be envisioned.

A crucial next step towards industrial-scale, bio-based AKG production is a comprehensive techno-economic analysis (TEA). Given that AKG is a comparatively low-value product with a market price in a range of 33 000 – 40 000 USD t^{-1}, profitability can only be expected at very large production scales, where the break-even point can be reached [167]. Even tough molasses is a side stream, current prices in ranges of 320 – 450 USD t^{-1} are in the same range than glucose and sucrose [168]. Additional expenses for fermentation, DSP, and utilities are more difficult to estimate without a detailed techno-economic analysis. Based on preliminary estimations, economic feasibility is likely to require the processing of at least ten tons of substrate per batch, corresponding to production scales in the range of 50 – 100 m^3 bioreactors.

Upstream process optimization should focus on investigation of the observed co-substrate limitation. A deeper understanding of the beneficial “molasses effect” could open further avenues for process improvement, including the recreation of defined or synthetic molasses compositions for more controlled fermentations. Given that this effect appears to be driven by a cheap component, its identification could provide an economically attractive strategy for process optimization. In addition, there is substantial potential to optimize the composition of the CGXII medium, ideally eliminating it entirely to reduce costs. Ultimately, process scale-up to larger reactors will be necessary to validate performance under industrially relevant conditions.

Downstream processing remains a significant challenge, particularly due to the large solvent volumes required and the generation of waste salts through acidification. Transitioning to a continuous downstream process, analogous to in situ product removal, could offer notable advantages. Even more promising may be the integration of pH-shift technology as outlined in Chapter 1.3.1 Figure 8C, which would further reduce waste generation. Depending on the

intended application of AKG, further decolorization and refinement steps may be needed to achieve the desired product purity. Additionally, downstream operations must be scalable to match future upstream improvements.

7.2 AKG production from 2nd gen. feedstock

The work on lignocellulosic feedstocks highlighted both the potential and the limitations of using second-generation hydrolysates for AKG production. Defined glucose-xylose mixtures could be successfully converted into AKG, demonstrating the basic feasibility of valorizing C5 and C6 sugars with engineered strains. In contrast, the use of real lignocellulosic hydrolysates revealed significant challenges: the presence of inhibitory compounds caused extended lag-phases and, in some cases, complete inhibition of growth and AKG production. Furthermore, the sequential utilization of carbon sources poses a challenge for large-scale process design such as fed-batch fermentations, since in the feeding phase only glucose is consumed while xylose accumulates. While successful fed-batch fermentations of *C. glutamicum* with the Weimberg pathway have been reported, these employed pure xylose as the feed substrate [82]. This approach, however, does not reflect the composition of a realistic xylose-containing waste stream. These findings emphasize that, beyond metabolic engineering, robust process strategies are required to overcome the complexity and variability inherent to lignocellulosic side streams.

Possible approaches include enabling true co-utilization of glucose and xylose or implementing modified feeding strategies, such as sequential or pulse feeding, where a new feed pulse is only initiated after complete xylose consumption.

In addition, a deeper understanding of the inhibitory compounds present in lignocellulosic hydrolysates, such as furfural and HMF, will be essential. These inhibitors may act synergistically, further exacerbating their toxic effects. Future strategies could therefore include targeted metabolic engineering approaches to introduce or enhance detoxification pathways, enabling the degradation or binding of such inhibitors. Complementarily, untargeted approaches such as ALE could accelerate the development of strains with increased tolerance or novel catabolic capacities for these compounds.

Beyond technical optimization, the economic and sustainability aspects of 2nd gen. feedstocks must also be critically considered. While 2nd gen. materials are often expected to reduce feedstock costs, additional pretreatment steps and substrate heterogeneity frequently diminish this advantage compared to first-generation sugars. At the same time, they offer clear sustainability benefits by avoiding direct competition with food production and reducing land use requirements. A comprehensive techno-economic analysis and life cycle assessment will therefore be essential to evaluate the true feasibility and environmental performance of AKG production from lignocellulosic substrates. In this context, CCU-derived feedstocks such as ethanol may represent a complementary route to further decouple chemical production from agricultural resources, although their competitiveness currently depends on technological progress and regulatory incentives.

7.3 AKG production with improved ethanol utilization

Chapter 5 demonstrated the general feasibility of AKG production from ethanol using *C. glutamicum*. However, substantial further research is required to enable an efficient and industrially relevant process. A key priority for future studies will be the systematic integration of the beneficial mutation identified during ALE into all established AKG production strains (AKG-1 – AKG-4), followed by comprehensive screening to identify the most promising candidates.

In addition to genetic optimization, process development should focus on minimizing the formation of undesired by-products such as acetate and succinate, in order to improve overall yields and simplify DSP. As with the molasses-based process, a thorough TEA is essential to assess the economic feasibility of AKG production from ethanol. Furthermore, it will be critical to evaluate whether ethanol-based production routes offer a genuine advantage in terms of sustainability, for example through a detailed life cycle analysis.

Beyond AKG production, the improved metabolic capacity of *C. glutamicum* for ethanol utilization may be broadly applicable for the synthesis of other platform chemicals.

7.4 Long-term repetitive batch ALE

The methodological advances introduced in this work, particularly the development of a workflow for long-term performance of rbALE, now enable the theoretically unlimited execution of rbALE experiments. By overcoming the previous technical limitations of the 48-well plate format and implementing automated well recycling without manual intervention, this development eliminates a major bottleneck for extended laboratory evolution studies.

This innovation paves the way for evolving microbial strains over substantially more generations, thereby increasing the likelihood of acquiring beneficial mutations. Further expanding the platform to accommodate even greater degrees of parallelization could accelerate evolutionary adaptation. For example, future developments might explore the feasibility of running multiple ALE groups in parallel, such as managing 24 evolution lines using only two wells, or by directly reseeding cultures into the same well after brief storage on the robotic deck.

For the design of effective ALE strategies, establishing a direct coupling between growth and product formation remains a crucial objective, as previously demonstrated by Stella et al. [169]. Such coupling ensures that only strains exhibiting both high growth and high production are enriched during the evolutionary process.

Importantly, the modular nature of this advanced rbALE workflow provides a blueprint for adapting and scaling ALE experiments to a broad range of microorganisms, substrates, and target products far beyond AKG. This methodological framework is readily transferable to other industrially relevant host organisms and enables the exploration of novel substrate-product combinations, thus greatly expanding the scope and impact of automated laboratory evolution in microbial biotechnology.

8. Materials and methods

8.1 Materials

8.1.1 Strain construction and maintenance

The bacterial strains utilized in this study (see Table 5) were engineered by Daniela Höppner from the 'Synthetic Cell Factories' research group at IBG-1, Forschungszentrum Jülich. All enzymes required for the experiments were obtained from Thermo Scientific (Schwerte, Germany). Standard molecular cloning techniques, including PCR and Gibson assembly, were applied as described by Gibson et al. and Sambrook & Russell [170, 171]. Transformation of *E. coli* DH5α was carried out using the heat shock method at 42 °C for 90 seconds, with chemically competent cells prepared via the RbCl protocol. *C. glutamicum* was transformed through electroporation, followed by a heat shock at 46 °C for 6 minutes in BHIS medium (BHI enriched with 90 g L^{-1} sorbitol). Cell regeneration was performed on a rotary shaker: 37 °C for 60 minutes for *E. coli*, and 30 °C for 120 minutes for *C. glutamicum* [102, 172]. Targeted gene deletions, including the in-frame removal of glutamate dehydrogenase (*gdh*), subunits of glutamine-2-oxoglutarate aminotransferase (*gltB*), the *odhA* gene encoding part of the oxoglutarate dehydrogenase complex, and the truncation of the *mscCG* mechanosensitive channel, were achieved using two-step homologous recombination with the pK19*mobsacB* plasmid system [131]. Verification of the deletion plasmids was performed by restriction enzyme analysis, and successful gene deletions were confirmed through colony PCR. All oligonucleotides used in this study can be found in the Appendix (Table S9).

Table 3 Bacterial strains and plasmids used in this study.

Strain or plasmid	Relevant characteristics	Source or Reference
E. coli		
DH5α	F$^-$ Φ80*lacZ*ΔM15 Δ(*lacZYA- argF*)U169 *recA1 endA1 hsdR17* (rK-, mK+) *phoA supE*44λ- *thi*-1 *gyrA96 relA1*	Invitrogen (Karlsruhe, Germany)
C. glutamicum		
ATCC 13032 (WT)	Biotin-auxotrophic wild type	Abe et al., 1967
WT_EtOH-Evo	Derivative of ATCC 13032 with (among others) G→A mutation 68 bp upstream of the *ald* (cg3096) start codon resulting from ALE	This work
WT::P01-*ald*	Derivative of ATCC 13032 with G→A mutation is introduced 68 bp upstream of the *ald* (cg3096) start codon	This work
P_{O6}-*iolT1*	Derivative of *C. glutamicum* ATCC 13032 with two mutations in the promoter of *iolT1* (cg0223) relative to the start codon at position -113 (A to G) and -112 (C to G)	Brüsseler et al., 2018
P_{O6}-*iolT1* Δ*gdh* (AKG-1)	Derivative of *C. glutamicum* ATCC 13032 P_{O6}-*iolT1* with in-frame deletion of *gdh* (cg2280)	This work
AKG-1 *mscCG*' (AKG-2)	Derivative of *C. glutamicum* AKG-1 with C-terminal truncation of 345 bp in *mscCG* (cg1434)	This work
AKG-2 Δ*gltB* (AKG-3)	Derivative of *C. glutamicum* AKG-2 with in-frame deletion of *gltB* (cg0229)	This work
AKG-3 Δ*odhA* (AKG-4)	Derivative of *C. glutamicum* AKG-3 with in-frame deletion of *odhA* (cg1280)	This work
P_{O6}-*iolT1*-xyl	Derivative of *C. glutamicum* P_{O6}-*iolT1*-xyl with plasmid pEKEx3-$xylXABCD_{opt}$	This work
AKG-1-xyl	Derivative of *C. glutamicum* AKG-1 with plasmid pEKEx3-$xylXABCD_{opt}$	This work
AKG-2-xyl	Derivative of *C. glutamicum* AKG-2 with plasmid pEKEx3-$xylXABCD_{opt}$	This work
AKG-3-xyl	Derivative of *C. glutamicum* AKG-3 with plasmid pEKEx3-$xylXABCD_{opt}$	This work
AKG-4-xyl	Derivative of *C. glutamicum* AKG-4 with plasmid pEKEx3-$xylXABCD_{opt}$	This work
Plasmids		
pK19*mobsacB*	Kan^r; vector for allelic exchange in *C. glutamicum* (pK18 oriV_{Ec} *sacB lacZα*)	Schäfer et al., 1994
pK19*mobsacB*-P_{01}-*ald*	Kan^R; derivative of pK19*mobsacB* for mutating the promoter in front of *ald* (cg3096). The G→A mutation is introduced 68 pb upstream of the ALD start codon.	This work

pK19*mobsacB*-Δ*gdh*	pK19*mobsacB* derivative for in-frame deletion of *gdh* (cg2280)	This work
pK19*mobsacB*-Δ*gltB*	pK19*mobsacB* derivative for in-frame deletion of *gltB* (cg0229)	This work
pK19*mobsacB*-Δ*mscCG'*	pK19*mobsacB* derivative for C-terminal truncation of 345 bp in *mscCG* (cg1434)	This work
pK19*mobsacB*-Δ*odhA*	pK19*mobsacB* derivative for in-frame deletion of *odhA* (cg1280)	Brüsseler et al., 2019
pEKEx3-*xylXABCD*$_{opt}$	Spec^R; pEKEx3 derivative for the heterologous expression of *xylXABCD* from *C. crescentus* in *C. glutamicum*	(Radek et al., 2017)

8.1.2 Cultivation media and other chemicals

All main cultivations were carried out in defined CGXII medium, following the formulation described by Keilhauer [173]. Modifications regarding carbon sources or additional supplements are detailed in the result Chapters 3 and 4. The standard composition of CGXII medium contained per liter of deionized water: 1 g K_2HPO_4, 1 g KH_2PO_4, 13.25 mg $CaCl_2$ • 2 H_2O, 0.25 g $MgSO_4$ • 7 H_2O, 10 mg $FeSO_4$ • 7 H_2O, 10 mg $MnSO_4$ • H_2O, 0.02 mg $NiCl_2$ • 6 H_2O, 0.313 mg $CuSO_4$ • 5 H_2O, 1 mg $ZnSO_4$ • 7 H_2O, 0.2 mg biotin and 30 mg protocatechuate. For cultivations without pH control, 5 g urea and 42 g MOPS were added.

For stock preparation, CGXII salts were dissolved in 900 mL of ultrapure water, and the pH was adjusted to 7.2 using 5 mol L^{-1} KOH pellets and a pH measurement device (SevenEasy, Mettler Toledo). The final volume was then adjusted to 1 L with water. Trace elements were first dissolved in 50 mL of ultrapure water, with 1 mol L^{-1} HCl added as necessary to ensure complete solubility. Protocatechuic acid was solubilized in 10 mL of 1 mol L^{-1} NaOH and subsequently diluted to a total volume of 50 mL with water. Separate stock solutions of biotin, $MgSO_4$, and $CaCl_2$ were also prepared in ultrapure water. Depending on component stability, sterilization was performed either by filtration through 0.2 µm pore-size membranes or by autoclaving at 120 °C for 20 minutes. Unless otherwise specified, all reagents used were of analytical grade and obtained from Sigma (Steinheim, Germany), Merck (Darmstadt, Germany), or Carl Roth (Karlsruhe, Germany).

8.2 Cultivation methods

8.2.1 Shake flask cultivations

Shake flask cultivations were performed under standardized conditions using an orbital shaking incubator (Multitron®, Infors HT, Germany) operated at 30 °C and 250 rpm, with a shaking diameter of 25 mm. Depending on the desired working volume, either 100 mL or 500 mL unbaffled Erlenmeyer flasks were employed, filled with 10 mL or 50 mL of medium, respectively. In cases requiring larger volumes (e.g., 100 mL), 1000 mL flasks were also used. Shake flask cultivations were primarily used for cryo-stock preparation and as pre-culture systems for subsequent experiments in shake flasks, microbioreactors, or bioreactors. A standardized two-step pre-culture protocol was followed unless stated otherwise. The first pre-culture was initiated by inoculating 10 mL of Brain Heart Infusion (BHI) medium in a non-baffled flask with an aliquot from a glycerol stock stored at -80 °C. After approximately 6 hours of incubation, 500 µL of this culture were transferred into a second pre-culture containing 50 mL of CGXII medium in a baffled flask, which was incubated for roughly 16 hours. Following growth, cells were harvested by centrifugation (4000 × g, 10 min, 4 °C), washed once with sterile 0.9 % (w v^{-1}) NaCl solution and resuspended in 0.9 % (w v^{-1}) NaCl solution for inoculation of the main culture. Unless specified otherwise, all main cultures were inoculated to an initial OD at 600 nm of 0.2.

8.2.2 Microbioreactor cultivation

For the characterization of *C. glutamicum* strains, small-scale cultivations were conducted using the BioLector® microbioreactor system (Beckman Coulter Life Sciences, CA, USA). Experiments were performed in 48-well FlowerPlates® (type BOH-1 with integrated optical sensors) with a working volume ranging from 800 to 1000 µL per well. Cultivations were carried out in CGXII medium supplemented with 20 g L^{-1} glucose, sucrose or molasses. The cultivation conditions were set to 30 °C, 1300 rpm shaking speed with a 3 mm orbit diameter, and a maintained relative humidity of over 80 % to reduce evaporation. Wells were sealed with gas-permeable, self-adhesive barrier films (F-GP-10 and F-GPRS48-10, m2p-labs, Baesweiler, Germany), allowing for sufficient oxygen transfer while minimizing liquid loss. The BioLector platform enables quasi-continuous monitoring of biomass via BS [174], as well as real-time measurement of pH and DO through integrated fluorescence-based optodes

positioned at the bottom of each well. Cultures were inoculated to an initial OD of 0.2 from actively growing shake flask pre-cultures.

8.2.3 Automated sampling and repetitive batch procedure

For time-resolved sampling, the Mini Pilot Plant technology for high-throughput microbial phenotyping was used [175, 176]. This setup facilitated automated "sacrifice" sampling of cultivation wells at defined time points, including cell separation via centrifugation and immediate storage of culture supernatants at 4 °C on a cooled platform. Subsequently, the supernatants were filtered using a 96-well AcroPrep filter plate (Pall Corporation, NY, USA), frozen at -20 °C, and later thawed, diluted with MilliQ water (dilution factor 0.5 to 0.1), and analyzed by HPLC as described in the following sections.

Automated repetitive batch cultivations were performed using the Mini Pilot Plant as described above, or an equivalent setup based on the PerkinElmer Janus robotic liquid handler (Waltham, Massachusetts, United States). Each platform is equipped with an eight-channel liquid handling arm with fixed tips and a robotic gripper for plate transport. Cultivations were carried out in 48-well FlowerPlates®, enabling high-throughput parallel processing. Real-time process control was achieved through the use of the integrated software agents *RoboLector* and *WinPrep*, which continuously monitored BS signals and triggered predefined actions based on logic rules implemented via Python scripts.

An advanced, long-term miniaturized ALE protocol was implemented based on the method proposed by Radek et al. [126]. For this purpose, individual wells on a 48-well microtiter plate were grouped into defined sequences, each representing a discrete ALE trajectory. Cultivations began in the first well of each sequence, which was inoculated from a shake flask pre-culture (as described in Section 7.2.1) and standardized to a starting OD_{600} of 0.2. The BS signal in each well was recorded every 15 minutes. Upon reaching 60 % of the maximum observed BS signal, the system automatically inoculated the subsequent well in the sequence with 50 µL of culture from the triggering well and added 800 µL of fresh medium. This process continued through the remaining wells of the sequence. To overcome the limitation imposed by the finite number of wells, a protocol for well recycling was developed and implemented.

As this extension constitutes a methodological innovation within the scope of this study, its detailed procedure and evaluation are provided in Chapter 4.1 of the results section.

8.2.4 Stirred tank reactor cultivations

Bioreactor cultivations were conducted using a parallel bioreactor system (DASGIP, Eppendorf, Jülich, Germany) equipped with two six-blade Rushton turbines and online sensors for pH (405-DPAS-SC-K80/225, Mettler Toledo, Urdorf, Switzerland), DO (Visiferm DO 225, Hamilton, Bonaduz, Switzerland), and exhaust gas composition (GA4, DASGIP). Temperature and aeration were maintained at 30 °C and 0.5 vvm, respectively. The pH was controlled at 7 through the automated addition of either 5 mol L^{-1} NH_4OH or 5 mol L^{-1} H_3PO_4 (or in some setups using 25 % $NaOH{\cdot}H_2O$ and 30 % H_3PO_4). The process was managed by DASGIP Control 5.6.0 software. DO concentration was regulated to maintain a minimum of 30 % using a two-step cascade strategy. Initially, DO levels were maintained by adjusting the stirrer speed between 400 and 1200 rpm (up to 1400 rpm in some experiments). If DO levels exceeded 80 %, the aeration rate was increased incrementally up to 1 vvm. Cultivations were inoculated from exponentially growing pre-cultures, which were previously prepared from cryo-preserved stocks in shake flasks. Unless otherwise stated, the main cultures were inoculated to an OD_{600} of 1, using 20 mL of inoculum. At the start of cultivation, stirrer speed and gas flow were initially set to 400 rpm and 0.1 vvm, respectively. To complete the initial culture volume of 1 L, 1 mL of antifoam agent was added immediately after inoculation. The batch phase was monitored via DO levels, with a sharp increase in the DO signal indicating depletion of the carbon source. This was further verified by HPLC analysis. Fed-batch operation of the AKG production process from molasses began approximately 94 hours after the start of cultivation, using a feed solution prepared from molasses containing 328 g L^{-1} sucrose. The molasses solution was diluted with purified water and sterilized by autoclaving at 121 °C for 20 minutes. The calibrated feed pump delivered this solution at a rate of 5 mL h^{-1}. Feeding was paused after 41.8 hours and resumed after approximately 8 hours. The entire process was terminated after 164 hours.

8.3 Purification methods

8.3.1 Recovery: Cell separation

To initiate the purification of AKG from the fermentation broth derived from molasses-based cultivations, cells and suspended solids were first removed. This was achieved by centrifugation (Avanti JXN-26, Beckman Coulter Life Sciences, CA, USA) followed by filtration to obtain a clarified supernatant. These steps served to eliminate biomass and other particulate matter that could interfere with the subsequent liquid-liquid extraction.

8.3.2 Isolation: Liquid-liquid extraction

The clarified supernatant was acidified to a pH of approximately 1 using hydrochloric acid to ensure protonation of both carboxyl groups of the dicarboxylic acid AKG. This step exploited the low pKa value of AKG (2.47), increasing its partitioning into the organic phase during extraction. Subsequently, ethyl acetate was added in a volume ratio of up to 5:1 (solvent to aqueous phase) in a separatory funnel. The mixture was thoroughly swirled to allow efficient mass transfer between phases. Upon settling, three phases were observed: a lower aqueous phase, a middle viscous interphase, and an upper organic phase. The aqueous phase was subjected to two additional extraction rounds with fresh ethyl acetate, while the viscous interphase was discarded. The organic layers containing the extracted AKG were collected and stored for further processing. A comparative study on four different extraction strategies revealed that sequential extractions using fresh solvent significantly increased the extraction efficiency.

8.3.3 Purification: Concentration

The combined organic phases were concentrated using a rotary evaporator (Rotavapor R-100, Büchi Labortechnik GmbH, Essen, Germany) to remove ethyl acetate, which was collected and recycled. The evaporation step yielded a concentrated solution of AKG, which was then further processed. This concentration not only facilitated downstream crystallization but also minimized solvent use and allowed for partial solvent recovery, improving process sustainability.

8.3.4 Polishing: Crystallization

The concentrated solution was cooled to 4 °C to induce crystallization of AKG. Crystals were formed and subsequently analyzed for purity by GC-ToF-MS.

8.4 Analytical methods

8.4.1 High-performance liquid chromatography measurements

Supernatants from bioreactor cultivations were obtained by centrifugation at 4000 × g for 10 minutes at 4 °C and subsequently sterile-filtered using cellulose acetate syringe filters (0.2 µm pore size, DIA-Nielsen, Düren, Germany). Filtered samples were either analyzed immediately or stored at -20 °C. Prior to HPLC analysis, frozen samples were thawed at room temperature, mixed thoroughly, and diluted 1:2 to 1:50 with high-purity water (Milli-Q). For high dilutions, multiple 1:10 steps were performed. Quantification of sugars (e.g., glucose, sucrose) and organic acids (e.g., acetate, succinate, pyruvate, α-ketoglutarate, lactate), was carried out using isocratic ion exchange chromatography. Separation was performed on a polymer-based cation exchange column (Isera Metab-AAC HPLC, 300 × 7.8 mm (Isera, Düren, Germany) using 0.1 M H_2SO_4 as the mobile phase at a flow rate of 0.6 mL min^{-1}. The column compartment was maintained at 45 – 80 °C depending on the target analyte. Injection volumes ranged from 10 to 20 µL. Detection was conducted using a refractive index detector (RID) and a diode array detector (DAD) at wavelengths of 215 nm or 230 nm, depending on the analyte.

For ethanol quantification, RID-based detection was used. A dilution series of an ethanol standard (1370 mM to 10.7 mM, 1:2 steps) was prepared and measured alongside samples.

Calibration curves were established for all measured compounds using external standards prepared from sterile-filtered 100 mM stock solutions stored at -20 °C. Data evaluation and uncertainty estimation were conducted using Python. Peaks were identified based on retention times and UV/Vis spectra compared to standards. Eight-step dilution series were measured and analyzed by linear regression using the *linregress* function from the scipy.stats Python package (v1.10.1). Sample concentrations were then calculated using the fitted slope and intercept. For signals outside the calibration range, additional dilutions were performed. Concentrations below the detection limit were reported as “not detectable”.

8.4.2 Quadrupol-Time-of-Flight (Q-ToF) mass spectrometry

Proteomic profiling of strains P_{O6}-*iolT1* and AKG-1 to AKG-3 cultivated on glucose, sucrose, and molasses was performed using biological triplicates. Cells were grown in FlowerPlates containing CGXII medium supplemented with the respective carbon source, as described in Section 7.2.2. Cultures were harvested during the exponential growth phase. Sampling and processing at this stage were conducted automatically using a Mini Pilot Plant. Cells were collected and temporarily stored on an intermediate plate to enable accurate pipetting. After centrifugation at 4,500 × g for 5 minutes, the pellets were washed with 0.9 % ($w\,v^{-1}$) NaCl solution and centrifuged again under identical conditions. The resulting pellets were manually transferred into designated tubes for proteomics and stored at -80 °C until analysis. Proteomic measurements were initiated with cell lysis, as outlined below.

For proteomic analysis of ethanol-grown cultures, both the evolved strain *C. glutamicum* WT_EtOH-Evo and the wild-type reference were cultivated in CGXII medium containing 171 mM ethanol. Cultivations were carried out in shake flasks at 30 °C and 250 rpm using biological triplicates. Sampling was performed at two predefined time points representing exponential (Evo(*t1*) = 28.25 h, WT(*t1*) = 52.5 h) and stationary (Evo(*t2*) = 52.5 h, WT(*t2*) = 74.0 h) growth phases. Cells were harvested by centrifugation at 12,500 × g for 10 minutes, followed by a wash step with 0.9 % ($w\,v^{-1}$) NaCl solution and another centrifugation under the same conditions.

Cell pellets were resuspended in a lysis buffer composed of 50 mM potassium phosphate buffer (pH 8.0), 2 mM EDTA, 2 mM DTT, and a complete protease inhibitor cocktail (1697 498, Roche Applied Science, Basel, Switzerland). Cell disruption was carried out using a Precellys homogenization system (Bertin Instruments, Montigny-le-Bretonneux, France) with a mixture of 0.1 – 0.2 mm glass beads and two 5 mm glass beads, applying three cycles of 30 seconds each at maximum speed. The supernatant containing crude protein extracts was collected and stored at -20 °C until further processing. Protein concentrations were determined via the Bradford assay (B6916, Sigma Aldrich, USA), using BSA as a standard. Untargeted LC-MS/MS analyses were conducted using an Infinity 1260 HPLC system (Agilent Technologies) coupled to a Q-ToF 6600 mass spectrometer (Sciex, Darmstadt, Germany), following procedures described previously [177]. Chromatogram acquisition and peak integration were carried out

using PeakView 2.1 software (Sciex), while protein identification was performed using ProteinPilot 5.1 (Sciex). Statistical comparisons using t-tests were conducted in MarkerView (Sciex). Further data processing and functional annotation were performed in Python, utilizing standard packages such as Biopython [178].

8.4.3 GC-ToF-MS analysis

For untargeted feedstock and product analysis, 130 µL and 13 µL of liquid or masses of less than 2 mg of solid particle were lyophilized using a freeze dryer (Christ LT-105, Martin Christ, Osterode am Harz, Germany). The dried samples were stored at -20 °C until further processing. Prior to gas chromatography-mass spectrometry (GC-MS) analysis, samples were derivatized in a two-step reaction: first, 50 µL of O-methylhydroxylamine hydrochloride in pyridine was added and incubated at 30 °C for 90 minutes at 600 rpm in a thermomixer (Eppendorf, Jülich, Germany). Subsequently, 80 µL of N-Methyl-N-(trimethylsilyl)trifluoroacetamide was added, and the mixture was incubated for another 90 minutes at 40 °C and 600 rpm.

The derivatized components were analyzed using a gas chromatography system (Agilent 6890N or Agilent 8890N, Agilent Technologies, Santa Clara, CA, USA), coupled to a high-resolution time-of-flight mass spectrometer (Waters Micromass GCT, Waters, Eschborn, Germany, or LECO GCxGC HRT+4D, LECO, Mönchengladbach, Germany). The analytical setup included a double split/splitless (SSL) injector and was equipped with a PAL3 autosampler (LECO). Method parameters and sample processing followed the protocol established by Paczia et al. [179]. Chromatographic and spectral data acquisition were controlled using ChromaToF software (LECO). Metabolite identification was performed by comparing baseline-corrected fragment spectra with entries from three reference databases: the in-house JuPoD library, the National Institute of Standards and Technology (NIST, Gaithersburg, USA) database, and the Golm Metabolome Database (GMD, Max Planck Institute for Molecular Plant Physiology, Golm, Germany).

8.4.4 Genomic sequencing

For whole-genome sequencing, genomic DNA was extracted from selected *C. glutamicum* samples, including the evolved strain *C. glutamicum* WT_EtOH-Evo. To isolate the evolved

strain, single colonies were obtained from agar plates and cultivated in brain heart infusion broth (BHI) (Carl Roth GmbH, Germany) in 50 mL shake flasks with a filling volume of 10 percent at 30 °C and 250 rpm. This preculture served to inoculate CGXII medium, and cells were harvested at the end of the exponential phase. Following centrifugation, cells were washed with 0.9 percent (w v^{-1}) sterile NaCl solution, centrifuged again, and the resulting pellet was used for genomic DNA extraction. DNA was isolated using the NucleoSpin Gel and PCR Clean-up kit (Macherey-Nagel, Germany), following the manufacturer's protocol.

Sequencing libraries were then prepared using the TruSeq DNA PCR-Free Sample Preparation Kit (Illumina). Genomic DNA (4 µg) was fragmented to an average size of 550 base pairs using the Bioruptor Pico sonication system (Diagenode). A 2 µg aliquot of the fragmented DNA was subjected to end repair and size selection using magnetic beads. A single adenine residue was ligated to the 3' ends of the fragments, and Illumina paired-end index adapters were added. The resulting indexed libraries were quantified using qPCR with the KAPA Library Quantification Kit (Peqlab), normalized to a concentration of 2 nM, and pooled. The pooled libraries were diluted to a final concentration of 10 pM and sequenced using a paired-end run (2 × 150 nucleotides) on an Illumina MiSeq system.

An automated workflow for sequence read analysis and variant identification was implemented using tools available in the CLC Genomics Workbench (Qiagen Aarhus A/S). Adapter sequences were removed, and reads were quality-trimmed to exclude bases and reads with a Phred quality score below 30. High-quality reads were aligned to the reference genome of *C. glutamicum* ATCC 13032 (GenBank accession number BX927147) using default alignment parameters. Single nucleotide variants, multiple nucleotide variants, insertions and deletions, as well as structural variants, were identified using quality-based variant calling tools. Detected variants from each sample were compiled using Microsoft Excel and further analyzed to evaluate their occurrence, frequency, and overlap across the different datasets.

8.4.5 Determination of cell dry weight

Cell dry weight (CDW) was determined gravimetrically using 2 mL samples collected from bioreactor cultivations. Prior to the experiment, 2 mL reaction tubes were labeled, pre-dried at 80 °C for at least 24 to 48 hours, allowed to equilibrate to room temperature in a desiccator,

and subsequently weighed. Upon sampling via the bioreactor sampling port, the culture broth was transferred into these pre-weighed tubes and centrifuged at 13,000 × g for 10 minutes using a benchtop centrifuge (e.g., "BIOFUGE PICO", Heraeus, Hanau, Germany). The supernatant was either discarded or stored at -20 °C for further analysis. The resulting cell pellet was washed to remove residual medium components using 0.9 % (w v^{-1}) NaCl or phosphate-buffered saline. The pellet was resuspended in 1 mL of the washing solution, centrifuged again under the same conditions, and the supernatant was discarded. This washing step was repeated once if necessary. The washed pellets were then dried in a laboratory drying oven at 80 °C for at least 16 hours, but not exceeding 24 hours, ensuring constant weight. After cooling to room temperature in a desiccator, the tubes were weighed again. Throughout the entire process, sample tubes were handled exclusively with gloved hands to prevent contamination or moisture uptake. The CDW (g/L) was calculated from the mass difference before and after drying, normalized to the sampled culture volume.

8.4.6 Determination of optical density

The OD at 600 nm was determined using a dual-beam UV-1800 spectrophotometer (Shimadzu, Duisburg, Germany) and standard 1 mL plastic cuvettes. As a reference, 0.9 % (w v^{-1}) NaCl solution was used. To ensure reliable absorbance values within the linear range of the device, samples were diluted as needed to obtain absorbance values between 0.05 and 0.35 arbitrary units (a.u.). Dilutions were typically performed in steps not exceeding a 1:10 ratio. If not otherwise specified, all measurements were carried out in analytical triplicates to ensure reproducibility and statistical validity.

8.5 Data evaluation methods

8.5.1 Bioprocess modelling of growth kinetics

Data from rbALE experiments were processed using Python 3.9.1 in combination with various libraries. Microbioreactor data, including plate layouts, were read and organized using the pandas and bletl packages [180]. BS values for each batch were normalized to the respective well before inoculation. Data analysis and visualization were performed with numpy, matplotlib, and seaborn, and all scripts were executed in Jupyter notebooks (v6.3.0).

Growth rate estimation for rbALE experiments was conducted with the pyFOOMB package, which allows the implementation of bioprocess models as systems of ordinary differential equations [181]. The modeling was based on the classical assumption that cell growth followed the Monod equation (Eqs. 8 – 10). For rbALE modelling, a substrate-independent specific growth rate ($\mu = \mu_{max}$) model was used, justified by substrate concentrations exceeding the affinity constants for *C. glutamicum*. A linear calibration mapped BS to biomass. Transfer events were implemented to model repetitive batch cycles and allow for evolving growth rates. Model parameters were estimated using advanced optimization and uncertainty analysis routines.

For bioreactor cultivations, classical Monod kinetics described biomass growth and substrate consumption. Parameters such as maximum specific growth rate (μ_{max}), Monod constant (k_S), and biomass yield ($Y_{X/S}$) were treated as global parameters across replicates, while initial biomass (c_{X_0}) and substrate concentrations (c_{S_0}) were defined locally.

$$\mu = \mu_{max} \frac{c_S}{k_S + c_S} \tag{8}$$

$$\frac{dc_X}{dt} = \mu \cdot c_X \qquad c_x(t_0) = c_{X_0} \tag{9}$$

$$\frac{dc_S}{dt} = -\frac{1}{Y_{X/S}} \cdot \frac{dc_X}{dt} \qquad c_S(t_0) = c_{S_0} \tag{10}$$

Parameter estimation was carried out using the *estimate_parallel* function, which applies an advanced metaheuristic optimization algorithm as described by Hemmerich et al. (2021) [181]. Required parameter bounds for the estimation were determined based on both literature values and exploratory data analysis.

8.5.2 KPIs to compare bioprocesses

For the comparison of different strains and process conditions, key performance indicators such as the biomass yield per substrate $Y_{X/S}$, the product yield per substrate $Y_{P/S}$, extraction efficiency EE and the space-time-yield (STY) were calculated for each cultivation according to the following equations (Eqs. 11 – 14). Biomass X is consistently reported as cell dry weight,

which was either determined directly by gravimetric measurement or estimated from OD or BS using a linear calibration curve. S_0 denotes the initial substrate concentration at the beginning of the cultivation, whereas X_{final} and $S_{final,}$ represent the cell dry weight and substrate concentrations, respectively, measured at the end of the cultivation (t_{final}). P_{res} denotes the residual product in the aqueous fermentation broth after solvent extraction, whereas P_{final} refers to the total product concentration prior to extraction.

$$Y_{X/S} = \frac{X_{final}[g]}{S_0[g]} \tag{11}$$

$$Y_{P/S} = \frac{P_{final}[mol] \cdot moles\ of\ carbon\ in\ P[C - mol\ \cdot mol^{-1}]}{S_0[mol] \cdot moles\ of\ carbon\ in\ S[\ C - mol\ \cdot mol^{-1}]} \tag{12}$$

$$EE = \left(1 - \frac{P_{res}[mol]}{P_{final}[mol]}\right) * 100\ \% \tag{13}$$

$$STY = \frac{P_{final}\ [g]}{volume\ [L] \cdot t_{final}[h]} \tag{14}$$

9. References

1. OPEC. *Distribution of oil demand in the OECD in 2023*. Statista 2025 [cited 2025 May 13]; Available from: https://www.statista.com/statistics/307194/top-oil-consuming-sectors-worldwide/.
2. NRCan. *Distribution of coal demand worldwide in 2022*. Statista 2024 [cited 2025 March 13]; Available from: https://www.statista.com/statistics/1279674/worldwide-coal-demand-share-by-sector/.
3. Energy-Post. *Fossil fuel demand worldwide from 1965 to 2020, with a forecast until 2050 by scenario*. Statista 2022 [cited 2025 March 13]; Available from: https://www.statista.com/statistics/1275666/fossil-fuel-supply-worldwide/.
4. Höök, M. and Tang, X., *Depletion of fossil fuels and anthropogenic climate change — A review.* Energy Policy, 2013. **52**: p. 797-809.
5. Houghton Filho, J.T., et al., *Climate Change 1995: The science of climate change.*, 1996.
6. *Mitigating climate change.* Working group III contribution to the sixth assessment report of the intergovernmental panel on climate change, 2022.
7. OPEC. *Demand for crude oil worldwide from 2005 to 2023, with a forecast for 2024*. Statista 2024 [cited 2025 March 13]; Available from: https://www.statista.com/statistics/271823/global-crude-oil-demand/.
8. BMLEH, *Nationale Bioökonomiestrategie: Kabinettversion 15.01.2020,* 2020.
9. Backhouse, M., et al., *Bioökonomie-Strategien im Vergleich: Gemeinsamkeiten, Widersprüche und Leerstellen.* 2017.
10. Jordan, N., et al., *Sustainable development of the agricultural bio-economy.* Science, 2007. **316**(5831): p. 1570-1571.
11. McCormick, K. and Kautto N., *The bioeconomy in Europe: An overview.* Sustainability, 2013. **5**(6): p. 2589-2608.
12. Heimann, T., *Bioeconomy and SDGs: Does the bioeconomy support the achievement of the SDGs?* Earth's Future, 2019. **7**(1): p. 43-57.
13. Hüsing, B., *Evaluation der "Nationalen Forschungsstrategie BioÖkonomie 2030": Wirksamkeit der Initiativen des BMBF-Erfolg der geförderten Vorhaben-Empfehlungen zur strategischen Weiterentwicklung: Abschlussbericht*. 2017: Fraunhofer-Institut für System-und Innovationsforschung (ISI).
14. Bachmann, M., et al., *Towards circular plastics within planetary boundaries.* Nature Sustainability, 2023. **6**(5): p. 599-610.
15. OECD. *Distribution of plastic waste management worldwide in 2019*. Statista 2022 [cited 2025 March 10]; Available from: https://www.statista.com/statistics/1358376/global-plastic-waste-management-share-by-region/.

16. PlasticsEurope. *Annual production of plastics worldwide from 1950 to 2023* Statista 2024 [cited 2025 March 10]; Available from: https://www.statista.com/statistics/282732/global-production-of-plastics-since-1950/.
17. Europe, P., *Plastics—The fast facts 2023.* Plastics Europe, 2023.
18. Naser, A.Z., et al., *Poly (lactic acid)(PLA) and polyhydroxyalkanoates (PHAs), green alternatives to petroleum-based plastics: A review.* RSC Advances, 2021. **11**(28): p. 17151-17196.
19. Pellis, A., et al., *Renewable polymers and plastics: Performance beyond the green.* New Biotechnology, 2021. **60**: p. 146-158.
20. Righetti, G.I.C., et al., *Embracing sustainability: The World of bio-based polymers in a mini review.* Polymers, 2024. **16**(7): p. 950.
21. *Bioplastics Market—Size, Share & Trends Analysis Report by Product (Biodegradable, Non-biodegradable), by Application (Packaging, Agriculture, Automotive & Transportation, Electronics, Textile), by Region, and Segment Forecasts, 2025 - 2030.* Market Analysis Report, 2024: p. 145.
22. de Albuquerque, T.L., et al., *Polylactic acid production from biotechnological routes: A review.* International Journal of Biological Macromolecules, 2021. **186**: p. 933-951.
23. da Silva, D., et al., *Biocompatibility, biodegradation and excretion of polylactic acid (PLA) in medical implants and theranostic systems.* Chemical Engineering Journal, 2018. **340**: p. 9-14.
24. Future Market Insights , *Polylactic acid market to reach USD 3,856.3 million by 2034, Booming demand for biodegradable solutions propels growth.* Future Market Insights Global and Consulting Pvt. Ltd., 2024.
25. RameshKumar, S., et al., *Bio-based and biodegradable polymers: State-of-the-art, challenges and emerging trends.* Current Opinion in Green and Sustainable Chemistry, 2020. **21**: p. 75-81.
26. Nakajima, H., et al., *The recent developments in biobased polymers toward general and engineering applications: Polymers that are upgraded from biodegradable polymers, analogous to petroleum-derived polymers, and newly developed.* Polymers, 2017. **9**(10): p. 523.
27. Siracusa, V., and Blanco, I., *Bio-polyethylene (Bio-PE), Bio-polypropylene (Bio-PP) and Bio-poly (ethylene terephthalate)(Bio-PET): Recent developments in bio-based polymers analogous to petroleum-derived ones for packaging and engineering applications.* Polymers, 2020. **12**(8): p. 1641.
28. Benavides, P.T., et al., *Life cycle greenhouse gas emissions and energy use of polylactic acid, bio-derived polyethylene, and fossil-derived polyethylene.* Journal of Cleaner Production, 2020. **277**: p. 124010.
29. Mortimer, C.E., *Chemie Das Basiswissen der Chemie*. Vol. 5., völlig neubearbeitete und erweiterte Auflage. 1987, New York: Georg Thieme Verlag Stuttgart. 660.

30. Becker, T., et al., *Open-and Closed-Loop Recycling: Highly Active Zinc Bisguanidine Polymerization Catalyst for the Depolymerization of Polyesters.* ChemSusChem, 2024. **17**(18): p. e202400933.
31. Wierckx, N., et al., *Plastic biodegradation: Challenges and opportunities.* Consequences of microbial interactions with hydrocarbons, oils, and lipids: biodegradation and bioremediation, 2018: p. 1-29.
32. Taib, N.-A.A.B., et al., *A review on poly lactic acid (PLA) as a biodegradable polymer.* Polymer Bulletin, 2023. **80**(2): p. 1179-1213.
33. Li, Y., et al., *Synthesis and investigation of sustainable long-chain branched poly (lactic acid-r-malic acid) copolymer as toughening agent for PLA blends.* Polymer, 2024. **293**: p. 126634.
34. Tenhaef, N., et al., *From Microbial Succinic Acid Production to Polybutylene Bio-Succinate Synthesis.* Chemie Ingenieur Technik, 2023. **95**(4): p. 587-595.
35. Voessing, T. et al., *Bio-based aniline: Scale-up of a sustainable innovative route to a strategic raw material.* Chemie Ingenieur Technik, 2022. **94**(9): p. 1295-1295.
36. Winter, B., et al., *Towards aromatics from biomass: Prospective Life Cycle Assessment of bio-based aniline.* Journal of Cleaner Production, 2021. **290**: p. 125818.
37. Sauer, M., et al., *Microbial production of organic acids: Expanding the markets.* Trends in Biotechnology, 2008. **26**(2): p. 100-108.
38. Pogrell, H.v., *Bioplastics market development update 2024*. 2025 [cited 2025 03. June]; Available from: https://www.european-bioplastics.org/market/#.
39. Pogrell, H.v., *What are bioplastics?* 2025 [cited 2025 03. June]; Available from: https://www.european-bioplastics.org/bioplastics/.
40. Bosoi, C.R. and C.F. Rose, *Identifying the direct effects of ammonia on the brain.* Metabolic Brain Disease, 2009. **24**: p. 95-102.
41. Bellon, G., et al., *Glutamine increases collagen gene transcription in cultured human fibroblasts.* Biochimica et Biophysica Acta (BBA)-Molecular Cell Research, 1995. **1268**(3): p. 311-323.
42. Kristensen, N.B., et al., *Absorption and metabolism of α-ketoglutarate in growing pigs.* Journal of Animal Physiology and Animal Nutrition, 2002. **86**(7-8): p. 239-245.
43. Velvizhi, S., et al., *Effects of α-ketoglutarate on antioxidants and lipid peroxidation products in rats treated with ammonium acetate.* Nutrition, 2002. **18**(9): p. 747-750.
44. Mailloux, R.J., et al., *α-ketoglutarate dehydrogenase and glutamate dehydrogenase work in tandem to modulate the antioxidant α-ketoglutarate during oxidative stress in Pseudomonas fluorescens.* Journal of Bacteriology, 2009. **191**(12): p. 3804-3810.
45. Lemire, J., et al., *Metabolic defence against oxidative stress: the road less travelled so far.* Journal of Applied Microbiology, 2017. **123**(4): p. 798-809.

46. Legendre, F., et al., *Biochemical pathways to α-ketoglutarate, a multi-faceted metabolite.* World Journal of Microbiology and Biotechnology, 2020. **36**(8): p. 123.
47. Little, J.P., et al., *Creatine, arginine α-ketoglutarate, amino acids, and medium-chain triglycerides and endurance and performance.* International Journal of Sport Nutrition and Exercise Metabolism, 2008. **18**(5): p. 493-508.
48. Coudray-Lucas, C., et al., *Ornithine α-ketoglutarate improves wound healing in severe burn patients: A prospective randomized double-blind trial versus isonitrogenous controls.* Critical Care Medicine, 2000. **28**(6): p. 1772-1776.
49. Sultana, S., et al., *Alpha ketoglutarate nanoparticles: A potentially effective treatment for cyanide poisoning.* European Journal of Pharmaceutics and Biopharmaceutics, 2018. **126**: p. 221-232.
50. Eckert, C., et al., *Ethylene-forming enzyme and bioethylene production.* Biotechnology for Biofuels, 2014. **7**: p. 1-11.
51. Wang, J.-P., et al., *Metabolic engineering for ethylene production by inserting the ethylene-forming enzyme gene (efe) at the 16S rDNA sites of Pseudomonas putida KT2440.* Bioresource Technology, 2010. **101**(16): p. 6404-6409.
52. Barrett, D.G. and Yousaf, M.N., *A tunable, chemoselective, and moldable biodegradable polyester for cell scaffolds.* ChemBioChem, 2008. **9**(1): p. 62-66.
53. Barrett, D.G. and Yousaf, M.N., *Thermosets synthesized by thermal polyesterification for tissue engineering applications.* Soft Matter, 2010. **6**(20): p. 5026-5036.
54. Barrett, D.G., et al., *One-step syntheses of photocurable polyesters based on a renewable resource.* Macromolecules, 2010. **43**(23): p. 9660-9667.
55. Barrett, D.G., et al., *Microfluidic etching and oxime-based tailoring of biodegradable polyketoesters.* Langmuir, 2008. **24**(17): p. 9861-9867.
56. Hermann, A., *Zur Polymerisationskatalyse nachwachsender Monomere mit Zink-N, N-Donor-Komplexen*. 2022, Dissertation, RWTH Aachen University, 2022.
57. Barrett, D.G. and Yousaf, M.N., *Preparation of a class of versatile, chemoselective, and amorphous polyketoesters.* Biomacromolecules, 2008. **9**(7): p. 2029-2035.
58. Hermann, A., et al., *Biologisch abbaubare Klebstoff-Zusammensetzung.* DE102020124314, 2020, PCT/EP2021/075471, 2021.
59. Liu, Z. and Yan, F., *Switchable adhesion: On-demand bonding and debonding.* Advanced Science, 2022. **9**(12): p. 2200264.
60. Luo, Z., et al., *Comparative analysis of the chemical and biochemical synthesis of keto acids.* Biotechnology Advances, 2021. **47**: p. 107706.
61. Utomo, R.N.C., et al., *Defined microbial mixed culture for utilization of polyurethane monomers.* ACS Sustainable Chemistry & Engineering, 2020. **8**(47): p. 17466-17474.
62. Saur, K.M., et al., *Holistic approach to process design and scale-up for itaconic acid production from crude substrates.* Bioengineering, 2023. **10**(6): p. 723.
63. Straathof, A., *The proportion of downstream costs in fermentative production processes*. Comprehensive Biotechnology, 2011. Elsevier. p. 811-814.
64. Chmiel, H., R. Takors, and D. Weuster-Botz, *Bioprozesstechnik*. 2018: Springer.

65. López-Garzón, C.S. and Straathof, A.J., *Recovery of carboxylic acids produced by fermentation.* Biotechnology Advances, 2014. **32**(5): p. 873-904.
66. Eggert, A., et al., *Integrated in-situ product removal process concept for itaconic acid by reactive extraction, pH-shift back extraction and purification by pH-shift crystallization.* Separation and Purification Technology, 2019. **215**: p. 463-472.
67. Kurzrock, T. and Weuster-Botz, D., *New reactive extraction systems for separation of bio-succinic acid.* Bioprocess and Biosystems Engineering, 2011. **34**: p. 779-787.
68. Kocks, C., et al., *Electrochemical crystallization concept for succinic acid reduces waste salt production.* Chemie Ingenieur Technik, 2020. **92**(3): p. 221-228.
69. Gausmann, M., et al., *Electrochemical pH-T-swing separation of itaconic acid for zero salt waste downstream processing.* ACS Sustainable Chemistry & Engineering, 2021. **9**(28): p. 9336-9347.
70. Datta, R. and Henry,M., *Lactic acid: recent advances in products, processes and technologies—a review.* Journal of Chemical Technology & Biotechnology: International Research in Process, Environmental & Clean Technology, 2006. **81**(7): p. 1119-1129.
71. Din, N.A.S., et al., *Lactic acid separation and recovery from fermentation broth by ion-exchange resin: A review.* Bioresources and Bioprocessing, 2021. **8**: p. 1-23.
72. Lee, H.D., et al., *Separation and purification of lactic acid from fermentation broth using membrane-integrated separation processes.* Industrial & Engineering Chemistry Research, 2017. **56**(29): p. 8301-8310.
73. Reifsteck, R.A., et al., *Techno-Economic Comparison of Bio-Cycling Processes for Mixed Plastic Waste Valorization.* Chemie Ingenieur Technik, 2023. **95**(8): p. 1247-1258.
74. Mousavi-Avval, S.H., et al., *Environmental impacts and techno-economic assessments of biobased products: A review.* Renewable and Sustainable Energy Reviews, 2023. **180**: p. 113302.
75. Hermann, B. and Patel, M., *Today's and tomorrow's bio-based bulk chemicals from white biotechnology: A techno-economic analysis.* Applied Biochemistry and Biotechnology, 2007. **136**: p. 361-388.
76. Zeng, W., et al., *Separation and purification of α-ketoglutarate and pyruvate from the fermentation broth of Yarrowia lipolytica.* Bioprocess and Biosystems Engineering, 2018. **41**: p. 1519-1527.
77. Carus, M. and Dammer, L., *Food or non-food: Which agricultural feedstocks are best for industrial uses?* Industrial Biotechnology, 2013. **9**(4): p. 171-176.
78. Straathof, A.J., *Transformation of biomass into commodity chemicals using enzymes or cells.* Chemical Reviews, 2014. **114**(3): p. 1871-1908.
79. Orfali, D.M., et al., *Ranking economic and environmental performance of feedstocks used in bio-based production systems.* Current Research in Biotechnology, 2025: p. 100275.

80. Mahapatra, S., et al., *Biofuels and their sources of production: A review on cleaner sustainable alternative against conventional fuel, in the framework of the food and energy nexus.* Energy Nexus, 2021. **4**: p. 100036.
81. Helm, T., et al., *Introducing molasses as an alternative feedstock into itaconate production using Ustilago sp..* New Biotechnology, 2023. **77**: p. 30-39.
82. Tenhaef, N., et al., *Microaerobic growth-decoupled production of α-ketoglutarate and succinate from xylose in a one-pot process using Corynebacterium glutamicum.* Biotechnology Journal, 2021. **16**(9): p. 2100043.
83. Blunt, M., et al., *Carbon dioxide in enhanced oil recovery.* Energy Conversion and Management, 1993. **34**(9-11): p. 1197-1204.
84. Orr Jr, F. and Taber, J., *Use of carbon dioxide in enhanced oil recovery.* Science, 1984. **224**(4649): p. 563-569.
85. Kongsjorden, H., et al., *Saline aquifer storage of carbon dioxide in the Sleipner project.* Waste Management, 1998. **17**(5-6): p. 303-308.
86. Al-Mamoori, A., et al., *Carbon capture and utilization update.* Energy Technology, 2017. **5**(6): p. 834-849.
87. Zhang, Z., et al., *Advances in carbon capture, utilization and storage*. 2020, Elsevier. p. 115627.
88. Sanz-Pérez, E.S., et al., *Direct capture of CO2 from ambient air.* Chemical Reviews, 2016. **116**(19): p. 11840-11876.
89. Castro-Munoz, R., et al., *A new relevant membrane application: CO2 direct air capture (DAC).* Chemical Engineering Journal, 2022. **446**: p. 137047.
90. Choi, S., J.H. Drese, and Jones, C.W., *Adsorbent materials for carbon dioxide capture from large anthropogenic point sources.* ChemSusChem: Chemistry & Sustainability Energy & Materials, 2009. **2**(9): p. 796-854.
91. Pace, G. and Sheehan, S.W., *Scaling CO2 capture with downstream flow CO2 conversion to ethanol.* Frontiers in Climate, 2021. **3**: p. 656108.
92. Ravikumar, D., et al., *The environmental opportunity cost of using renewable energy for carbon capture and utilization for methanol production.* Applied Energy, 2020. **279**: p. 115770.
93. Haszeldine, R.S., et al., *Negative emissions technologies and carbon capture and storage to achieve the Paris Agreement commitments.* Philosophical Transactions of the Royal Society A: Mathematical, Physical and Engineering Sciences, 2018. **376**(2119): p. 20160447.
94. Ondrey, G., *Linde and Heidelberg Materials Announce Large-Scale Carbon Capture Project*. Chemical Engineering, 2023, Access Intelligence: chemengonline.com. p. 1.
95. Buckel, A., *KIT-IMVT-Research-Technology Transfer-ICODOS.* 2022.
96. Haas, T., et al., *Technical photosynthesis involving CO2 electrolysis and fermentation.* Nature Catalysis, 2018. **1**(1): p. 32-39.
97. Esposito, D., *Scaling it up.* Nature Catalysis, 2021. **4**(10): p. 828-829.

98. Mihalcea, C., et al., *R&D&I and Industry examples: LanzaTech's gas fermentation*, in *CO2 and CO as Feedstock: Sustainable Carbon Sources for the Circular Economy*. 2024, Springer. p. 333-343.
99. Wenda, S., et al., *Industrial biotechnology—the future of green chemistry?* Green Chemistry, 2011. **13**(11): p. 3007-3047.
100. Kinoshita, S., et al., *Studies on the amino acid fermentation Part I. Production of L-glutamic acid by various microorganisms.* The Journal of General and Applied Microbiology, 1957. **3**(3): p. 193-205.
101. Wendisch, V.F., et al., *Updates on industrial production of amino acids using Corynebacterium glutamicum.* World Journal of Microbiology and Biotechnology, 2016. **32**: p. 1-10.
102. Eggeling, L. and Bott, M., *Handbook of Corynebacterium glutamicum*. 2005: CRC press.
103. Kalinowski, J., et al., *The complete Corynebacterium glutamicum ATCC 13032 genome sequence and its impact on the production of L-aspartate-derived amino acids and vitamins.* Journal of Biotechnology, 2003. **104**(1-3): p. 5-25.
104. Becker, J. and Wittmann, C., *Bio-based production of chemicals, materials and fuels–Corynebacterium glutamicum as versatile cell factory.* Current Opinion in Biotechnology, 2012. **23**(4): p. 631-640.
105. Uhde, A., et al., *Glucosamine as carbon source for amino acid-producing Corynebacterium glutamicum.* Applied Microbiology and Biotechnology, 2013. **97**: p. 1679-1687.
106. Chen, Z., et al., *Metabolic engineering of Corynebacterium glutamicum for the production of 3-hydroxypropionic acid from glucose and xylose.* Metabolic Engineering, 2017. **39**: p. 151-158.
107. Henke, N.A., et al., *Carotenoid production by Corynebacterium: The workhorse of industrial amino acid production as host for production of a broad spectrum of C40 and C50 carotenoids*. IntechOpen, 2017.
108. Kallscheuer, N., et al., *A novel synthetic pathway enables microbial production of polyphenols independent from the endogenous aromatic amino acid metabolism.* ACS Synthetic Biology, 2017. **6**(3): p. 410-415.
109. Smith, K.M., et al., *Engineering Corynebacterium glutamicum for isobutanol production.* Applied Microbiology and Biotechnology, 2010. **87**: p. 1045-1055.
110. Arndt, A., et al., *Ethanol catabolism in Corynebacterium glutamicum.* Journal of Molecular Microbiology and Biotechnology, 2008. **15**(4): p. 222-233.
111. Kiefer, D., et al., *High cell density cultivation of Corynebacterium glutamicum on bio-based lignocellulosic acetate using pH-coupled online feeding control.* Bioresource Technology, 2021. **340**: p. 125666.

112. Käß, F., et al., *Assessment of robustness against dissolved oxygen/substrate oscillations for C. glutamicum DM1933 in two-compartment bioreactor.* Bioprocess and Biosystems Engineering, 2014. **37**: p. 1151-1162.
113. Limberg, M.H., et al., *Plug flow versus stirred tank reactor flow characteristics in two-compartment scale-down bioreactor: Setup-specific influence on the metabolic phenotype and bioprocess performance of Corynebacterium glutamicum.* Engineering in Life Sciences, 2016. **16**(7): p. 610-619.
114. Limberg, M.H., et al., *Metabolic profile of 1, 5-diaminopentane producing Corynebacterium glutamicum under scale-down conditions: blueprint for robustness to bioreactor inhomogeneities.* Biotechnology and Bioengineering, 2017. **114**(3): p. 560-575.
115. Kawaguchi, H., et al., *Engineering of a xylose metabolic pathway in Corynebacterium glutamicum.* Applied and Environmental Microbiology, 2006. **72**(5): p. 3418-3428.
116. Buschke, N., et al., *Metabolic engineering of Corynebacterium glutamicum for production of 1, 5-diaminopentane from hemicellulose.* Biotechnology Journal, 2011. **6**(3): p. 306-317.
117. Meiswinkel, T.M., et al., *Accelerated pentose utilization by Corynebacterium glutamicum for accelerated production of lysine, glutamate, ornithine and putrescine.* Microbial Biotechnology, 2013. **6**(2): p. 131-140.
118. Mutz, M., et al., *Metabolic engineering of Corynebacterium glutamicum for the production of anthranilate from glucose and xylose.* Microbial Biotechnology, 2024. **17**(1): p. e14388.
119. Weimberg, R., *Pentose oxidation by Pseudomonas fragi.* Journal of Biological Chemistry, 1961. **236**(3): p. 629-635.
120. Stephens, C., et al., *Genetic analysis of a novel pathway for D-xylose metabolism in Caulobacter crescentus.* Journal of Bacteriology, 2007. **189**(5): p. 2181-2185.
121. Shen, L., et al., *A combined experimental and modelling approach for the Weimberg pathway optimisation.* Nature Communications, 2020. **11**(1): p. 1098.
122. Borgström, C., et al., *Identification of modifications procuring growth on xylose in recombinant Saccharomyces cerevisiae strains carrying the Weimberg pathway.* Metabolic Engineering, 2019. **55**: p. 1-11.
123. Wasserstrom, L., et al., *Exploring D-xylose oxidation in Saccharomyces cerevisiae through the Weimberg pathway.* AMB Express, 2018. **8**(1): p. 33.
124. Nerke, P., et al., *Metabolic bottlenecks of Pseudomonas taiwanensis VLB120 during growth on D-xylose via the Weimberg pathway.* Metabolic Engineering Communications, 2024. **18**: p. e00241.
125. Radek, A., et al., *Engineering of Corynebacterium glutamicum for minimized carbon loss during utilization of D-xylose containing substrates.* Journal of Biotechnology, 2014. **192**: p. 156-160.

126. Radek, A., et al., *Miniaturized and automated adaptive laboratory evolution: Evolving Corynebacterium glutamicum towards an improved d-xylose utilization.* Bioresource Technology, 2017. **245**: p. 1377-1385.
127. Brüsseler, C., et al., *The myo-inositol/proton symporter IolT1 contributes to d-xylose uptake in Corynebacterium glutamicum.* Bioresource Technology, 2018. **249**: p. 953-961.
128. Nielsen, J., *Metabolic engineering: Techniques for analysis of targets for genetic manipulations.* Biotechnology and Bioengineering, 1998. **58**(2-3): p. 125-132.
129. Van der Rest, M., C. Lange, and D. Molenaar, *A heat shock following electroporation induces highly efficient transformation of Corynebacterium glutamicum with xenogeneic plasmid DNA.* Applied Microbiology and Biotechnology, 1999. **52**: p. 541-545.
130. Kirchner, O. and Tauch, A., *Tools for genetic engineering in the amino acid-producing bacterium Corynebacterium glutamicum.* Journal of Biotechnology, 2003. **104**(1-3): p. 287-299.
131. Schäfer, A., et al., *Small mobilizable multi-purpose cloning vectors derived from the Escherichia coli plasmids pK18 and pK19: Selection of defined deletions in the chromosome of Corynebacterium glutamicum.* Gene, 1994. **145**(1): p. 69-73.
132. Notley-McRobb, L. and Ferenci, T., *The generation of multiple co-existing mal-regulatory mutations through polygenic evolution in glucose-limited populations of Escherichia coli.* Environmental Microbiology, 1999. **1**(1): p. 45-52.
133. Portnoy, V.A., et al., *Adaptive laboratory evolution—harnessing the power of biology for metabolic engineering.* Current Opinion in Biotechnology, 2011. **22**(4): p. 590-594.
134. Dragosits, M. and Mattanovich,D., *Adaptive laboratory evolution–principles and applications for biotechnology.* Microbial Cell Factories, 2013. **12**: p. 1-17.
135. Stella, R.G., et al., *Evolutionary engineering of Corynebacterium glutamicum.* Biotechnology Journal, 2019. **14**(9): p. 1800444.
136. Cheng, K.-K., et al., *Global metabolic network reorganization by adaptive mutations allows fast growth of Escherichia coli on glycerol.* Nature Communications, 2014. **5**(1): p. 3233.
137. Gresham, D. and Hong, J., *The functional basis of adaptive evolution in chemostats.* FEMS Microbiology Reviews, 2015. **39**(1): p. 2-16.
138. Bromig, L. and Weuster-Botz, D., *Accelerated adaptive laboratory evolution by automated repeated batch processes in parallelized bioreactors.* Microorganisms, 2023. **11**(2): p. 275.
139. Lee, S. and Kim, P., *Current status and applications of adaptive laboratory evolution in industrial microorganisms.* Journal of Microbiology and Biotechnology, 2020. **30**(6): p. 793.
140. Klaffl, S., et al., *Complex regulation of the phosphoenolpyruvate carboxykinase gene pck and characterization of its GntR-type regulator IolR as a repressor of myo-inositol*

utilization genes in Corynebacterium glutamicum. Journal of Bacteriology, 2013. **195**(18): p. 4283-4296.

141. Bäumchen, C., et al., *Myo-inositol facilitators IolT1 and IolT2 enhance D-mannitol formation from D-fructose in Corynebacterium glutamicum.* FEMS Microbiology letters, 2009. **290**(2): p. 227-235.
142. Ikeda, M., et al., *Identification and application of a different glucose uptake system that functions as an alternative to the phosphotransferase system in Corynebacterium glutamicum.* Applied Microbiology and Biotechnology, 2011. **90**: p. 1443-1451.
143. Fukui, K., et al., *Corynebacterium glutamicum CgynfM encodes a dicarboxylate transporter applicable to succinate production.* Journal of Bioscience and Bioengineering, 2019. **127**(4): p. 465-471.
144. Nakamura, J., et al., *Mutations of the Corynebacterium glutamicum NCgl1221 gene, encoding a mechanosensitive channel homolog, induce L-glutamic acid production.* Applied and Environmental Microbiology, 2007. **73**(14): p. 4491-4498.
145. Kataoka, N., et al., *Development of a 2-hydroxyglutarate production system by Corynebacterium glutamicum.* Applied Microbiology and Biotechnology, 2023. **107**(19): p. 5987-5997.
146. Marienhagen, J., et al., *Functional analysis of all aminotransferase proteins inferred from the genome sequence of Corynebacterium glutamicum.* Journal of Bacteriology, 2005. **187**(22): p. 7639-7646.
147. Kholy, E.R.B.-E., et al., *Glutamate dehydrogenase is not essential for glutamate formation by Corynebacterium glutamicum.* Applied and Environmental Microbiology, 1993. **59**(7): p. 2329-2331.
148. Krahn, I., et al., *Evolving a new efficient mode of fructose utilization for improved bioproduction in Corynebacterium glutamicum.* Frontiers in Bioengineering and Biotechnology, 2021. **9**: p. 669093.
149. Noack, S., et al., *The linkage between nutrient supply, intracellular enzyme abundances and bacterial growth: New evidences from the central carbon metabolism of Corynebacterium glutamicum.* Journal of Biotechnology, 2017. **258**: p. 13-24.
150. Wendisch, V.F., et al., *Quantitative determination of metabolic fluxes during coutilization of two carbon sources: comparative analyses with Corynebacterium glutamicum during growth on acetate and/or glucose.* Journal of Bacteriology, 2000. **182**(11): p. 3088-3096.
151. Peters-Wendisch, P.G., et al., *Pyruvate carboxylase as an anaplerotic enzyme in Corynebacterium glutamicum.* Microbiology, 1997. **143**(4): p. 1095-1103.
152. Witthoff, S., et al., *C1 metabolism in Corynebacterium glutamicum: an endogenous pathway for oxidation of methanol to carbon dioxide.* Applied and Environmental Microbiology, 2013. **79**(22): p. 6974-6983.

153. Stansen, C., et al., *Characterization of a Corynebacterium glutamicum lactate utilization operon induced during temperature-triggered glutamate production.* Applied and Environmental Microbiology, 2005. **71**(10): p. 5920-5928.
154. Rückert, C., et al., *Functional genomics and expression analysis of the Corynebacterium glutamicum fpr2-cysIXHDNYZ gene cluster involved in assimilatory sulphate reduction.* BMC Genomics, 2005. **6**: p. 1-18.
155. Nishimura, T., et al., *ArnR, a novel transcriptional regulator, represses expression of the narKGHJI operon in Corynebacterium glutamicum.* Journal of Bacteriology, 2008. **190**(9): p. 3264-3273.
156. Nolden, L., et al., *Sensing nitrogen limitation in Corynebacterium glutamicum: the role ofglnK andglnD [sup†].* Molecular Microbiology, 2001. **42**(5).
157. Jakoby, M., et al., *Isolation of the Corynebacterium glutamicum glnA gene encoding glutamine synthetase I.* FEMS Microbiology Letters, 1997. **154**(1): p. 81-88.
158. Kohl, T.A. and Tauch, A., *The GlxR regulon of the amino acid producer Corynebacterium glutamicum: Detection of the corynebacterial core regulon and integration into the transcriptional regulatory network model.* Journal of Biotechnology, 2009. **143**(4): p. 239-246.
159. Chen, X., et al., *Pathway engineering of Escherichia coli for α-ketoglutaric acid production.* Biotechnology and Bioengineering, 2020. **117**(9): p. 2791-2801.
160. Sakai, S., et al., *Effect of lignocellulose-derived inhibitors on growth of and ethanol production by growth-arrested Corynebacterium glutamicum R.* Applied and Environmental Microbiology, 2007. **73**(7): p. 2349-2353.
161. Tsuge, Y., et al., *Detoxification of furfural in Corynebacterium glutamicum under aerobic and anaerobic conditions.* Applied Microbiology and Biotechnology, 2014. **98**(20): p. 8675-8683.
162. Tsuge, Y., et al., *FudC, a protein primarily responsible for furfural detoxification in Corynebacterium glutamicum.* Applied Microbiology and Biotechnology, 2016. **100**(6): p. 2685-2692.
163. Pfeifer-Sancar, K., et al., *Comprehensive analysis of the Corynebacterium glutamicum transcriptome using an improved RNAseq technique.* BMC Genomics, 2013. **14**: p. 1-23.
164. Auchter, M., et al., *Dual transcriptional control of the acetaldehyde dehydrogenase gene ald of Corynebacterium glutamicum by RamA and RamB.* Journal of Biotechnology, 2009. **140**(1-2): p. 84-91.
165. Jungwirth, B., et al., *High-resolution detection of DNA binding sites of the global transcriptional regulator GlxR in Corynebacterium glutamicum.* Microbiology, 2013. **159**(Pt_1): p. 12-22.
166. Toyoda, K., et al., *Genome-wide identification of in vivo binding sites of GlxR, a cyclic AMP receptor protein-type regulator in Corynebacterium glutamicum.* Journal of Bacteriology, 2011. **193**(16): p. 4123-4133.

167. *Alibaba product listing for 2-oxoglutaric acid by Guangzhou Harworld Life Sciences Co., Ltd.* archived 2025-08-21 Available from: https://web.archive.org/web/20250821092622/https://www.alibaba.com/product-detail/Alpha-Ketoglutaric-Acid-2-Oxoglutaric-Acid_1601430861336.html.
168. *Alibaba product listing for fodder/sugarcane molasses by Takimex Global Co., LTD*. archived 2025-08-21 Available from: https://web.archive.org/web/20250821101807/https://www.alibaba.com/product-detail/Vietnam-Black-Molasses-for-Fodder-Sugarcane_11000010703790.html.
169. Stella, R.G., et al., *Biosensor-based growth-coupling and spatial separation as an evolution strategy to improve small molecule production of Corynebacterium glutamicum.* Metabolic Engineering, 2021. **68**: p. 162-173.
170. Gibson, D.G., et al., *Enzymatic assembly of DNA molecules up to several hundred kilobases.* Nature Methods, 2009. **6**(5): p. 343-345.
171. Sambrook, J. and Russell, D.W., *Detection of DNA in agarose gels.* Molecular Cloning, A Laboratory Manual,(3rd Ed.) Cold Spring Harbor Laboratory Press, New York, 2001: p. 5-14.
172. Hanahan, D., *Studies on transformation of Escherichia coli with plasmids.* Journal of Molecular Biology, 1983. **166**(4): p. 557-580.
173. Keilhauer, C., et al., *Isoleucine synthesis in Corynebacterium glutamicum: Molecular analysis of the ilvB-ilvN-ilvC operon.* Journal of Bacteriology, 1993. **175**(17): p. 5595-5603.
174. Kensy, F., et al., *Validation of a high-throughput fermentation system based on online monitoring of biomass and fluorescence in continuously shaken microtiter plates.* Microbial Cell Factories, 2009. **8**: p. 1-17.
175. Hemmerich, J., et al., *Combinatorial impact of Sec signal peptides from Bacillus subtilis and bioprocess conditions on heterologous cutinase secretion by Corynebacterium glutamicum.* Biotechnology and Bioengineering, 2019. **116**(3): p. 644-655.
176. Unthan, S., et al., *Bioprocess automation on a Mini Pilot Plant enables fast quantitative microbial phenotyping.* Microbial Cell Factories, 2015. **14**: p. 1-11.
177. Voges, R. and Noack, S., *Quantification of proteome dynamics in Corynebacterium glutamicum by 15N-labeling and selected reaction monitoring.* Journal of Proteomics, 2012. **75**(9): p. 2660-2669.
178. Cock, P.J., et al., *Biopython: Freely available Python tools for computational molecular biology and bioinformatics.* Bioinformatics, 2009. **25**(11): p. 1422.
179. Paczia, N., et al., *Extensive exometabolome analysis reveals extended overflow metabolism in various microorganisms.* Microbial Cell Factories, 2012. **11**: p. 1-14.
180. Osthege, M., et al., *bletl-A Python package for integrating BioLector microcultivation devices in the Design-Build-Test-Learn cycle.* Engineering in Life Sciences, 2022. **22**(3-4): p. 242-259.

181. Hemmerich, J., et al., *pyFOOMB: Python framework for object oriented modeling of bioprocesses.* Engineering in Life Sciences, 2021. **21**(3-4): p. 242-257.

10. List of figures

11. List of tables

12. Appendix

Table S 1 Measurement of relevant trace elements in molasses.[81]

Analyte	Unit	Measurement	Error	Method
C	% w w^{-1}	34.1	0.2	
H	% w w^{-1}	7.18	0.09	EA
N	% w w^{-1}	2.45	0.1	EA
S	% w w^{-1}	< 0,6		EA
O	% w w^{-1}	49.8	0.1	EA
Ca	mg kg^{-1}	630	20	EA
Fe	mg kg^{-1}	5.87	0.98	ICP-OES
K	mg kg^{-1}	39300	500	ICP-OES
Mg	mg kg^{-1}	50.5	1.6	ICP-OES
Na	mg kg^{-1}	8200	300	ICP-OES
P	mg kg^{-1}	199	8	ICP-OES
NH_4^+	% w w^{-1}	0.0732		ICP-OES
PO_4^{3-}	% w w^{-1}	0.0013		CFA
Cl^-	% w w^{-1}	0.3131	0.03	CFA
NO_3^-	% w w^{-1}	0.4507	0.05	IC
SO_4^{2-}	% w w^{-1}	0.6097	0.06	IC

Table S 2 Certificate of analysis of the lignocellulosic hydrolysate feedstock from Fibenol.

Analyte	Unit	Measurement
Dry matter content	% w w^{-1}	57,6
pH		3,8
Glucose	g L^{-1}	99,9
Xylose	g L^{-1}	257,0
Galactose	g L^{-1}	17,9
Arabinose	g L^{-1}	10,6
Mannose	g L^{-1}	20,9
Formic acid	g L^{-1}	0,9
Acetic acid	g L^{-1}	5,0
HMF	g L^{-1}	4,0
Furfural	g L^{-1}	1,4

Table S 3 Metabolic comparison of AKG-3 on defined media with complex molasses. Significantly regulated proteins in the direct comparison of *C. glutamicum* AKG-3 grown on molasses versus sucrose. Proteomic analyses identified 48 proteins significantly regulated between molasses and sucrose.

Protein	FC_mol_suc	Gene	Locus	Regulated by
Probable aldehyde dehydrogenase	4.8	*msmA*	cg0199	GlxR, IolR
Putative zinc-type alcohol dehydrogenase transmembrane protein	4.22	*adhE*	cg0387	
Sugar kinase, ribokinase family	3.71	*iolC*	cg0197	GlxR, IolR
Glyceraldehyde-3-phosphate dehydrogenase	3.26	*gap*	cg1791	GlxR, RamA, SigA, SigB, SugR
Nitrate reductase 2, alpha subunit	3.12	*narG*	cg1344	ArnR, GlxR, RipA, RosR, SigA
Homolog of lactam utilization protein B	2.99	-	cg1141	GlxR, Pred
Conserved hypothetical protein fragment	2.73		cg2651	
Phosphate isomerase/epimerase	2.68	*iolE*	cg0203	GlxR, IolR
Putative L-lactate dehydrogenase	2.34	*lldA*	cg3227	GlxR, LldR, RamA, SigA
Bacterial extracellular solute-binding protein, family A	2.28	-	cg0834	LexA
Alcohol dehydrogenase, class C	2.23	*adhC*	cg0400	
tRNA methylthiotransferase	2.22	*miaB*	cg2135	
Molybdopterin cofactor synthesis protein	2.2	*moaC*	cg0260	
Imidazoleglycerol-phosphate synthase, amidotransferase	2.16	*hisH*	cg2300	
Sulfite reductase (hemoprotein)	2.14	*cysI*	cg3118	CysR, DtxR, McbR, SigA
Probable phosphoenolpyruvate carboxykinase protein	2.05	*pck*	cg3169	GlxR, IolR, RamA, RamB, SigA
Glyoxalase/bleomycin resistance/dioxygenase superfamily protein	2.02	-	cg1373	
Putative nucleoside-diphosphate-sugar epimerase	0.49	-	cg1740	
Prolyl oligopeptidase	0.49	*ptrB*	cg2873	ClgR
Mg-chelatase subunit ChlI	0.49	-	cg1203	
Probable methylisocitric acid lyase	0.49	*prpB2*	cg0760	GlxR, PrpR, RamA, SigA
Inositol-monophosphate dehydrogenase	0.48	*guaB1*	cg2964	
Glyoxalase/bleomycin resistance protein/dioxygenase	0.47	-	cg0141	
Esterase/lipase/thioesterase family protein	0.47	-	cg0120	

Dihydroxy-acid dehydratase	0.47	*ilvD*	cg1432	SigA
Iron-regulated ABC transporter ATPase subunit	0.46	*sufC*	cg1762	OxyR, SigH, SigM, SufR
Thioredoxin reductase	0.46	*trxB*	cg3422	SigH, SigM, WhcA, WhcB, WhcE
Components of an uncharacterized iron-regulated ABC-type transporter	0.45	*sufD*	cg1763	OxyR, SigH, SigM, SufR
Component of an uncharacterized iron-regulated ABC-type transporter	0.45	*sufB*	cg1764	OxyR, SigH, SigM, SufR
Nitroreductase family protein	0.45	-	cg0404	SigH, WhcA
Putative NADH-dependent flavin oxidoreductase	0.45	-	cg3370	
Putative secreted protein	0.44	-	cg2052	MtrA
Putative membrane protein fragment	0.43	-	cg2657	
Putative transcriptional regulator	0.41	-	cg2112	LexA, SigA
Cysteine sulfinate desulfinase/cysteine desulfurase or related enzyme	0.41	-	cg1214	NdnR, SigH, WhcA
Putative excinuclease ATPase subunit, UvrA-like protein	0.41	-	cg1234	
Putative secreted protein	0.37	-	cg4005	CysR
ABC-type cobalamin/Fe^{3+}-siderophore transport system protein	0.37	-	cg0924	DtxR
Putative glutathione reductase	0.37	*gor*	cg2194	SigH
Predicted acetyltransferase	0.36	-	cg2835	SigH
Ribosomal large subunit pseudouridine synthase D	0.36	*rluD*	cg2346	
Quinolinate synthase	0.35	*nadA*	cg1216	NdnR, SigH, WhcA
Aldehyde dehydrogenase	0.34	-	cg3096	GlxR, RamA, RamB, SigA
Flavin-containing monooxygenase (FMO)	0.33	-	cg3195	GlxR, IpsA
ATPase component of ABC transporters with duplicated ATPase domains	0.33	-	cg2475	
Hypothetical protein Cg0511	0.33	-	cg0511	
Aspartyl aminopeptidase	0.29	*pepC*	cg1693	
ABC-type Mn/Zn transport system, secreted Mn/Zn-binding (lipo)protein (surface adhesin)	0.03	-	cg2911	SigA

Table S 4 Proteom comparison of AKG-3 and the parental strain P_{O6}-*iolT1* on glucose. Differentially synthesized proteins of *C. glutamicum* AKG-3 in comparison to the control strain *C. glutamicum* P_{O6}-*iolT1* with glucose as sole carbon and energy source. Proteins with statistically significant changes (*p*-value < 0.01, Log2(Fold-Change) > 0.5 for upregulated proteins and Log2(Fold-Change) < -0.5 for down-regulated proteins of conditions during exponential growth are shown.

Protein	FC_AKG-4_P_{O6}_glc	Gene	Locus
Rhodanese-related sulfurtransferase	0.141	*sseA2*	cg1613
Ribosomal L32p protein family	0.161	*rpmF*	cg0995
Low molecular weight phosphotyrosine protein phosphatase	0.214	-	cg1706
Universal stress protein UspA or related nucleotide-binding protein	0.221	*uspA2*	cg1595
Probable phospho-2-dehydro-3-deoxyheptonate aldolase	0.256	*aroF*	cg1129
Conserved hypothetical protein	0.262	-	cg0895
Putative transcriptional accessory protein, RNA binding	0.262	-	cg2241
Cold-shock protein CspA	0.273	*cspA*	cg0215
3-isopropylmalate dehydratase (small subunit)	0.282	*leuD*	cg1488
Trypsin-like serine protease	0.296	-	cg0998
Putative chorismate mutase	0.298	-	cg0975
Phosphoadenosine-phosphosulfate reductase	0.303	*cysH*	cg3116
Sensor histidine kinase of two-component system, fragment	0.324	-	cg0228
Putative glycerate kinase	0.336	*glxK*	cg2282
Ribosomal protein S15	0.34	*rpsO*	cg2167
Putative UDP-N-acetylglucosamine pyrophosphorylase	0.344	*glmU*	cg1076
Secreted protein potentially involved into thiamin biosynthesis	0.351	*thiX*	cg2561
30S ribosomal protein S16	0.351	*rpsP*	cg2253
Putative phage integrase (N-terminal fragment)	0.353	*int2'*	cg2071
30S ribosomal protein S18	0.353	*rpsR*	cg0988
Nitroreductase family	0.359	-	cg0404
Ribosomal protein L36	0.36	-	cg2791
50S ribosomal protein L18	0.372	*rplR*	cg0630
50S ribosomal protein L2	0.379	*rplB*	cg0598
Ribosomal protein S10	0.383	*rpsJ*	cg0593
Conserved hypothetical protein	0.383	-	cg2106
50S ribosomal protein L28	0.383	*rpmB*	cg0991
Glutamate 5-kinase protein	0.384	*proB*	cg2588
NADP-specific glutamate dehydrogenase	0.39	*gdh*	cg2280

Sulfite reductase (hemoprotein)	0.395	*cysI*	cg3118
50S ribosomal protein L11	0.398	*rplK*	cg0563
Trigger factor, PPIase involved into cell division, molecular chaperone	0.399	*tig*	cg2647
Penicillin tolerance protein	0.403	*lytB*	cg1164
50S ribosomal protein L27	0.404	*rpmA*	cg2594
30S ribosomal protein S14	0.406	*rpsN*	cg0989
Predicted nucleoside-diphosphate-sugar epimerase	0.407	-	cg1553
Putative secreted protein	0.411	-	cg1636
50S ribosomal protein L9	0.411	*rplI*	cg3306
50S ribosomal protein L23	0.414	*rplW*	cg0597
Translation initiation factor IF3 protein	0.42	*infC*	cg1563
50S ribosomal protein L20	0.42	*rplT*	cg1565
50S ribosomal protein L29	0.42	*rpmC*	cg0603
50S ribosomal protein L10	0.422	*rplJ*	cg0572
50S ribosomal protein L35	0.429	*rpmI*	cg1564
3-isopropylmalate dehydratase large subunit	0.43	*leuC*	cg1487
50S ribosomal protein L30	0.435	*rpmD*	cg0632
Ribosomal protein L22	0.441	*rplV*	cg0600
50S ribosomal protein L16	0.447	*rplP*	cg0602
Chaperone with DnaK, heat shock protein (DnaJ protein)	0.448	*dnaJ*	cg3098
Putative secreted protein	0.448	-	cg1859
Ribosomal protein S12	0.45	*rpsL*	cg0581
30S ribosomal protein S17	0.452	*rpsQ*	cg0604
50S ribosomal protein L4	0.461	*rplD*	cg0596
Conserved hypothetical protein	0.462	-	cg0282
Putative polyribonucleotide phosphorylase / guanosine pentaphosphate synthetase	0.467	*gpsI*	cg2166
GTPase involved into stress response	0.469	-	cg1248
50S ribosomal protein L3	0.47	*rplC*	cg0594
Shikimate kinase I	0.473	*aroK*	cg1828
Putative glucose-6-phosphate dehydrogenase assembly protein OpcA	0.477	*opcA*	cg1779
Carbonic anhydrase	0.477	*cynT*	cg2954
Putative transcriptional termination/antitermination factor	0.477	*nusA*	cg2178
30S ribosomal protein S3	0.481	*rpsC*	cg0601

Conserved hypothetical protein	0.482	-	cg1597
30S ribosomal protein S20	0.483	*rpsT*	cg2573
Ribosomal protein L15	0.485	*rplO*	cg0634
30S ribosomal protein S19	0.491	*rpsS*	cg0599
Protein deacetylase, SIR2 family	0.494	-	cg0745
Cysteine desulfhydrase / selenocysteine lyase	0.496	*nifS2*	cg1761
Ribosomal protein S11	0.496	*rpsK*	cg0653
Transcription termination factor Rho	0.497	*rho*	cg1354
Putative integral membrane protein	0.499	-	cg0952
Bacterial regulatory protein, MarR family	2.006	-	cg3315
Branched-chain amino acid aminotransferase	2.009	*ilvE*	cg2418
Fumarate hydratase	2.015	*fum*	cg1145
Cyclopropane-fatty-acyl-phospholipid synthase	2.036	*cma*	cg0663
Thiamine biosynthesis protein	2.06	*thiC*	cg1476
Serine/threonine-specific protein phosphatase	2.07	-	cg2172
Conserved hypothetical protein	2.072	-	cg0192
Phosphocarrier protein HPr	2.074	*ptsH*	cg2121
Acetohydroxyacid synthase small subunit	2.082	*ilvN*	cg1436
Membrane protease subunit, stomatin/prohibitin homologs	2.089	-	cg3396
Phosphoenolpyruvate carboxylase	2.095	*ppc*	cg1787
L-gulonolactone oxidase	2.097	-	cg0238
Quinolinate synthetase	2.097	*nadA*	cg1216
Putative secreted protein	2.101	-	cg3032
CTP synthase	2.102	*pyrG*	cg1606
Transcriptional regulator, TetR family	2.102	-	cg1738
3-phosphoshikimate 1-carboxyvinyltransferase	2.103	*aroA*	cg0873
Conserved hypothetical protein	2.116	-	cg2283
Mg-chelatase subunit ChlI	2.12	-	cg1203
Hypothetical protein predicted by Glimmer/Critica	2.122	-	cg3016
Probable FeSuccinyl-CoA:3-ketoacid-coenzyme A transferase subunit	2.13	*scoA*	cg2623
ABC-type cobalamin/Fe3+-siderophores transport system	2.141	-	cg0924
Cystathionine beta-lyase	2.174	*aecD*	cg2536
Uncharacterized proteins, LmbE homolog	2.176	-	cg1127
Thiamin biosynthesis protein	2.184	*thiG*	cg2239

ATP synthase C chain	2.185	*atpE*	cg1363
ABC-type peptide transport system, secreted component	2.188	-	cg2181
Conserved hypothetical protein	2.204	-	cg2079
Conserved hypothetical protein	2.213	-	cg2498
Lipoate-protein ligase	2.217	*lplA*	cg1222
Putative shikimate / quinate 5-dehydrogenase	2.228	*aroE2*	cg1283
Putative nicotinate-nucleotide pyrophosphorylase	2.234	*nadC*	cg1215
Phosphopantetheine adenylyltransferase	2.279	*coaD*	cg1501
Putative transcriptional regulator	2.301	-	cg3414
3'-Phosphoadenosine 5'-phosphosulfate (PAPS) 3'-phosphatase	2.346	*cysQ*	cg0967
L-2,3-butanediol dehydrogenase/acetoin reductase	2.347	*butA*	cg2958
Cyclomaltodextrinase	2.379	-	cg1012
Succinate dehydrogenase CD	2.381	*sdhCD*	cg0445
Nicotinamidase/ pyrazinamidase	2.383	*pncA*	cg2734
Malto-oligosyltrehalose trehalohydrolase	2.393	*treZ*	cg2333
Glutamate secreted binding protein	2.443	*gluB*	cg2137
Predicted acetyltransferase	2.452	-	cg2605
Conserved hypothetical protein	2.455	-	cg0935
ATP synthase F0 subunit 6	2.487	*atpB*	cg1362
Conserved hypothetical protein	2.489	-	cg2850
Cysteine sulfinate desulfinase/cysteine desulfurase or related enzyme	2.501	-	cg1214
Uncharacterized enzyme related to sulfurtransferases	2.547	-	cg3319
Predicted transcriptional regulator	2.649	-	cg1687
Tetrahydrodipicolinate succinylase	2.691	*dapD*	cg1256
Probable methylisocitric acid lyase	2.746	*prpB2*	cg0760
Putative secreted or membrane protein	2.751	-	cg2994
Haloacid dehalogenase-like hydrolase	2.825	-	cg0154
Putative phosphopantothenoylcysteine synthetase/decarboxylase	2.868	-	cg1907
Hypothetical protein predicted by Glimmer/Critica	2.902	-	cg3009
Putative secreted or membrane protein	2.91	-	cg2195
ABC-type cobalt transport system, permease component CbiQ	2.918	-	cg1229
Conserved hypothetical protein	2.986	-	cg1045
Methylcitrate synthase	3.015	*prpC2*	cg0762

Component of an uncharacterized iron-regulated ABC-type transporter	3.085	*sufB*	cg1764
Putative secreted protein	3.088	-	cg4005
Aldehyde dehydrogenase	3.108	-	cg3096
Phospholipid-binding protein	3.159	-	cg1718
Putative acetyl-CoA:acetyltransferase	3.209	*pcaF*	cg2625
Porin	3.276	*porA*	cg3008
Conserved hypothetical protein	3.403	-	cg2772
NADPH-dependent FMN reductase	3.424	-	cg3223
Ferritin-like protein	3.552	*ftn*	cg2782
Putative carboxymuconolactone decarboxylase subunit	3.602	-	cg3212
Catechol 1,2-dioxygenase	3.665	*catA1*	cg2636
ADP-ribose pyrophosphatase	3.667	-	cg1218
Aconitase	3.806	*acn*	cg1737
Propionate catabolism protein PrpD	4.246	*prpD2*	cg0759
Conserved hypothetical protein	4.36	-	cg0338
Hypothetical protein predicted by Glimmer/Critica	4.536	-	cg2665
Superfamily II DNA/RNA helicases, SNF2 family	4.538	-	cg1316
Uncharacterized enzyme involved in biosynthesis of extracellular polysaccharides	4.985	-	cg2962
Starvation-induced DNA protecting protein	5.232	*dps*	cg3327
Decarboxylase	5.254	-	cg2343
ATPase component of ABC transporters with duplicated ATPase domains	5.478	-	cg2475
Conserved hypothetical protein	6.412	-	cg2247
Glutamine synthetase I	7.83	*glnA*	cg2429
Nitrogen regulatory protein PII	16.464	*glnK*	cg2260

Table S 5 Proteom comparison of AKG-3 and the parental strain P_{O6}-*iolT1* on sucrose. Differentially synthesized proteins of *C. glutamicum* AKG-3 in comparison to the control strain *C. glutamicum* P_{O6}-*iolT1* with sucrose as sole carbon and energy source. Proteins with statistically significant changes (*p*-value < 0.01, Log2(Fold-Change) > 0.5 for upregulated proteins and Log2(Fold-Change) < -0.5 for down-regulated proteins of conditions during exponential growth are shown.

Protein	FC_AKG-4_P_{O6}_suc	Gene	Locus
Ribosomal L32p protein family	0.173	*rpmF*	cg0995
Universal stress protein UspA or related nucleotide-binding protein	0.236	*uspA2*	cg1595
Putative L-lactate dehydrogenase	0.309	*lldA*	cg3227
Probable phospho-2-dehydro-3-deoxyheptonate aldolase	0.327	*aroF*	cg1129
Putative integral membrane protein	0.347	-	cg0952
Conserved hypothetical protein	0.362	-	cg2106
3-isopropylmalate dehydratase (small subunit)	0.391	*leuD*	cg1488
Aldehyde dehydrogenase	0.393	-	cg3096
Conserved hypothetical protein	0.395	-	cg0895
Phosphoribosyl pyrophosphate synthase isozyme 2 PR	0.395	*prsA*	cg1075
50S ribosomal protein L28	0.405	*rpmB*	cg0991
Na+/proline, Na+/pantothenate symporter or related permease	0.407	-	cg0953
50S ribosomal protein L33	0.411	*rpmG*	cg0990
Isocitrate lyase	0.432	*aceA*	cg2560
Sensor histidine kinase of two-component system, fragment	0.433	-	cg0228
Threonyl-tRNA synthetase	0.436	*thrS*	cg1880
Cold-shock protein CspA	0.438	*cspA*	cg0215
D-alanine:D-alanine-adding enzyme	0.44	*murF*	cg2373
50S ribosomal protein L17	0.444	*rplQ*	cg0656
3-isopropylmalate dehydratase large subunit	0.446	*leuC*	cg1487
Ribosomal protein L36	0.447	-	cg2791
Conserved hypothetical protein	0.448	-	cg0282
30S ribosomal protein S16	0.451	*rpsP*	cg2253
NADP-specific glutamate dehydrogenase	0.453	*gdh*	cg2280
Trigger factor, PPIase involved into cell division, molecular chaperone	0.459	*tig*	cg2647
ABC-type cobalamin/Fe3+-siderophores transport system, ATPase component	0.463	-	cg0928
Ribosomal protein L22	0.465	*rplV*	cg0600
50S ribosomal protein L11	0.469	*rplK*	cg0563

30S ribosomal protein S20	0.473	*rpsT*	cg2573
50S ribosomal protein L3	0.475	*rplC*	cg0594
50S ribosomal protein L29	0.48	*rpmC*	cg0603
30S ribosomal protein S18	0.484	*rpsR*	cg0988
30S ribosomal protein S7	0.484	*rpsG*	cg0582
Acetyltransferase	0.488	-	cg1612
Ribosomal protein S10	0.49	*rpsJ*	cg0593
Na+-dependent transporters of the SNF family	0.494		cg1169
Rhodanese-related sulfurtransferase	0.495	*sseA2*	cg1613
ABC-type cobalamin/Fe3+-siderophores transport system	0.499	-	cg0924
Putative phosphopantothenoylcysteine synthetase/decarboxylase	2.025	-	cg1907
NADPH-dependent FMN reductase	2.027	-	cg3223
DNA or RNA helicase of superfamily II	2.041	-	cg3398
Succinate dehydrogenase A	2.042	*sdhA*	cg0446
Putative acylphosphatase	2.063	-	cg2266
Putative phosphomethylpyrimidine kinase	2.088	*thiD2*	cg3409
Thiol peroxidase	2.095	*tpx*	cg1236
Tetrahydrodipicolinate succinylase	2.113	*dapD*	cg1256
Cyclomaltodextrinase	2.125		cg1012
Dihydrolipoamide dehydrogenase	2.135	*lpd*	cg0441
Conserved hypothetical protein	2.136	-	cg1045
Conserved hypothetical protein	2.172	-	cg1374
Succinate dehydrogenase B	2.193	*sdhB*	cg0447
Bacterial regulatory proteins, DeoR family	2.255	-	cg0139
Phosphoenolpyruvate carboxylase	2.272	*ppc*	cg1787
Cytochrome c oxidase chain II	2.285	*ctaC*	cg2409
Glutamate secreted binding protein	2.297	*gluB*	cg2137
Single-stranded DNA-binding protein	2.317	*ssb*	cg3307
Polypeptide deformylase	2.35	*def1*	cg3034
Conserved hypothetical protein	2.361	-	cg1728
Hypothetical protein predicted by Glimmer/Critica	2.391	-	cg1240
Uncharacterized enzyme involved in biosynthesis of extracellular polysaccharides	2.405	-	cg2962
CTP synthase	2.41	*pyrG*	cg1606

Ferritin-like protein	2.414	*ftn*	cg2782
Conserved hypothetical protein	2.447	-	cg1370
Protein synthesis inhibitor, putative	2.468	-	cg2435
Permease	2.496	-	cg0683
ADP-ribose pyrophosphatase	2.511	-	cg1218
Succinate dehydrogenase CD	2.515	*sdhCD*	cg0445
Probable FeSuccinyl-CoA:3-ketoacid-coenzyme A transferase subunit	2.525	*scoA*	cg2623
rRNA or tRNA methylase	2.556	-	cg2100
Putative excinuclease ATPase subunit-UvrA-like protein	2.562	-	cg1234
Chloromuconate cycloisomerase	2.576	*catB*	cg2635
1,4-alpha-glucan branching enzyme	2.59	*glgB*	cg1381
Ribulose-5-phosphate-3-epimerase	2.599	*rpe*	cg1801
Transcriptional regulator, TetR family	2.631	-	cg1738
Catechol 1,2-dioxygenase	2.712	*catA1*	cg2636
ABC-type peptide transport system, secreted component	2.809	-	cg2181
Putative carboxymuconolactone decarboxylase subunit	2.832	-	cg3212
Putative acetyl-CoA:acetyltransferase	2.924	*pcaF*	cg2625
Haloacid dehalogenase-like hydrolase	2.989	-	cg0154
Phosphoserine transaminase	3.024	*serC*	cg0948
Porin	3.108	*porA*	cg3008
7,8-dihydro-6-hydroxymethylpterin-pyrophosphokinase	3.16	*folK*	cg2979
Catalase	3.226	*katA*	cg0310
Conserved hypothetical protein	3.45	-	cg2247
Putative penicillin binding protein	3.58	-	cg2478
Conserved hypothetical protein	3.985	-	cg2514
Putative nicotinate-nucleotide pyrophosphorylase	4.006	*nadC*	cg1215
Esterase/lipase/thioesterase family protein	4.476	-	cg0120
Aconitase	4.487	*acn*	cg1737
GTP cyclohydrolase	4.58	*folE*	cg2983
Starvation-induced DNA protecting protein	4.954	*dps*	cg3327
Glutamine synthetase I	10.777	*glnA*	cg2429
Nitrogen regulatory protein PII	18.943	*glnK*	cg2260

Table S 6 Proteom comparison of AKG-3 and the parental strain P_{O6}-*iolT1* on molasses. Differentially synthesized proteins of *C. glutamicum* AKG-3 in comparison to the control strain *C. glutamicum* the parental strain P_{O6}-*iolT1* with molasses as carbon and energy source. Proteins with statistically significant changes (*p*-value < 0.01, Log2(Fold-Change) > 0.5 for upregulated proteins and Log2(Fold-Change) < -0.5 for down-regulated proteins of conditions during exponential growth are shown.

Protein	FC_AKG-4_P_{O6}_suc	Gene	Locus
Zn-dependent alcohol dehydrogenase	0.052	*adhA*	cg3107
Aldehyde dehydrogenase	0.109	-	cg3096
Flavin-containing monooxygenase (FMO)	0.127	-	cg3195
Probable respiratory nitrate reductase oxidoreductase	0.223	*narH*	cg1343
Secreted sugar-binding protein	0.224	-	cg1413
Molybdate-binding secreted protein	0.228	*modA*	cg0263
NADP-specific glutamate dehydrogenase	0.237	*gdh*	cg2280
Acetyltransferase	0.251	-	cg1612
Universal stress protein UspA or related nucleotide-binding protein	0.26	*uspA2*	cg1595
Putative integral membrane protein	0.282	-	cg0952
Probable methylisocitric acid lyase	0.289	*prpB2*	cg0760
Homocysteine methyltransferase	0.292	*metE*	cg1290
Na+-dependent transporters of the SNF family	0.294	-	cg1169
Na+/proline, Na+/pantothenate symporter or related permease	0.296	-	cg0953
Methylcitrate synthase	0.324	*prpC2*	cg0762
Hypothetical protein predicted by Glimmer/Critica	0.33	-	cg2564
Putative excinuclease ATPase subunit-UvrA-like protein	0.332	-	cg1234
Putative ribokinase protein	0.334	*rbsK1*	cg1546
Cold-shock protein CspA	0.353	*cspA*	cg0215
Anion-specific porin precursor	0.366	*porB*	cg1109
Metal-dependent hydrolases of the beta-lactamase superfamily III	0.367	-	cg2761
Conserved hypothetical protein	0.369	-	cg0895
Conserved hypothetical protein	0.387	-	cg2089
3-isopropylmalate dehydratase large subunit	0.401	*leuC*	cg1487
Nitrate reductase 2, alpha subunit	0.402	*narG*	cg1344
Quinolinate synthetase	0.416	*nadA*	cg1216
3-isopropylmalate dehydratase (small subunit)	0.426	*leuD*	cg1488
Conserved hypothetical protein	0.438	-	cg1632
Phosphoribosyl pyrophosphate synthase isozyme 2 PR	0.453	*prsA*	cg1075

Folylpolyglutamate synthase	0.457	*folC*	cg2608
Helicase	0.462	-	cg0843
ABC-type cobalamin/Fe3+-siderophores transport system	0.465	-	cg0924
lycosyl transferase	0.467	-	cg0394
Ribosomal protein L36	0.48	-	cg2791
Rhodanese-related sulfurtransferase	0.483	*sseA2*	cg1613
Propionate catabolism protein PrpD	0.489	*prpD2*	cg0759
RNA polymerase sigma factor, putative	0.49	*pvdS1*	cg1046
Putative transcriptional regulator	0.495	-	cg2112
DTDP-glucose 4,6-dehydratase	2.006	*rmlB1*	cg0403
Inositol monophosphatase	2.011	-	cg0910
Component of an uncharacterized iron-regulated ABC-type transporter	2.016	*sufB*	cg1764
Putative transcriptional regulator	2.045	-	cg3414
Phosphoenolpyruvate carboxylase	2.056	*ppc*	cg1787
Branched-chain amino acid aminotransferase	2.06	*ilvE*	cg2418
Benzaldehyde dehydrogenase	2.085	*xylC*	cg2953
Uncharacterized enzyme involved in biosynthesis of extracellular polysaccharides	2.102	-	cg2962
Cyclomaltodextrinase	2.112	-	cg1012
Succinate dehydrogenase B	2.132	*sdhB*	cg0447
Succinate dehydrogenase CD	2.188	*sdhCD*	cg0445
Putative riboflavin synthase	2.451	*ribC*	cg1799
Permease	2.569	-	cg0683
Transcriptional regulator, TetR family	2.613	-	cg1738
Conserved hypothetical protein	2.628	-	cg1374
Dihydrolipoamide dehydrogenase	2.64	*lpd*	cg0441
Creatinine deaminase	2.641	*codA*	cg0104
Conserved hypothetical protein	2.643	-	cg0338
Holliday junction resolvasome helicase subunit	2.684	*ruvB*	cg1869
Delta-aminolevulinic acid dehydratase	2.7	*hemB*	cg0512
CTP synthase	2.765	*pyrG*	cg1606
Molybdopterin co-factor synthesis protein	2.844	*moaC*	cg0260
Tetrahydrodipicolinate succinylase	2.962	*dapD*	cg1256
Ferritin-like protein	3.004	*ftn*	cg2782

Conserved hypothetical protein	3.041	-	cg1433
Hypothetical protein cg0571	3.062	-	cg0571
Starvation-induced DNA protecting protein	3.16	*dps*	cg3327
Putative phage integrase (C-terminal fragment)	3.31	*'int2*	cg2070
Aconitase	3.462	*acn*	cg1737
Conserved hypothetical protein	4.464	-	cg0987
Putative membrane protein	5.686	-	cg1082
Glyceraldehyde-3-phosphate dehydrogenase	5.741	*gap*	cg1791
Glutamine synthetase I	6.88	*glnA*	cg2429
Nitrogen regulatory protein PII	13.912	*glnK*	cg2260

Table S 7 Proteom comparison of WT_EtOH-evo and the WT strain on ethanol Differentially synthesized proteins of *C. glutamicum* WT_EtOH-Evo in comparison to the control strain *C. glutamicum* WT with ethanol as sole carbon and energy source. Proteins with statistically significant changes (*p*-value < 0.01, Log2(Fold-Change) > 0.5 for upregulated proteins and Log2(Fold-Change) < -0.5 for down-regulated proteins) as intersection of the four sampled conditions during exponential growth (EVO(t_1), WT(t_1)) and stationary phase (EVO(t_2), WT(t_2)) are shown

Identified protein	Gene	Locus	FC	*p*-value
Putative protein of nitroreductase-family	-	cg0404	0.15	6.39e-05
Uncharacterized ACR, double-stranded □-helix domain	-	cg3277	0.151	1.55e-06
Predicted nucleoside-diphosphate-sugar epimerase	-	cg3375	0.168	5.82e-05
Pyruvate:quinone oxidoreductase	*pqo (poxB)*	cg2891	0.172	6.53e-07
Conserved hypothetical protein	-	cg1131	0.181	0.0002
Iron-regulated ABC transporter ATPase subunit	*sufC*	cg1762	0.185	3.69e-06
O-Acetylhomoserine (Thiol)-Lyase	*metY*	cg0755	0.191	3.18e-10
Uracil phosphoribosyltransferase	*upp*	cg0786	0.197	2.07e-07
Electron transfer flavoprotein, α subunit	*fixB*	cg1387	0.2	2.18e-08
Putative secreted protein	-	cg4005	0.209	2.47e-05
Riboflavin synthase subunit β	*ribH*	cg1797	0.213	3.65e-05
Fe-S cluster assembly protein	*sufB*	cg1764	0.224	0.00128
Cu^{2+}/cation-transporting ATPase transmembrane protein	*copB*	cg3281	0.226	4.81e-06
6-phosphogluconolactonase	*pgi (devB)*	cg1780	0.228	1.6e-07
Citrate uptake transporter	*tctC*	cg3127	0.232	0.0161
Putative membrane-bound protease modulator	*ppmA*	cg3138	0.257	5.51e-09
Putative alkanal monooxygenase □ chain, FMN-linked	-	cg2538	0.265	1.62e-06
Electron transfer flavoprotein, □ subunit	*fixA*	cg1386	0.29	3.46e-08
Putative homoserine O-acetyltransferase	-	cg0961	0.295	0.00119
Cysteinyl-tRNA synthetase	*cysS2*	cg1709	0.3	5.34e-08
Peptide methionine sulfoxide reductase	*msrA*	cg3236	0.306	8.49e-05
30S ribosomal protein S10	*rpsJ*	cg0593	0.314	8.78e-05
High affinity ABC-type methionine transporter	*metQ*	cg0737	0.317	2.1e-07
Bifunctional 3,4-dihydroxy-2-butanone 4-phosphate synthase/ GTP cyclohydrolase II protein	*ribA*	cg1798	0.333	7.86e-11
2-methycitrate dehydratase	*prpD2*	cg0759	0.334	0.000257
Homoserine kinase	*thrB*	cg1338	0.336	0.00277
Putative protein, CsbD-family, probably involved in stress response	*cybD*	cg0282	0.352	9.33e-08
Putative coenzyme F420-dependent N5,N10-methylene tetrahydromethanopterin reductase or related flavin-depende	-	cg2329	0.357	1.16e-05
Thioredoxin reductase	*trxB*	cg3422	0.362	1.35e-11
Putative Fe-S cluster assembly protein	-	cg1759	0.363	0.0157

Putative lysine decarboxylase-family protein	-	cg1261	0.364	7.8e-08
Pyruvate carboxylase	*pyc*	cg0791	0.365	0.00976
Putative NADPH quinone reductase or Zn-dependent oxidoreductase	-	cg3405	0.374	0.0357
Fe-S cluster assembly membrane protein	*sufD*	cg1763	0.391	0.00857
Cysteine desulfhydrase	*sufU*	cg1760	0.404	0.0161
N-acetylglucosaminyl transferase	*murG*	cg2369	0.429	6.36e-07
30S ribosomal protein S19	*rpsS*	cg0599	0.433	2.51e-07
ATP-dependent helicase PCRA	*pcrA*	cg0976	0.444	6.82e-06
30S ribosomal protein S17	*rpsQ*	cg0604	0.456	1.22e-06
Oxaloacetate decarboxylase	*odx*	cg1458	0.457	0.0047
Cytochrome aa3 oxidase, subunit 1	*ctaD*	cg2780	2.116	0.000383
Conserved hypothetical protein	-	cg0935	2.136	2.38e-05
Hypothetical protein	-	cg0452	2.379	0.00031
Phosphate acetyltransferase	*pta*	cg3048	2.637	1.79e-09
Thiosulfate sulfurtransferase	*thtR*	cg0803	2.886	1.47e-07
Cysteine desulfurase-like protein involved in Fe-S cluster assembly	*nadS*	cg1214	2.965	1.1e-05
Putative metallo-β-lactamase superfamily protein	-	cg0349	3.641	1.34e-06
Conserved hypothetical protein	-	cg2464	3.788	4.09e-07
Aldehyde dehydrogenase	*ald*	cg3096	4.082	3.71e-10
Putative signal-transduction protein containing cAMP-binding and CBS domain	-	cg1456	4.18	4.92e-09
4-hydroxy-3-methylbut-2-enyl diphosphate reductase	*lpsH (lytB)*	cg1164	4.316	8.57e-08
Conserved hypothetical protein	-	cg2363	4.316	1.44e-06
Putative secreted protein	-	cg2949	5.16	2.34e-09
Trehalose uptake system, ABC-type, bacterial extracellular solute-binding protein	*tusE*	cg0834	5.429	0.00051
Quinolinate synthetase	*nadA*	cg1216	9.182	1.63e-11
δ-aminolevulinate dehydratase	*hemB*	cg0512	9.736	4.19e-06
Conserved hypothetical protein	-	cg1045	14.999	1.21e-10
Putative NADPH-dependent FMN reductase	-	cg3223	20.12	7.7e-08
Phosphoenolpyruvate carboxykinase	*pck*	cg3169	26.869	1.94e-07

Table S 8 Single nucleotide variants (SNV) of rbALE EtOH R3 compared to the WT identified by genome sequencing appearing with a frequency of at least 75 %.

Position and mutation on DNA level	Frequency (%)	Locus tag, gene name, annotation	Mutation and interpretation[a]
829516_SNV_T_A	99.32	cg0896, putative membrane protein	cg0896 Y967*, no promoter affected
923955_SNV_G_T	99.3	cg0987, conserved hypothetical protein	cg0987 A12D, no promoter affected
381944_SNV_T_G	100	P_{cg0435}, *udgA1*, UDP-glucose 6-dehydrogenase	Mutation between RBS and TLS, 4 bp upstream of ATG, presumably no effect
512738_SNV_G_A	100	P_{cg0576}, *rpoB*, DNA-directed RNA polymerase β subunit	Mutation between TSS and TLS, 175 bp upstream of TLS, regulation not known.
1096559_SNV_A_G	100	cg1189, hypothetical protein	cg1189 I38V, no promoter affected
1813816_SNV_G_C	100	cg1935, *gntR2*, gluconate responsive repressor 2, involved in gluconate metabolism and the pentose phosphate pathway.	GntR2 V13L , no promoter affected
1993795_SNV_T_C	100	NCgl1815, hypothetical protein, CGP4	NCgl1815 R109R, silent mutation, no promoter affected
1993797_SNV_G_T	100	NCgl1815, hypothetical protein, CGP4	NCgl1815 R109R, silent mutation, no promoter affected
1993809_SNV_A_G	100	NCgl1815, hypothetical protein, CGP4	NCgl1815 L105L, silent mutation, no promoter affected
1993912_SNV_C_T	100	NCgl1815, hypothetical protein, CGP4	NCgl1815 P70P, silent mutation, no promoter affected
2368804_SNV_A_C	100	cg2452, *galK*, putative galactokinase	cg2452 Q338P, no promoter affected
2981767_SNV_G_A	75.61	P_{cg3096}, *ald*, acetaldehyde dehydrogenase	Located in the GlxR binding site upstream of cg3096, presumably effect on transcription of *ald*.

[a] RBS, Ribosome binding site; TLS, Translational start site; TSS, Transcriptional start site

Table S 9 Oligonucleotides used in this study.

Oligonucleotide	Sequence (5' → 3')
Construction of pK19*mobsacB*-Δ*gdh*	
gdh_up_fw	TGCATGCCTGCAGGTCGACTGTACCAATTCCATTTGAGG
gdh_up_rev	CGTCAGCTACCTGCTCATCAACTGTCATG
gdh_down_fw	TGATGAGCAGGTAGCTGACGCGATGCTG
gdh_down_rev	TTGTAAAACGACGGCCAGTGCAACTACGGTCTGGAACC
gdh_check_fw	AACGGTCGCCCAATTGAGGAGTGGGTCCAT
gdh_check_rev	AAGCCTTTGCCCAAAGGCCCGCTTAAGCTG
Construction of pK19*mobsacB*-Δ*gltB*	
gltB_up_fw	TGCATGCCTGCAGGTCGACTGAGAATTCCAAAGACATTTTG
gltB_up_rev	TTGCTGGGTCGAGTCCTTGTGGTTTCATG
gltB_down_fw	ACAAGGACTCGACCCAGCAATCAAGATCATGGAGGC
gltB_down_rev	TTGTAAAACGACGGCCAGTGGTGGCCTGCGCGGGTGAG
gltB_check_fw	AAGCTGCAACGCCTTCGATTTTTCC
gltB_check_rev	GCCGTAGCGCATGAGGCCGCCGAGG
Construction of pK19*mobsacB*-Δ*mscCG'*	
mscCG'_up_fw	TGCATGCCTGCAGGTCGACTGGCGGATCGACCACGGCT
mscCG'_up_rev	CAGCGTCCTAGACCTTAAATAGTGACAGCAAGAGCAGC
mscCG'_down_fw	ATTTAAGGTCTAGGACGCTGATTACAGAC
mscCG'_down_rev	TTGTAAAACGACGGCCAGTGGTAGCCGTCTTCTTGAAC
mscCG'_check_fw	CGCCCGGGTGTGGATGGTGTGCTGG
mscCG'_check_rev	GAAAGCTCCTTCTGCTGCTTCGGCC
Construction of plasmid pK19*mobsacB*-P01-*ald* and PCR-analysis of the resulting mutants	
PLZM056	CAGCTATGACCATGATTACGCCATCCACACCGAAAAAATCCAACG
PLZM057	TTGTAAAACGACGGCCAGTGAATTTCATTGGGTCTCCTTTGGGCCAC
M13-fw	CGCCAGGGTTTTCCCAGTCAC
M13-rv	AGCGGATAACAATTTCACACAGGA
P01-ald-Test-fw	CGGGCCAGAACCGCTAGACG
P01-ald-Test-rv	GCCACCAATGTAGTTCTCGTAGCGC
Universal pK19*mobsacB* oligonucleotides	
rsp	CACAGGAAACAGCTATGACCATG
univ	CGCCAGGGTTTTCCCAGTCACGAC

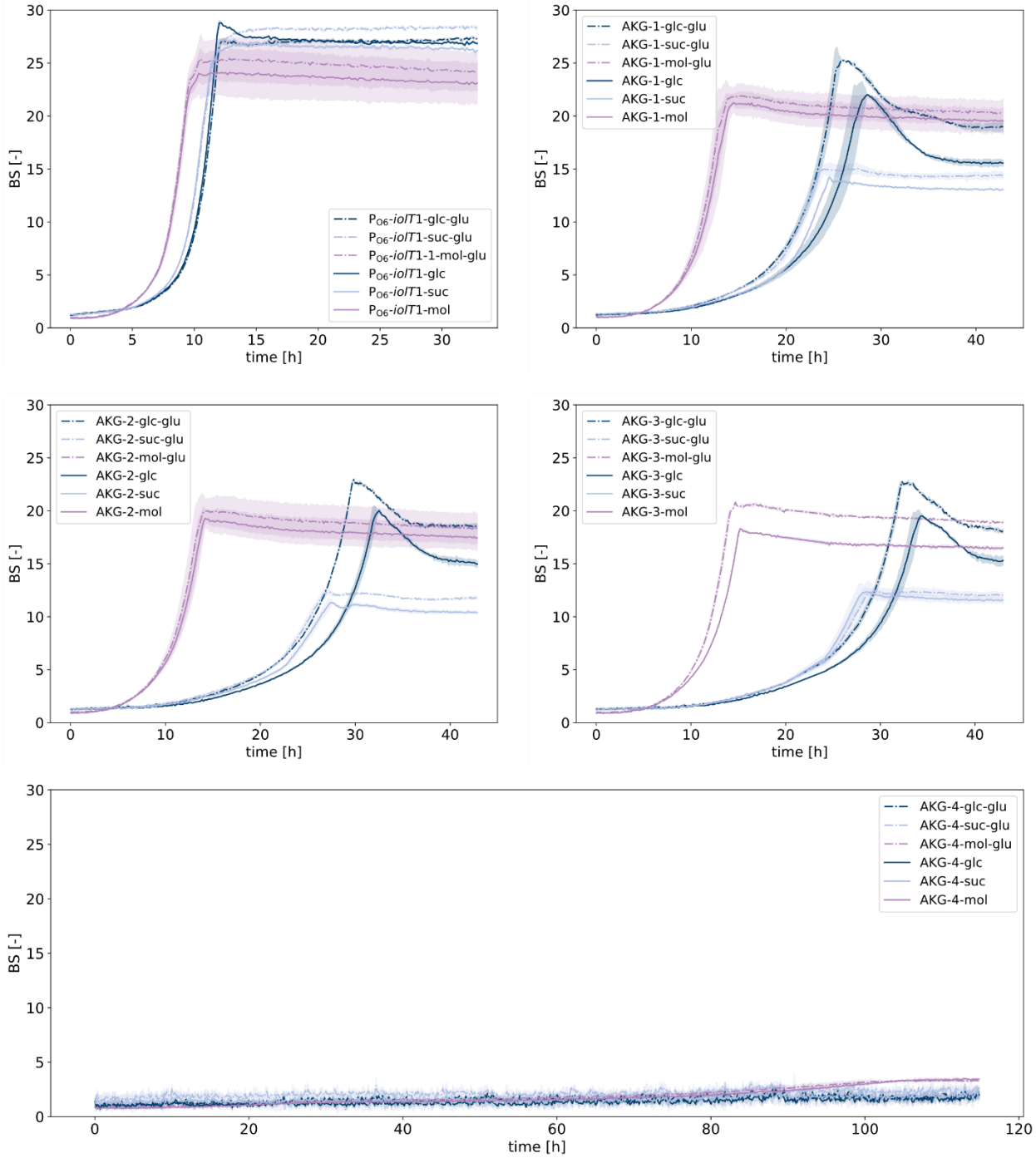

Figure S 1 Glutamate supplementation experiment to test the ability of growth recovery. All five *C. glutamicum* strains (P$_{O6}$-*iolT1* and AKG-1 to AKG-4) were cultivated separately on glucose, sucrose and molasses (20 g/L C-source) with and without supplementation of 15 mM glutamate.

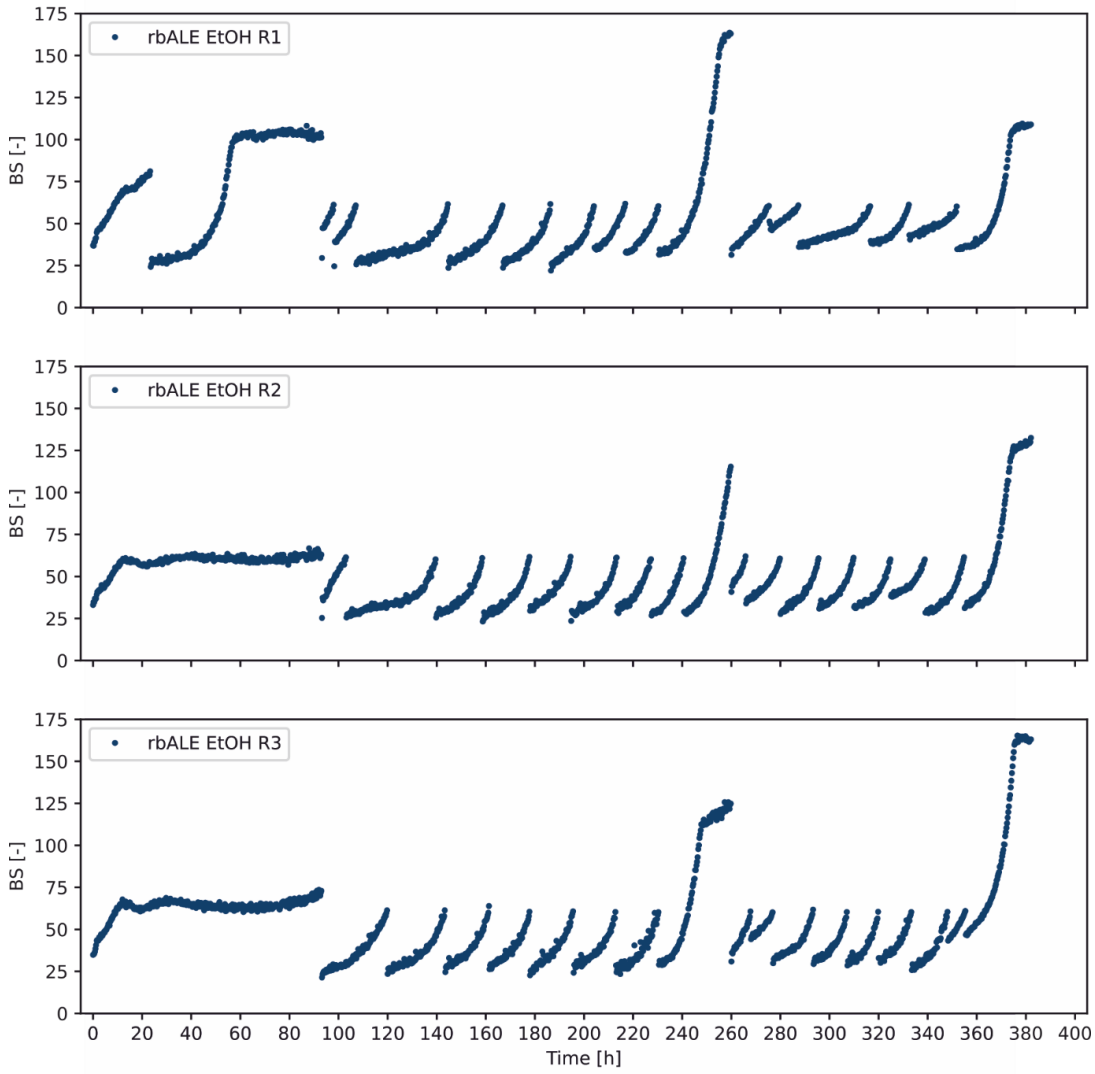

Figure S 2 Long-term rbALE experiment to improve ethanol utilizationof *C. glutamicum* WT. A total of three replicate runs in one FlowerPlate were performed. *C. glutamicum* WT was cultivated for a total number of 16 to 18 repetitive batches in one FlowerPlate and defined CGXII medium with 428 mM ethanol as sole carbon and energy source. The resulting online BS measurements against cultivation time are shown.

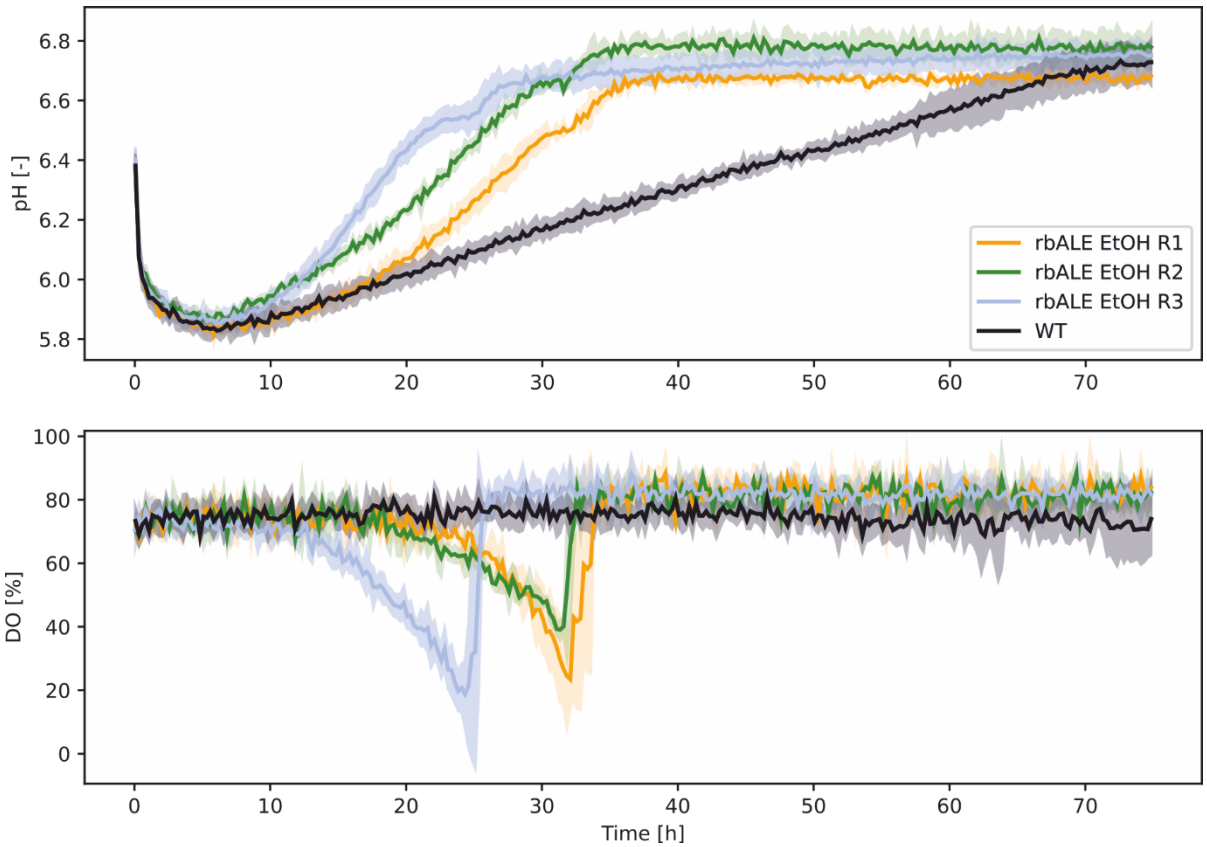

Figure S 3 Additional online data (pH and dissolved oxygen (DO)) for the phenotyping experiments of the three evolved mutant strains in comparison to *C. glutamicum* WT (cf. Figure 3C).